Sudan University of science and Technology

Collage of Graduate Studies

Spectroscopic Variability and Optical Properties of Sudanese Edible Oils Using Spectroscopy Methods

التباين الطيفي والخصائص البصرية لزيوت الطعام السودانية باستخدام طرق التحليل الطيفي

A Thesis Submitted in Fulfillment of the Requirements for the Degree of Ph.D. in Laser Applications in physics

By

Mahasin Mohamed Daffalla Banaga

Supervised by:

Prof. Dr.Abul Moneim. M. Awad elgied

2022

الآيه

ٱللَّهُ نُورُ ٱلسَّمَٰوَٰتِ وَٱلۡأَرۡضِۚ مَثَلُ نُورِهِۦ كَمِشۡكَوٰةٖ فِيهَا مِصۡبَاحٌۖ ٱلۡمِصۡبَاحُ فِي زُجَاجَةٍۖ ٱلزُّجَاجَةُ كَأَنَّهَا كَوۡكَبٞ دُرِّيّٞ يُوقَدُ مِن شَجَرَةٖ مُّبَٰرَكَةٖ زَيۡتُونَةٖ لَّا شَرۡقِيَّةٖ وَلَا غَرۡبِيَّةٖ يَكَادُ زَيۡتُهَا يُضِيٓءُ وَلَوۡ لَمۡ تَمۡسَسۡهُ نَارٞۚ نُّورٌ عَلَىٰ نُورٖۚ يَهۡدِي ٱللَّهُ لِنُورِهِۦ مَن يَشَآءُۚ وَيَضۡرِبُ ٱللَّهُ ٱلۡأَمۡثَٰلَ لِلنَّاسِۗ وَٱللَّهُ بِكُلِّ شَيۡءٍ عَلِيمُۢ

النور (35)

Acknowledgements

It is a pleasure to thank all the people who have accompanied and supported me throughout this scientific work. I am honoured to pay my sincere thanks to my research supervisor **Prof. Dr. Abdelmoneim Awadelgied** for giving me the opportunity to work in his research group. I most gratefully record that the work imbibed in this project is solely due to deep insight and vision of my guide and supervisor, **Prof. Dr Nafie Abdallatief Al Muslet.** Besides being morally supportive all through the execution of my work, his critical discussions and meticulous approach towards my theoretical back ground have not only proved valuable for the project but they, I am sure, will go a long way to mold my future career and for this I shall ever remain indebted. I acknowledge **Dr. Nadir Shams Eldin Osman** for his excellent guidance which was instrumental for the success of this research.

Lastly, I would like to thank all the past and present colleagues at for the pleasant working atmosphere.

Most importantly, I am ever so grateful to my dearest **Mom**, Sisters, brother, aunts for their moral support, endless love, trust, and understanding during my study. Their motivational nature and enthusiasm in both good and difficult times will remain in my memory. Without them this would not be possible.

Abstract

In this study, nondestructive test was applied on six types of edible oils (corn, extra virgin olive, sunflower, pressed sesame, factory sesame and peanuts) using spectroscopic methods. Raman spectroscopy and Fourier infrared spectroscopy were carried out to identify functional groups presence on oils while ultraviolet visible was used to study optical properties of edible oils.

From Raman spectra of edible oils samples, the major bands can be found at (1084, 1266, 1303, 1441, 1657, 1749,) cm^{-1}. It is of particularly significance for edible oils that stretching of C=C bonds gave rise to strong Raman signals and C=O stretching bands were very weak; the contrary can be found in infrared spectra. FTIR spectrum of all samples in range from (400-4000) cm^{-1}. From comparison of IR and Raman spectra of edible oil samples, the frequencies of some characteristic peaks were identical, while the relative intensities differed markedly. On the contrary, Raman scattering signal at (560, 969) cm^{-1} was quite weak, but corresponding infrared absorption peak was obvious.

The general appearance of the IR spectra of these vegetable oils was found to be very similar to a previously reported study. In the Raman spectrum, the spectrum of peanut and presses sesame differed from the previous studies. Thus, the combination of these two different methods has been very useful in the study of the oil which provides comprehensive information about the chemical compositions of edible oils.

FTIR spectral data collected in MIR range 4000-400 cm^{-1} showed major peaks representing triglyceride functional groups which could be observed around 2925 cm^{-1} [C−H stretching (asymmetry)], 2854 cm^{-1}

[C− H stretching (symmetry)], 1747 cm^{-1} [C=O stretching], 1463 cm^{-1} [C−H bending (scissoring)], 1238, 1163, 1118 and 1097 cm-1 [C−O stretching] and 722 cm^{-1} [C−H bending (rocking)]. A peak around 1653 cm^{-1} is attributed to C=C stretching (*cis*). A band shift at 3007 cm^{-1}; assigned to C–H stretching vibration of cis- double bond (=C–H) characteristic to samples oils.

The absorption spectrum of six important Sudanese oils can be divided into three main absorption regions the first region is from the beginning of the spectrum to 340 nm, the second region is (400 - 500) nm and the last region is from (600-800) nm. The shift in absorption peaks of these oils refer to different chemical group that oils contain. Absorption coefficient and refractive index of all oils under study were different because structure components of each oil were different and this confirm with Raman and FTIR results. High values of the absorption coefficient indicate the possibility of direct electronic transitions between the valence and conduction bands at these energies.

المستخلص

في هذه الدراسة تم إجراء اختبار غير تدميري على ستة أنواع من الزيوت الصالحة للأكل (الذرة ، الزيتون البكر الممتاز ، عباد الشمس ، سمسم المصنع ، السمسم المعصور والفول السوداني) باستخدام طرق التحليل الطيفي. تم إجراء التحليل الطيفي لرامان ومطياف فوريه بالأشعة تحت الحمراء لتحديد وجود المجموعات الوظيفية على الزيوت بينما تم استخدام الأشعة فوق البنفسجية المرئية لدراسة الخصائص البصرية لزيوت الطعام.

من أطياف رامان لعينات زيوت الطعام ، يمكن العثور على العصابات الرئيسية في (1084 ، 1266 ، 1303 ، 1441 ، 1657 ، 1749) سم $^{-1}$. ومن الأهمية بمكان بالنسبة لزيوت الطعام أن شد روابط C = C أدى إلى ظهور إشارات Raman قوية وأن أشرطة التمدد C = O كانت ضعيفة جدًا ؛ يمكن العثور على العكس في أطياف الأشعة تحت الحمراء. طيف FTIR لجميع العينات في المدى من (400-4000) سم $^{-1}$. من مقارنة طيفي الأشعة تحت الحمراء ورامان لعينات زيت الطعام ، كانت ترددات بعض القمم المميزة متطابقة ، بينما اختلفت الشدة النسبية بشكل ملحوظ. على العكس من ذلك ، كانت إشارة تشتت رامان عند (560 ، 969) سم $^{-1}$ ضعيفة جدًا ، لكن ذروة امتصاص الأشعة تحت الحمراء المقابلة كانت واضحة.

أظهرت البيانات الطيفية FTIR التي تم جمعها في نطاق MIR 4000-400 سم $^{-1}$ قمم رئيسية تمثل مجموعات وظيفية من الدهون الثلاثية والتي يمكن ملاحظتها حول 2925 سم $^{-1}$ [تمدد C - H (عدم تناسق)] ، 2854 سم $^{-1}$ [تمدد C – H (تناظر)] ، 1747 سم $^{-1}$ [تمديد C = O]، 1463 سم $^{-1}$ [انحناء C – H (مقص)] ، 1238 ، 1163 ، 1118 و 1097 سم $^{-1}$ [إطالة C – O و 722 سم $^{-1}$ [الانحناء) C - H هزاز)]. تُعزى ذروة حوالي 1653 سم $^{-1}$ إلى تمدد) C = C رابطة الدول المستقلة). إزاحة

الفرقة عند 3007 سم $^{-1}$ ؛ المخصصة لامتداد H - C الاهتزاز للرابطة المزدوجة (=C - H) المميزة لعينات الزيوت.

تم العثور على المظهر العام لأطياف الأشعة تحت الحمراء لهذه الزيوت النباتية ليكون مشابهًا جدًا لدراسة تم الإبلاغ عنها سابقًا. في طيف رامان ، اختلف طيف الفول السوداني و السمسم المعصور عن الدراسات السابقة. وبالتالي ، فإن الجمع بين هاتين الطريقتين المختلفتين كان مفيدًا جدًا في دراسة التركيبات الكيميائية لزيوت الطعام.

يمكن تقسيم طيف ستة زيوت سودانية مهمة إلى ثلاث مناطق امتصاص رئيسية المنطقة الأولى من بداية الطيف إلى 340 نانومتر ، والمنطقة الثانية (400-500) نانومتر والمنطقة الأخيرة من(600-800) نانومتر.

يشير التحول في قمم امتصاص هذه الزيوت إلى مجموعة كيميائية مختلفة تحتويها الزيوت. كان معامل الامتصاص ومعامل الانكسار لجميع الزيوت قيد الدراسة مختلفين لأن مكونات بنية كل زيت مختلفة وهذا يؤكد نتائج Raman و .FTIR تشير القيم العالية لمعامل الامتصاص إلى إمكانية حدوث انتقالات إلكترونية مباشرة بين نطاقي التكافؤ والتوصيل في هذه الطاقات.

Table of Contents

List of figures

List of Tables

Acronyms

Item	Definition
FT-IR	Fourier transform infrared
UV-VIS	Ultraviolet – visible
IR	infrared spectroscopy
Ppm	Part per million
FFA	free fatty acids
REMPI	Resonance-enhanced multiphoton ionization
NMR	Nuclear magnetic resonance
Rf radiation	radiofrequency radiation
LIBS	Laser-induced breakdown spectroscopy
LIPS	Laser-induced plasma spectroscopy
LSS	laser spark spectroscopy
LIF	Laser-induced fluorescence
FFA	free fatty acids
SERS	surface enhanced Raman scattering
LOD	Limits of detection
MS	Mass spectroscopy
NIR	near-infrared
R^2	coefficients of determination
MSE	mean-squared error
SBS	stimulated Brillouin scattering
ν^4	excitation frequency
CCD	Charge-coupled device
RR	resonance Raman
DU	Degree of unsaturation
IOP's	Intrinsic optical properties
AOP's	Apparent optical properties
RMSEP	root-meansquare error of the prediction
PCA	principal component analysis
OPLS-D	Orthogonal partial least square-discriminant analysis
PLS	partial least squares
CO	canola oil

FWHM	full width at half maximum
ATR	attenuated total reflection
LCD	liquid-crystal display
EVOO	Extra-Virgin Olive Oil
GUI	graphical user interface

Chapter One

Introduction

1.1 Introduction

Spectroscopic techniques are rapid analytical methods have been widely used for edible oil detection. The spectrum of oil can provide information to identify and analyze it is molecular structure, particularly the functional groups. Fourier transform infrared (FT-IR) spectroscopy has been used to detect and quantify the adulteration of edible oils with other types of oil evaluate functional compounds in edible oil, and determine the acid values of edible oils. As a complement to infrared spectroscopy, Raman spectroscopy has been used to predict the fatty acid content of oil and discriminate the of edible oils. On the other hand, the near UV-VIS spectroscopic absorption technique has been used mainly to evaluate the total amount of carotenoids and the total amount of chlorophylls' derivatives from absorbance values obtained on edible oil samples.

Edible oils are a group of products which are characterized by a high variability of their chemical and physical properties. The chemical analysis of vegetable oils is arduous because they consist of complex mixtures of chemical compounds and the evaluation of the results can also be disturbed by a matrix effect. However, characterization of these oils can be performed using a great variety of analytical methods and chemometric methodologies. Different techniques for fats and oils analysis have been developed so far and a large part of them is based on liquid or gas chromatography. There has been a growing demand to replace

traditional analytical methods with instrumental methods. The superiority of the latter is due to their high sensitivity, low limits of detection, speed of analysis and automated operation. Modern instrumental techniques include spectroscopic methods that are successfully used in qualitative and quantitative analysis in various industries, including the chemical and food industries, electronics or metallurgy. Furthermore, spectroscopic methods can be used in conjunction with advanced separation methods, which apart from comprehensive qualitative and quantitative analysis of isolated intermediates, enable the direct analysis of final products. Numerous scientific publications prove the usefulness of spectroscopic methods in the study of the properties of vegetable oils and, above all, the assessment of the quality of edible oils. The analysis of vegetable oils can be carried out with the use of absorption spectroscopy in the area of the ultraviolet-visible spectral region (UV-Vis), infrared spectroscopy (IR), and Raman spectroscopy.

1.2 Problems Statement

Quality tests of oils are often carried out using chemical methods which take a long test time, in addition to adding waste to environment. In this study, quantitative analysis of edible oils was applied through nondestructive testing by spectroscopic methods.

1.3 General Objectives

Variability spectroscopic and optical properties for Sudanese edible oils using spectroscopy methods

1.4 Specific Objectives

- To determine functional groups on edible oils (corn, extra virgin olive, sunflower, pressed sesame, factory sesame and peanuts) by using Raman spectroscopy.
- To determine functional groups on edible oils (corn, extra virgin olive, sunflower, pressed sesame, factory sesame and peanuts) by using Fourier infrared spectroscopy.
- To compare results obtained from Raman and Fourier infrared spectroscopy.
- To measurement optical absorbance and calculated optical properties of edible oils (corn, extra virgin olive, sunflower, pressed sesame, factory sesame and peanuts) using ultraviolet visible spectroscopy.
- To investigate the relation between optical properties and functional groups of edible oils (corn, extra virgin olive, sunflower, pressed sesame, factory sesame and peanut).

1.5 Methodology

Six types of edible oils (corn, extra virgin olive, sunflower, pressed sesame, factory sesame and peanuts) were collected from local market. Raman spectroscopy and Fourier infrared spectroscopy were applied to identify functional groups presence on oils, ultraviolet visible was used to study optical properties of edible oils.

1.6 Thesis Layout:

The thesis consists of the four chapters. chapter one contains introduction, chapter two is the theoretical background about

edible oils and spectroscopy and previous studies while chapter tree is experimental procedures and chapter four is concerned with results, analysis, discussion, conclusion and recommendation.

Chapter Two

Theoretical Background and Previous Studies

2.1 Introduction

This chapter consist of theoretical background about edible oils and spectroscopy in addition to previous studies related to research.

2.2 Edible Oils

Edible fats and oils comprise one of the three major classes of foods, the others being carbohydrates and proteins. Edible fats and oils can be obtained from terrestrial or aquatic animals, from the seeds or leaves of many plants, from the pulp, or from the nut/stone of many fruits. Edible fats and oils are used in many products not only to make food palatable but also to make them functional. The terms “fat” and “oil” are used according to the physical state of the material at room temperature. Fats are in a semi solid state, but the appearance is of a solid, while oils are in a liquid state. Chemically, fats and oils are mixtures comprised of more than 95% triacyl glyceride (TAGs) molecules mixed with minor components. Triacyl glycerides can also be found in the literature with the name triglycerides or triacylglycerols. These minor components can include phospholipids, glycolipids, free fatty acids, monoglycerides (MAGs) or diacylglycerides (DAGs) [Peyronel Fernanda, (2018)].

2.2.1 The difference between saturated and unsaturated fats

1. Saturated fat

Saturated fats do not have any double bonds in their chemical structure, because they are saturated with hydrogen atoms, and their chemical composition may have a role in their consistency at room temperatures.

Saturated fats are usually solid at room temperature. As for its food sources, it includes meat and dairy products, which are foods that contain high levels of saturated fat. The most important examples of this are:

Cheese, butter, ice cream, cuts of meat that are high in fat, palm oil, and coconut oil are also high in saturated fat. But it should be noted that the American Heart Association recommends eating foods containing this type of fat with less than 5 -6% of daily calories. This is because high intake of saturated fats is likely to lead to many diseases and serious health conditions such as; Atherosclerosis, increased risk of heart disease, and others.

2. Unsaturated fats

They are usually liquid at room temperature because unsaturated fats contain one or more double bonds in their chemical structure. Therefore, unsaturated fats can be classified based on their chemical structure into each of the following:

- **Monounsaturated fat**

They are those that contain in their chemical structure a single double bond, are usually liquid at room temperature, and also include olive oil and canola oil.

- **unsaturated fats**

Those with two or more double bonds in their chemical structure, are also liquid at room temperature, and may include; Corn oil and sunflower oil. The American Heart Association also recommends that most of the fat we eat daily should come from trans fats, whether monounsaturated fats or polyunsaturated fats, which are considered to be best for the health of the body.

As for the dietary sources of unsaturated fats, they are also varied and numerous, most notably. Avocado oil, olive oil that contains high levels of unsaturated fats, sunflower and corn.

Hence, the addition of hydrogen results in the reduction of unsaturated fatty acids to saturated fatty acids, which enhances the van der Waals interactions between the aliphatic chains to form solidified oils. The conversion of oleic acid (monounsaturated fatty acid) to stearic acid (saturated fatty acid) is schematically shown in Figure (2.1)

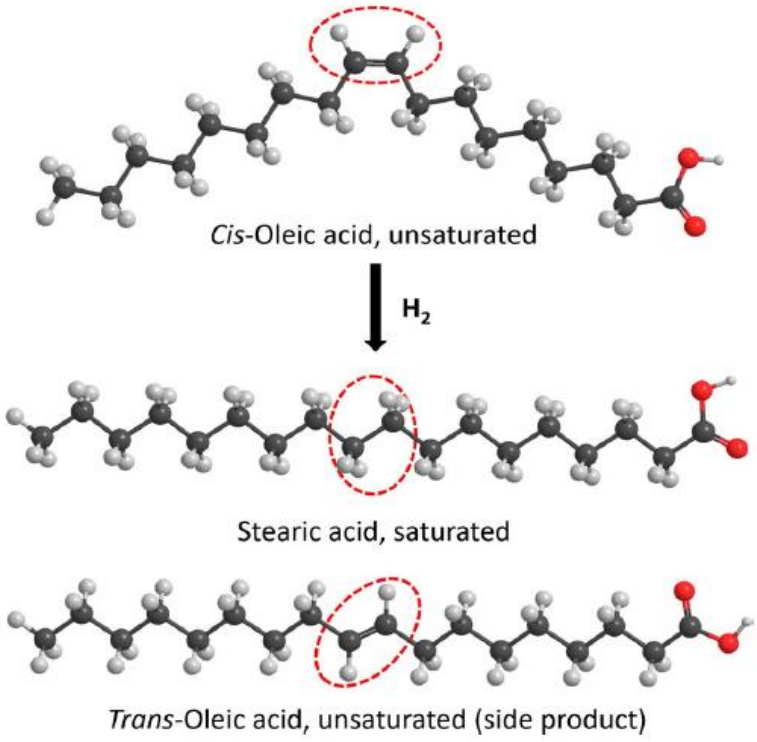

Figure 2.1 Conversion of oleic acid to stearic acid, showing the formation of *trans* oleic acid during partial hydrogenation.

2.2.2 Carotenoids and chlorophyll derivatives

The role of chlorophylls as natural pigments accounting for greenish colors and in photosynthesis is well known. There are also some reports about the benefits of dietary chlorophylls for human health. The structure of chlorophyll pigments, consisting of one tetra pyrrole macrocycle, coordinated to a Mg++ ion to form a planar complex, is responsible for the absorption in the visible region of the spectrum of oils. Here, both the bluish-green chlorophyll-a and the yellowish-green chlorophyll-b can be found. Chlorophylls in olive oils are mostly converted to pheophytins, due to the exchange of the central Mg++ ion with acid protons. Pheophytin-a (see Figure 2.2 a) is predominant with respect to pheophytin-b. In the case of bad storage conditions, pheophytins are further degraded to pyro pheophytins. The main carotenoids present in oils are lutein and β-carotene see figures (2.2 a, b, c). The level of pigments ranges from a few ppm to almost 100 ppm. Fresh edible oils usually have a higher pigments content. The major components are pheophytin-a followed by β-carotene and lutein. Carotenoids are isoprenoid compounds having a hydrocarbon structure with carbon double bonds that are responsible for many of their properties. Carotenoids can be divided into carotenes (carotenoids containing only carbon and hydrogen) and xanthophylls (carotenoids that also contain oxygenated functions, such as epoxide, hydroxyl, acetate, carbonyl and carboxylic groups, among others). In edible oils, the main carotenoids are β-carotene and lutein. The carotenoid fraction of olive oil also includes other xanthophyll's. [Cristina Lazzerini, et al, (2016),]

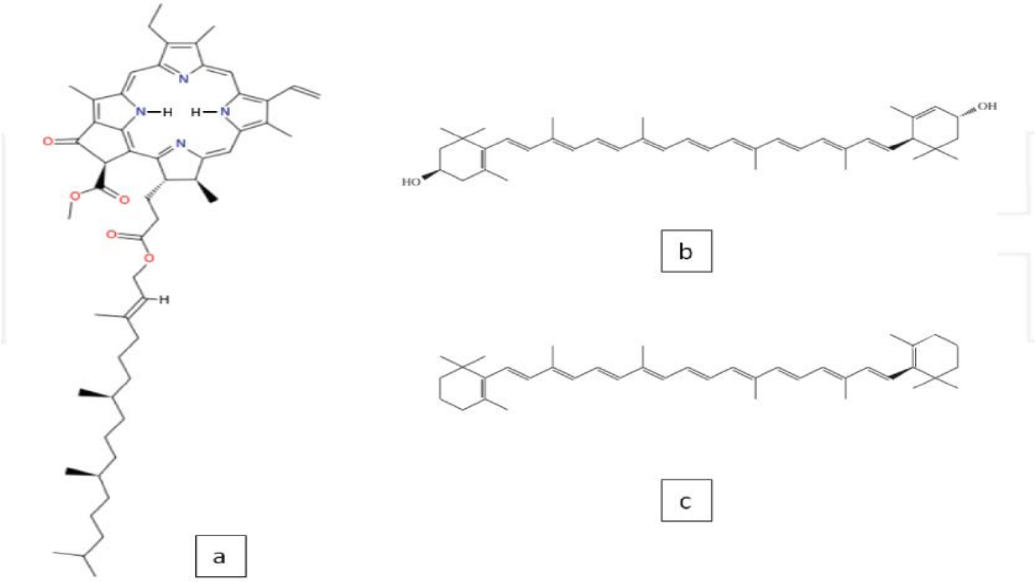

Figure (2.2) Molecular structure of (a) pheophytin-a, (b) lutein and (c) β-carotene

2.2.3 Corn oil

(Maize oil) is oil extracted from the germ of corn (maize). Its main use is in cooking, where it is high smoke point makes refined corn oil a valuable frying oil. It is also a key ingredient in some margarines. Corn oil is generally less expensive than most other types of vegetable oils. Corn oil is also a feedstock used for biodiesel. Other industrial uses for corn oil include soap, salve, paint, erasers, rust proofing for metal surfaces, inks, textiles, nitroglycerin, and insecticides. It is sometimes used as a carrier for drug molecules in pharmaceutical preparations. Almost all corn oil is expeller-pressed, then solvent-extracted using hexane or 2-methylpentane (is hexane). The solvent is evaporated from the corn oil, recovered, and re-used. After extraction, the corn oil is then refined by degumming and/or alkali treatment, both of which remove phosphatides. Alkali treatment also neutralizes free

fatty acids and removes color (bleaching). Final steps in refining include winterization (the removal of waxes), and deodorization by steam distillation of the oil at 232–260 °C (450–500 °F) under a high vacuum [Daniel Barrera-Arellano, et al, (2019)].

2.2.4 Olive Oils

Olive oil has a high nutritional value and significant health benefits. It is an essential component of the Mediterranean diet. According to the European Union (EU), olive oils are classified into various categories ranging from the high-quality extra-virgin olive oil to the low-quality olive pomace oil. Extra virgin olive oils are produced using only cold pressing techniques without any thermal or chemical treatments, while olive pomace oil, a fully refined olive oil, is obtained by solvent extraction processes from olive pomace. Extra-virgin olive oils are the most desirable on account of their high quality and nutritional properties compared to low-quality pomace olive oil and are therefore the most expensive grades. [R.M. El-Abassy, et al (27 April 2009)] [R.M. El-Abassy, et al (July 2005)]

2.2.5 Sunflower Oil

Sunflower oil is the non-volatile oil pressed from the seeds of sunflower (Helianthus annuus). Sunflower oil is one of the most popular vegetable oils and in Sudan it is preferred to peanut, cottonseed and corn oils . Sunflower oil has some unique characteristics that are popular with consumers, who use the oil in cooking and salad dressings. The oil can be used to make any product for the domestic or industrial food market and in cosmetic formulations as an emollient. The plant is grown in limited

areas in the world and this restricts the growth potential for the oil [Wikipedia, the free encyclopedia,(2021)].

2.2.6 Peanut Oil

Peanut oil is extracted from the seeds of Arachis hypogaea. known as groundnut, groundnut or ground nut because the seeds develop underground. Worldwide, frying and cooking make up the largest use of peanut oil by far. The high burning point of 229.4°C is one of the main reasons for using peanut oil for deep frying in fat. crude oil usually has a nutty smell but after refinement the oil becomes odorless. However, the hydrolysis of glycerides that occurs during frying leads to an increase in free fatty acids (FFA) and a lower smoke point. Early attempts to use peanut oil as a diesel fuel or as an additive were successful but not economically viable [FRANK D. GUNSTONE, (2000), p {231}].

2.2.7 Sesame Oil

Sesame (Sesamum indicum) is one of the oldest oil seed crops known to mankind and is the only cultivated Sesamum species. Sesame seed has been considered to be important because of it is high oil content (42–56%) and protein (20–25%), and also because it is a good source of minerals, particularly calcium, phosphorus, potassium and iron. Moreover, sesame oil is highly resistant to oxidation and displays several medicinal effects for instance, it is written in Chinese ancient books that sesame seeds (called ‘Chih-Ma’ in Chinese) increase energy and prevent ageing. The oil obtained from sesame seeds, called ‘Tila’ in Sanskrit or simply ‘Til’ these days, has been used as domestic Ayurveda medicine in India. Actually, the name sesame comes from the

Arabic word ‘semsin’. Researchers now believe that the actual origin of sesame was from Sudan where many wild species are found and not India [FRANK D. GUNSTONE, (2000), p {297}].

2.2.8 Pressed sesame oil

Pressed Sesame oil is obtained from sesame seeds. The oil is extracted from sesame seeds either by simply crushing them or roasting them over low heat. The first method provides cold-pressed sesame oil. While cold-pressed sesame oil is a pale yellow, hot-processed sesame oils have darker shades and a significantly different flavor. Apart from the light and nutty flavor of cold-pressed sesame oil, it has a higher percentage of fatty acids than sesame oil obtained from hot seeds. In addition, the sesamolin content in cold-pressed sesame oil protects it from oxidation, and thus increases its shelf life.

Cold-pressed sesame oil is a good source of vitamin E, containing 11.8 mg of the vitamin per 100 grams of oil. Vitamin E gives sesame oil its antioxidant properties. It is also high in fatty acids, including omega-6 polyunsaturated fatty acids and omega-9 monounsaturated fatty acids. Other components of cold pressed sesame oil include zinc, copper, magnesium, calcium, iron, as well as vitamin B6. Zinc contributes to bone health. Copper is useful for managing rheumatoid arthritis. Calcium is necessary for the prevention of osteoporosis, migraine headaches and colon cancer. And magnesium contributes to the health of the respiratory system. [https://www.livestrong.com/article/498331-cold-pressed-sesame-oil-benefits 20/6/2022]

[Wolf Hamm, et al, (2013)]

2.2.9 physical Properties of Edible Oils

Table (2.1) Properties of Edible Oils

Properties	Corn oil	Olive oil	Sunflower oil	Peanut oil	Sesame oil
Colour (visual)	Light yellow	Green	slightly amber	Light yellow	green
Smoke point °	230 to 238	190–215	232	229.4	232°
Boiling Point	400-500	299	475-500	410-450	450
Melting point	−11 to −8	−6.0	-17	0–3◦C	-6
Fire point	360	410	341	363	410
Density (kg/m^3)	922	920	918.8	910	928
Relative density	0.9188	0.9090-0.9150	0.9160 – 0.9210	0,9100 – 0,9150	0.9203-0.9237
Refractive index	1,4740 - 1,4760	1.4677-1.4705	1,4740 – 1,4760	1.46–1.465	1,4730-1,4760
Viscosity (Pa.s)	0.047	0.1	0.051	0.0355	0.0351

2.3 Spectroscopy

Spectroscopy occupies a very special position in chemistry, physics and in science in general. It is capable of providing accurate answers to some of the most searching questions, particularly those concerning atomic and molecular structure. For small molecules, it can provide accurate values of bond lengths and bond angles. For larger molecules, details of conformation can be obtained. Spectroscopy is basically an experimental subject and is concerned with the absorption, emission or scattering of electromagnetic radiation by atoms or molecules. electromagnetic radiation covers a wide wavelength range, from radio waves to γ-rays, and the atoms or molecules may be in the gas, liquid or solid phase [J. Michael Hollas (2004) {p 1}].

The first spectroscopic studies dealt with emission spectra or atomic absorption in 1885, JJ Balmer investigated the spectrum of the hydrogen atom. He observed four light lines in the spectrum located at (656, 486, 434, and 410) nm. In fact, it was shown later that the Balmer series extends in the ultraviolet region to the wavelength of 365 nm. Other experiments have shown that additional series of light lines exist in the ultraviolet and infrared regions [Éric Dufour (2009)].

Spectroscopy is mainly used for studying the structure of molecules and atoms. Spectroscopy will use a large wavelength to investigate the structure and electron configurations of atoms and molecules. Spectroscopy also provides a precise analytical method for finding the constituents in material having unknown chemical composition. In a typical spectroscopic analysis, a concentration of a few parts per million of a trace-elements in a material can be detected through its emission spectrum. In astronomy the study of the spectral emission lines of distant galaxies led to the discovery that the universe is expanding rapidly and isotopically (independent of direction). During the 1920s, the American astronomer Edwin Hubble identified the diffuse elliptical and spiral objects that had been observed as galaxies. He went on to discover and measure a roughly linear relationship between the distance of these galaxies from Earth and their Doppler shift. In any direction one looks, the farther the galaxy appears, the faster it is receding from Earth.

2.3.1 Atomic Spectroscopy

The basic structure of an atom., As shown in Figure (2.3), it's a positively charged nucleus surrounded by a cloud of negative

electrons, and each of these electrons moves in its own orbit around the nucleus. When energy is absorbed by the atom, the energy goes to the electrons. They move faster, or in different orbits. The crucial point is that only certain orbits are possible for a given electron, so the atom can absorb only certain amounts of energy. And once the atom has absorbed some energy, it can lose energy only in specified amounts because the electron can return only to allowed lower-energy orbits.

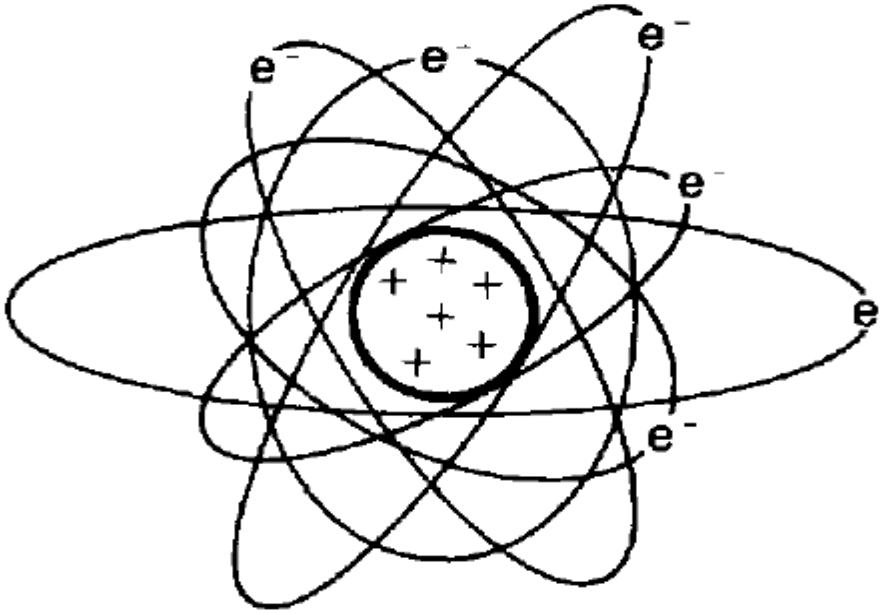

Figure (2.3) structure of atom.

The allowed energies for the atom are represented by different levels in the diagram. An atom in the ground state has energy E_0, while an atom in the first excited state has energy E_I, and so on. The atom loses energy $E = E_1 — E_0$ when it moves from level 1 to level 0. But an atom in level 1 cannot lose any other amount of energy; it must either keep all its energy or lose an amount equal to $E_I - E_0$ all at once [Breck Hitz, et al, (2001) {p 66}].

In analytical chemistry, atomic absorption spectroscopy is a technique for determining the concentration of a particular metal element in a sample. The technique can be used to analyze the concentration of over 70 different metals in a solution. Although atomic absorption spectroscopy dates to the nineteenth century, the modern form was largely developed during the 1950s by a team of Australian chemists. They were led by Alan Walsh and worked at the CSIRO Division of Chemical Physics in Melbourne, Australia. The technique makes use of absorption spectrometry to assess the concentration of an analyte in a sample. It relies therefore heavily on Beer-Lambert law.

$$I = I_0(10)^{-\varepsilon bC} \ldots. (2.1)$$

$I \equiv$ intensity I transmitted

$I_0 \equiv$ incident intensity

$c \equiv$ molar concentration

$\varepsilon \equiv$ absorption coefficient

In short, the electrons of the atoms in the atomizer can be promoted to higher orbital for a short amount of time by absorbing a set quantity of energy (i.e. light of a given wavelength). This amount of energy (or wavelength) is specific to a particular electron transition in a particular element, and in general, each wavelength corresponds to only one element. This gives the technique it is elemental selectivity. As the quantity of energy (the power) put into the flame is known, and the quantity remaining at the other side (at the detector) can be measured, it is possible, from Beer-Lambert law, to calculate how many of these transitions took place, and thus get a signal that is proportional to

the concentration of the element being measured [Muhammad Akhyar Farrukh. 2011]

2.3.2 Molecular Spectroscopy

A molecule is formed by the binding of two or more atoms in such a way that the total energy is lower than the sum of the energies of the constituents. The bonds are normally of *ionic* or *covalent* nature. Particularly weak bonds occur in Vander Waals molecules. The energy-level diagrams of molecules are significantly more complicated than those of atoms since, apart from energy levels corresponding to different electronic arrangements, there are also different states corresponding to vibrational and rotational motion. The structure is schematically shown in Figure (2.4) [Sune Svanberg (2001) {p31}].

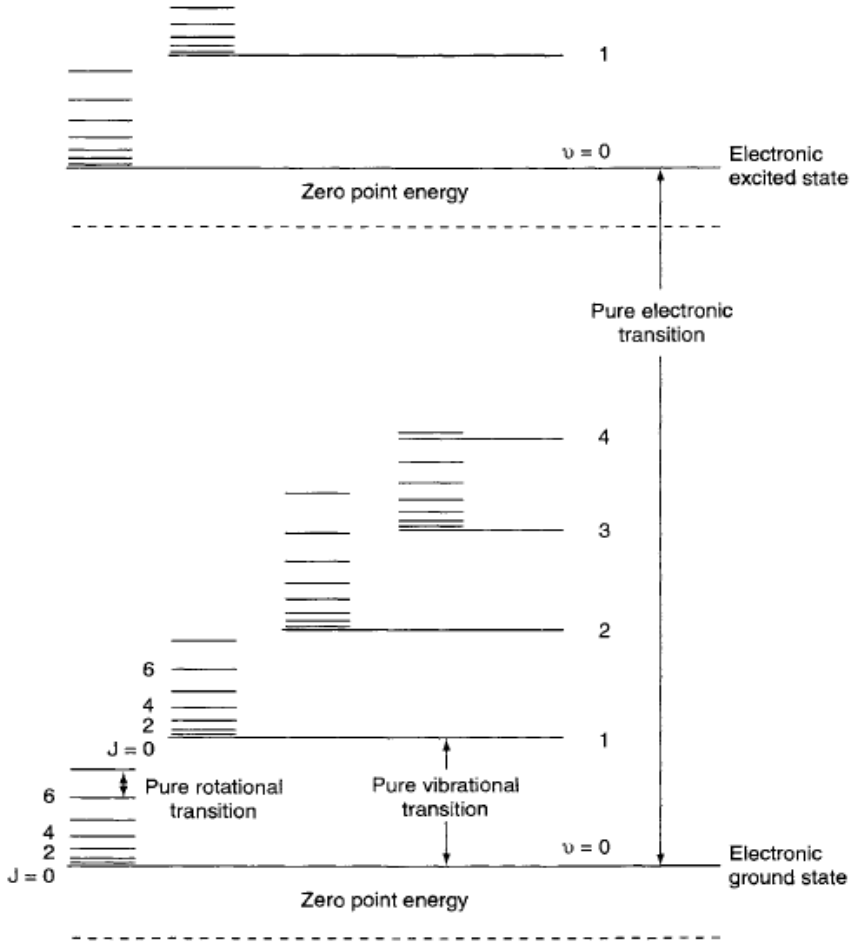

Figure (2.4) schematic molecular energy level diagram with electronic, vibrational and rotational levels

Consider a rotating diatomic molecule, as shown in Figure (2.5) with the atomic masses m_1 and m_2 at distances r_1 and r_2 from the centre of gravity. The moment of inertia with respect to the rotational axis is *I.* We have

$$r = r_1 + r_2 \ ,$$

$$m_1 r_1 = m_2 r_2$$

And

$$I = m_1 r_1^2 + m_2 r_2^2 \ldots\ldots (2.2)$$

We then obtain

$$I = \frac{m_1 m_2}{m_1 + m_2} (r_1 + r_2)^2 = \mu r^2 \ \ldots\ldots\ (2.3)$$

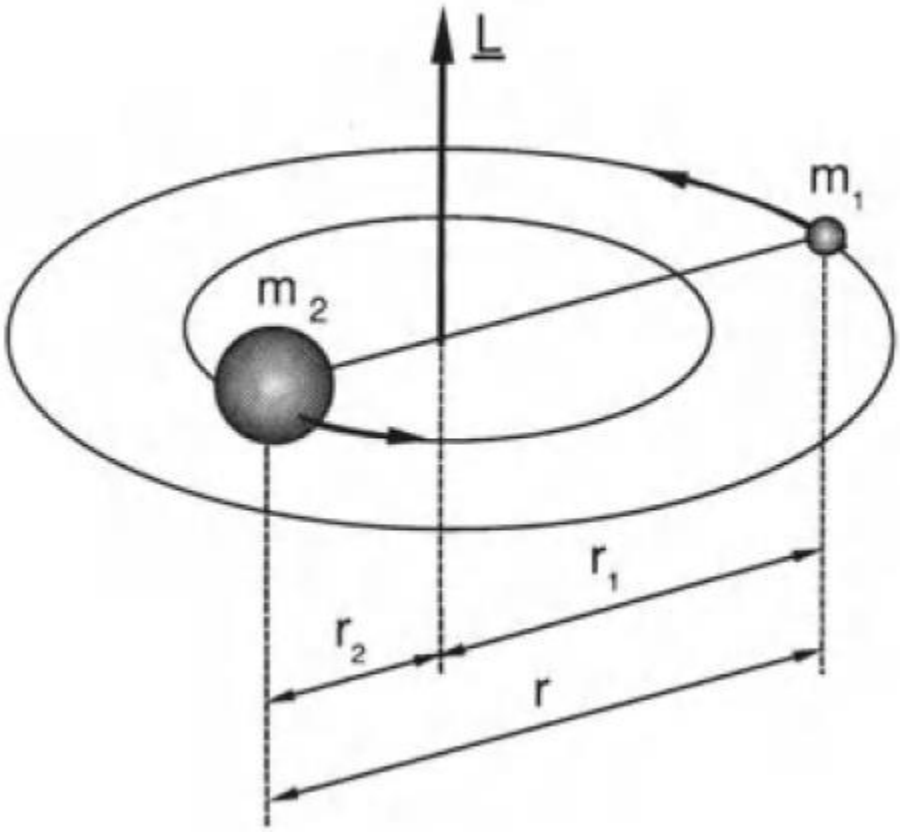

Figure (2.5) Rotation of a diatomic molecule

Where μ is the reduced mass. Classically, the angular momentum L and the energy E are given by

$$\left.\begin{aligned} L &= I\omega/\hbar \\ E &= I\omega^2/2 \end{aligned}\right\} \Rightarrow E = \frac{L^2\hbar^2}{2I} \quad \ldots. (2.4)$$

Where ω is the angular frequency vector, Quantum mechanically, L is given by

$$|L| = \sqrt{J(J+1)} \quad \text{,J= 0,1,2,3 …} \quad (2.5)$$

and thus, the quantized energy of the rotator is given by

$$E_J = \frac{J(J+1)\hbar^2}{2I} = BJ(J+1) \ldots\ldots \quad (2.6)$$

This energy expression leads to energy levels such as those in Figure (2.6)

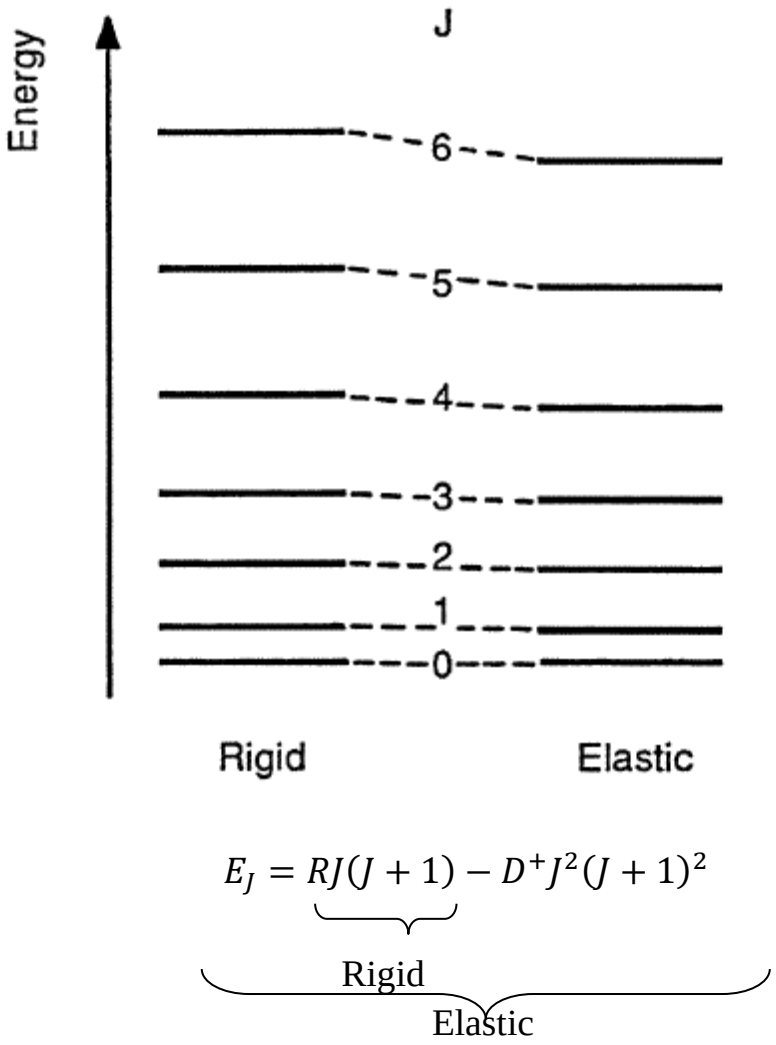

$$E_J = \underbrace{RJ(J+1)}_{\text{Rigid}} - D^+J^2(J+1)^2$$

Elastic

Figure (2.6) Rotational levels for a rigid rotator (left) and an elastic rotator (right)

Where

R is the rotational constant

D is the centrifugal distortion constant and is always positive for diatomic molecules.

If the rotator is not completely rigid it is slightly extended in higher rotational states. Then I increase and E_J will decrease. This results in a successive downward movement of the upper energy levels [Sune Svanberg (2001) {p 35}].

IR and Raman spectra results from transitions between quantized vibrational energy states. Molecular vibrations can range from the simple motion of the two atoms of a diatomic molecule to the more complex motion of every atom in a large polyatomic molecule. A mode of vibration in a molecule is a periodic contortion in which the Centre of mass of the molecule or it is orientation does not change as a result of the vibration and all of the atoms pass through their linear equilibrium position coincidentally. The position of a molecule in three-dimensional space can be described by using an x, y and z co-ordinate for each atom.

This means that a molecule comprised of n atoms has $3n$ Cartesian co-ordinates required to describe it is shape, position and orientation. The motion can be described by a change Δx, Δy and Δz in these Cartesian axes. There are $3n$ fundamental distinct molecular motions which are called degrees of freedom. Molecular motions consist of translations, rotations and vibrations. Three of the degrees of freedom are translations of the whole molecule along the x, y or z axis. A non-linear molecule also has three pure rotations about these axes while a linear molecule has only two. The translational and rotational degrees of freedom, which do not change the relative positions of the atoms in the molecule, are often called non-genuine modes. Thus, a non-linear molecule possesses $3n$-6 fundamental modes of vibration, whilst a linear molecule has $3n$-5. Of these, the number of

stretching modes is equal to the number of bonds in the molecule (*n*-1 for an acyclic molecule) and the remainder of the vibrations are bending modes. During these normal modes of vibrations all the atoms move in phase and with the same frequency. Various atoms in a molecule may be regarded as balls of different masses and the covalent bonds between them as weightless tiny springs holding such balls together. There are two types of fundamental molecular vibrations (Figure (2.7)

Stretching vibrations: in stretching vibrations, the distance between two atoms increase or decrease, but the atoms remain in the same bond axis.

Stretching vibrations are of two types:

- Symmetrical stretching: in this mode of vibration, the movement of atoms with respect to the common (or central) atom is in the same direction along the same bond axis.
- Asymmetrical stretching: in this vibrational mode, one atom approaches the common atom while the other departs away from it.

Bending Vibrations (Deformations):

In such vibrations, the positions of the atoms change with respect to their original bond axes. Bending vibrations are of four types:

- ***Scissoring***: In this mode of vibration, the movement of atoms is in the opposite direction with change in their bond axes as well as in the bond angle they form with the central atom.
- ***Rocking***: in this vibration, the movement of atoms takes place in the same direction with change in their bond axes. Scissoring and rocking are in-plane bending.
- ***Wagging***: in this vibration, two atoms simultaneously move above and below the plane with respect to the common atom.

- ***Twisting***: in this vibration, one of the atom moves up and the other moves down the plane with respect to the common atom [Hendra, P., Jones, C., Warnes, G., (1991) and Esam M A, Ali (2016)].

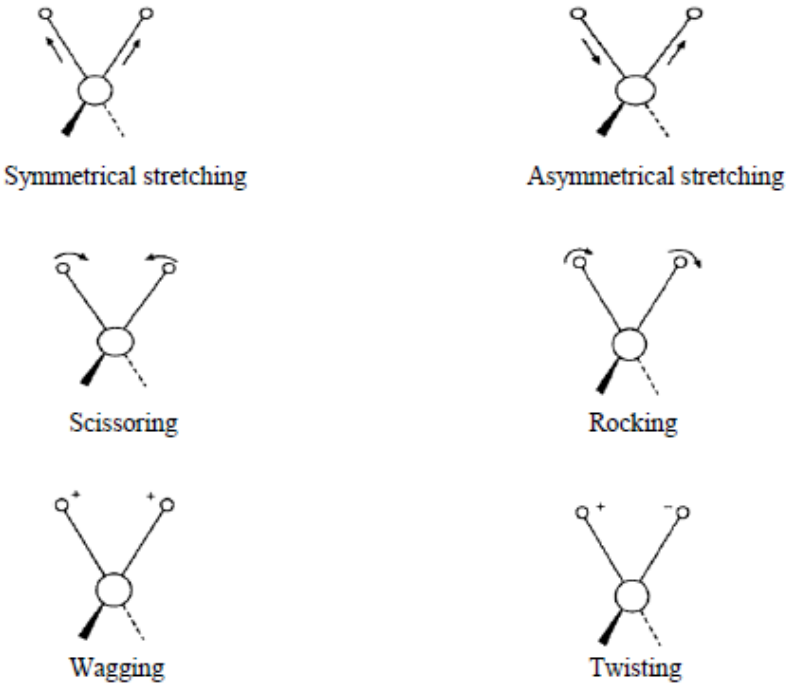

Figure (2.7) Stretching and Bending vibrations (+ and – signs indicate movement perpendicular to the plane of the paper).

2.3.3 NMR Spectroscopy

NMR spectroscopy is based on the absorption of energy in the radiofrequency region of electromagnetic spectrum by the nuclei of atoms. NMR spectra arise from a property that some nuclei have, usually called spin. Spinning of charged nuclei generates a magnetic field. When a sample is subjected to an external magnetic field, the nuclei align themselves with or against the applied magnetic field. Protons that align with the applied field

are in the lower-energy α-spin state and protons that align against the field are in the higher-energy β-spin state. When the sample is subjected to radiofrequency radiation (Rf radiation) whose energy corresponds to the difference in energy between the α- and β-spin states, the α- and β-spin states are made to interconvert i.e. flipping the spin. This flipping of the proton from one magnetic alignment to the other by the radio waves is known as the resonance condition. When the nuclei relax to their original states, they emit electromagnetic signals with frequencies that depend on the difference in energy between the α- and β-spin states. Since NMR experiment started with excess of nuclei in the α-spin states, there is a net absorption of energy which is displayed as a plot of frequency versus amount of absorbed energy. Nuclei in different parts of the molecule experience different local magnetic fields according to the molecular structure, and so they absorb the Rf radiation at different frequencies [Macomber, R.S., (1998)].

This difference is called the chemical shift. NMR has been applied to distinguish between drugs that have effects similar to narcotics and stimulants **[**Doi, K., et al., 2006**]** NMR in conjunction with MS and IR has been used for the identification and detection of contaminants in synthesized amphetamines **[**Blachut, D., Wojtasiewicz, K., Czarnocki, Z., (2002**)]** and for the characterization of derivatives of MDMA. It also has been applied for the detection of aminorex material in confiscated drug samples **[**Baudot, P., et al., **(**1999)]**.** Incident light wavelength λ; Knowledge of the absorption cell geometry and sample concentration (ε). Beer's law is applicable only when the incident light intensity I_o is low enough that the molecular state population are essentially unperturbed by it; the redistribution of molecules

into excited states by the light beam would otherwise materially change ε for different photons within the beam. In a ddition Beer's law is strictly valid only in very thin optical samples [WALTER S. STRUVE, (1989)].

2.3.4 uv-visible spectroscopy

UV-VIS spectroscopy is one of the oldest methods in molecular spectroscopy. The definitive formulation of the Bouguer-Lambert law in 1852 created the basis for the quantitative evaluation of absorption measurements at an early date. This led firstly to colorimetry, then to photometry and finally to spectrophotometry. This evolution ran parallel with the development of detectors for measuring light intensities, i.e. from the human eye via the photoelement and photocell, to the photomultiplier and from the photographic plate to the present silicon-diode detector both of which allow simultaneous measurement of the complete spectrum [H. Charlotte Grinter and Dr. T. L. Threlfall, 1992].

Ultraviolet (UV) and visible radiation comprise only a small part of the electromagnetic spectrum, which includes such other forms of radiation as radio, infrared (IR), cosmic, and X rays see Figure (2.8). Nevertheless, this range is of extreme importance, since the energy differences correspond to those of the electronic states of atoms and molecules; hence the concept of "electronic spectroscopy". Furthermore, in the visible spectral region the interactions between matter and electromagnetic radiation manifest themselves as color.

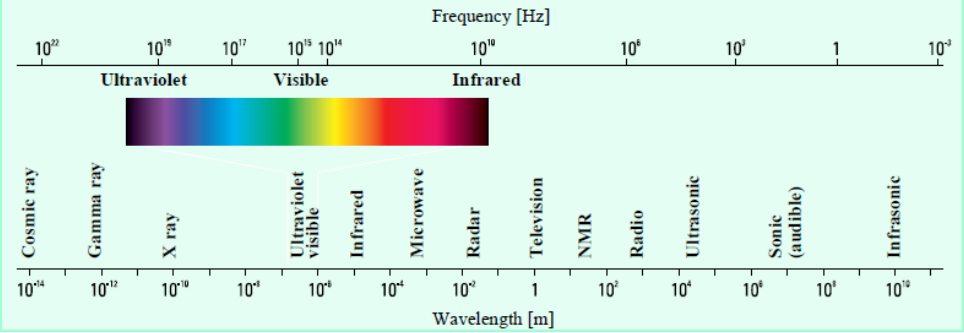

Figure (2.8) electromagnetic spectrum

In UV-visible spectroscopy, wavelength λ usually is expressed in nanometers (1 nm = 10^{-9} m). It follows from the above equations that radiation with shorter wavelength has higher energy. In UV-visible spectroscopy. In some cases, this energy is sufficient to cause unwanted photochemical reactions when measuring sample spectra [Hewlett-Packard, (1996). {p 10}]

Absorbed or emitted radiation of frequency v or wavenumber $\breve{\nu}$ can thus be assigned to specific energy differences or, applying the definition of the 'term value' (energy level), to specific energy-level differences:

$$\breve{\nu} = \frac{\Delta E}{ch} = \frac{E_2}{hc} - \frac{E_1}{hc} = T_2 - T_1 \ldots\ldots (2.7)$$

The Bouguer-Lambert law forms the mathematical-physical basis of light-absorption measurements on gases and solutions in the UV-VIS and IR region figure (2.9)

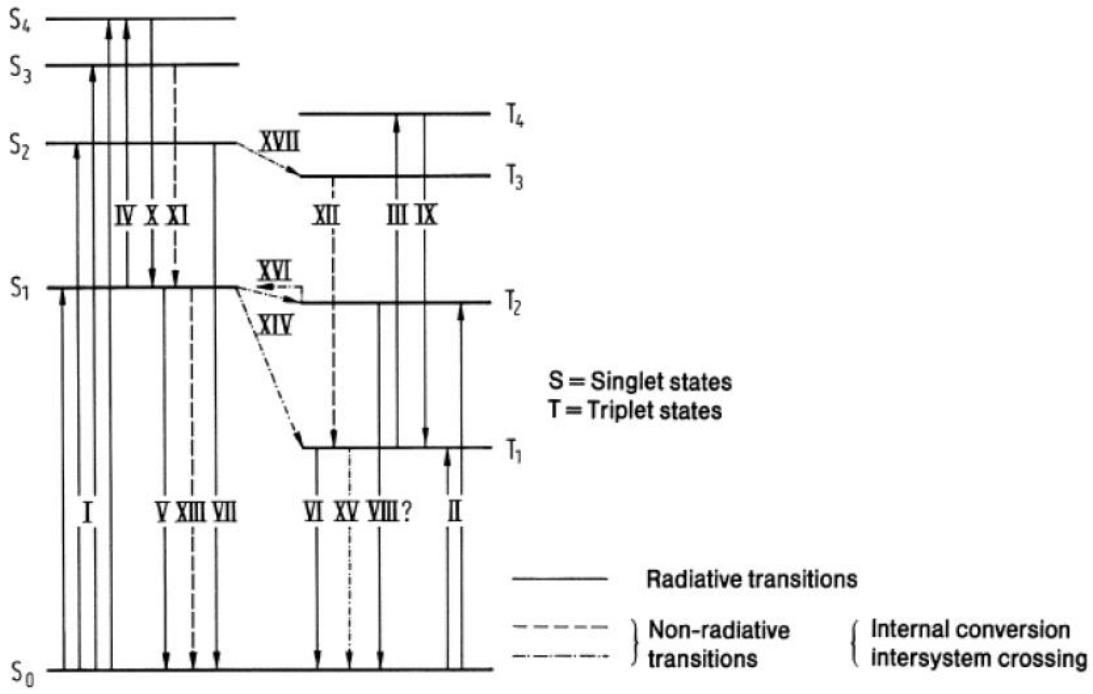

Figure (2.9). General energy-level diagram for electronic excitation

$$\log\left(\frac{I_0}{I}\right)_{\tilde{\nu}} = \log\left(\frac{100}{T\%}\right)_{\tilde{\nu}} = A_{\tilde{\nu}} = \varepsilon_{\tilde{\nu}} \cdot c \cdot d \ \ldots\ldots (2.8)$$

Where

$A_{\tilde{\nu}} = \log\left(\frac{I_0}{I}\right)_{\tilde{\nu}}$ is the absorbance

$T_{\tilde{\nu}} = \frac{I}{I_0} \cdot 100$ in % ≡ the transmittance

$\varepsilon_{\tilde{\nu}}$ ≡ the molar decadic extinction coefficient.

I_0 ≡ the intensity of the monochromatic light entering the sample

I ≡ the intensity of this light emerging from the sample;

c ≡ the concentration of the light-absorbing substance

d ≡ the path length of the sample in cm.

The molar decadic extinction coefficient, $\varepsilon_{\tilde{\nu}}$, is a quantity characteristic of the substance which also depends on wavenumber $\tilde{\nu}$ (cm^{-1}) or on wavelength λ (nm).

The functional correlation between $\varepsilon_{\tilde{\nu}}$ and wavenumber $\tilde{\nu}$ is called the "absorption spectrum" of a compound. Since the extinction coefficient can vary by several orders of magnitude within the absorption spectrum of a single inorganic or organic compound, the logarithmic value $\log\varepsilon = f(\check{\nu})$ can be used instead of $\varepsilon = f(\check{\nu})$ to plot an absorption spectrum.

According to Equation. (2.8), the application of the Bouguer-Lambert-Beer law presupposes a measurement of the relationship between the light intensities I and I_0, However, when measuring in quartz cuvettes (UV-VIS region) or cuvettes made of special optical glass (VIS region), part of the light is lost through reflection at the cuvette surfaces. In order to eliminate this source of error, a reference measurement is made in a cuvette with the same pathlength but not containing the substance to be measured. Since most UV-VIS spectroscopy is carried out with solutions, the standard cuvette contains the pure solvent, which ideally should not absorb in the spectral region under consideration [Hewlett-Packard, (1996)].

2.3.5 Infrared Spectroscopy

Infrared spectroscopy is the most commonly used spectroscopic method. There are a number of reasons for its great success and dissemination. The method is rapid, sensitive, easy to handle and provides many different sampling techniques for gases, liquids and solids. Important aspects are the convenient qualitative and quantitative evaluation of the spectra. The standard format of an IR spectrum is transmittance [$\%T$] versus wavenumber [cm^{-1}]. The features of an IR spectrum (number of infrared absorption bands, their intensities and their shapes) are directly related to the

molecular structure of a compound. The IR spectrum is a unique physical property of an individual compound; it is its molecular fingerprint. The IR region comprises fundamental vibrations of bound atoms. Whenever such bound atoms vibrate, they absorb infrared energy, i. e. they exhibit IR absorption bands. The condition for a normal vibration j to be IR active is a change in molecular dipole moment μ during vibration:

$$\mu_j = \mu_0 + \left(\frac{\delta\mu}{\delta q_j}\right) q_j + \frac{1}{2}\left(\frac{\delta^2\mu}{\delta q_j^2}\right) q_j^2 \quad \text{.... (2.9)}$$

q stands for the normal coordinate describing the motion of atoms during a normal vibration. With respect to the direction of the vibrational movement we may distinguish between stretching vibrations (changes of bond lengths) and deformation vibrations (changes of bond angles). Deformation vibrations may be subdivided into bending modes, twisting or torsion modes, wagging modes and rocking modes. Further subdivision refers to the symmetry of the vibration (e. g., symmetric or antisymmetric, in-plane or out-of-plane). Complications in evaluation of IR spectra are the overlapping of individual bands and the appearance of additional bands, e. g. overtone and combination bands, which may be caused by anharmonicity of some vibrations. In the NIR region, all bands are overtone or combination bands. They are always weaker in intensity than the corresponding fundamental bands. Originally considered as a drawback, the weak intensity of the NIR bands turned out to be the background for the large success of NIR spectroscopy in process analysis [Günter Gauglitz and Tuan Vo-Dinh (2003) {p 41}].

2.3.5.1 Optical systems in infrared instruments

A typical NIR instrument consists of a radiation source, a wavelength selection device such as a monochromator, a sample holder, a photoelectric detector that measures the intensity of detected light and converts it to electrical signals, and a computer system that acquires and processes spectral data. Traditional dispersive grating MIR spectrometers had similar optical systems. An optical diagram of a traditional dispersive grating MIR apparatus is shown in Figure 2.10

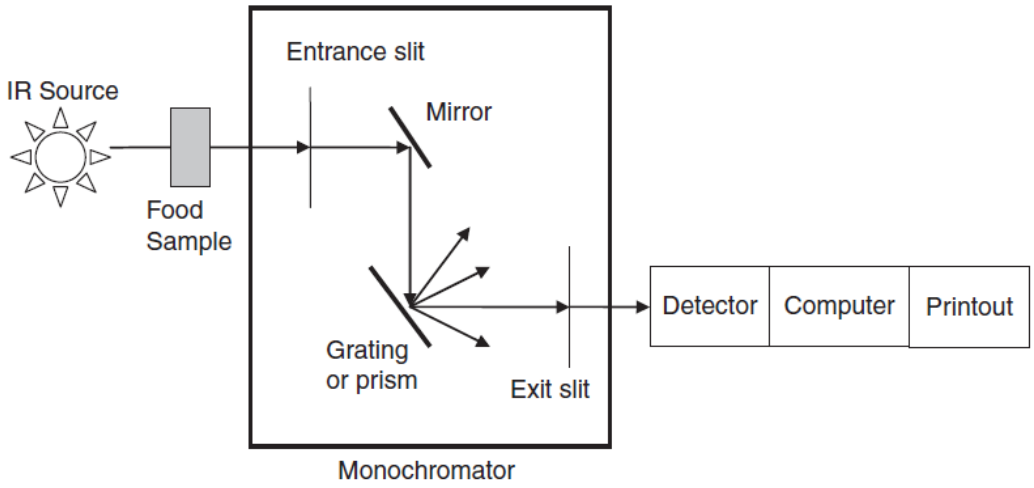

Figure 2.10 Dispersion of a single infrared beam by a diffracting grating. The angle of diffraction of lights depends on both the wavelength and the order of diffraction.

2.3.5.2 Single-beam and double-beam optics

IR optics consists of a specific arrangement of IR instrumental components such as single-beam or double-beam optics. A single-beam arrangement is used for all spectroscopic emission systems, while double-beam optics are common for spectroscopic absorption systems. Figure (2.11) shows a diagram of a single-beam transmittance apparatus that is

well suited for the reliable quantitative analysis of food samples. The PerkinElmer IR instrument model 12 was such a single-beam instrument. Single-beam IR instruments were quite popular until 1949 when double-beam instruments became available. A major problem associated with early single-beam systems was the fluctuation of the intensity of the source radiation, which led to an analytical error called “drift.” In addition, it required tedious manual replotting to obtain a standardized spectrum.

These problems were solved by the use of double-beam systems (Figure 2.12). In double-beam optics, the light intensity of the IR beam is measured before and after passing through a food sample by splitting the source radiation with the aid of a beam splitter (a half mirror). The light is usually split into two beams of equal energy, with one passing through the reference side called “the reference beam,” and the other passing through the sample called “the sample beam.” After passing through the sample, the sample beam merges with the reference beam and together they pass through a monochromator then to a detector. The ratio of the reference beam to the sample beam can be measured, and this ratio is not influenced by the fluctuation of radiation source intensity and other factors such as the drift. By constantly comparing the relative intensity of the sample and reference beams, the double-beam systems offer more stable and rapid measurements than single-beam systems.

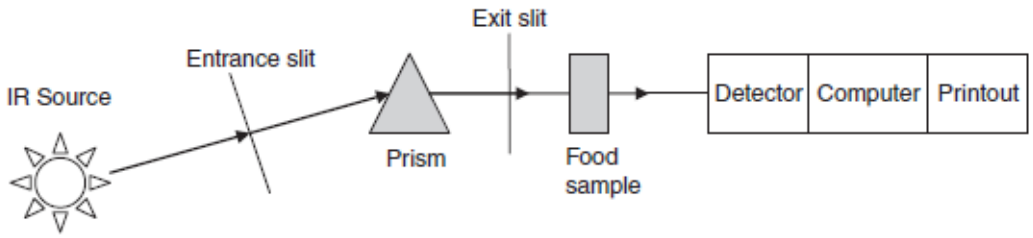

Figure 2.11 A single-beam transmittance apparatus.

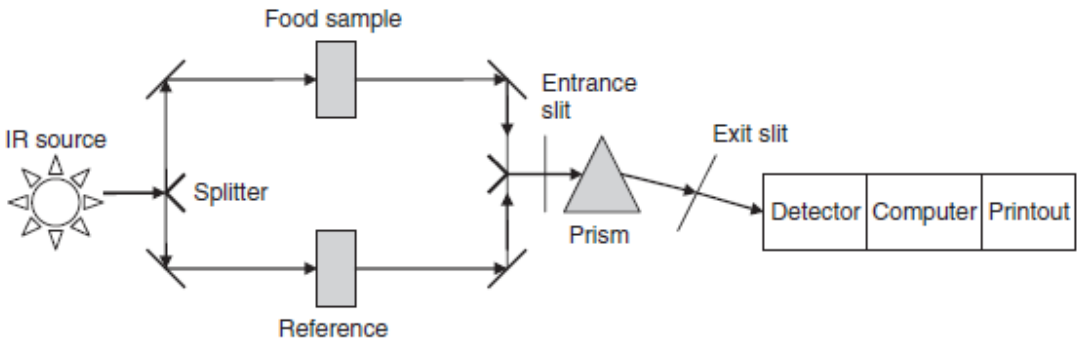

Figure 2.12 A double-beam transmittance apparatus.

2.3.6 Laser in Spectroscopy

The wide applicability of lasers in spectroscopy is due to several factors. As we have seen, very high intensities can be obtained with the advent of tunable lasers, completely new types of experiments have become possible and investigations that were only barely possible with conventional light sources can now be readily performed. small frequency interval. The favourable spatial properties of laser beams with the possibility of very good focusing is also of great importance. It is fair to state that tunable lasers have revolutionized optical spectroscopy [Sune Svanberg (2001) {p 287}]. Laser radiation has four very remarkable properties:

Directionality: The laser beam emerging from the output mirror of the cavity is highly parallel, which is a consequence of the strict requirements for the alignment of the cavity mirrors. Divergence of the beam is typically a few milliradians.

Monochromaticity: refers to a pure spectral color of a single wavelength. A beam is more and more monochromatic if the line spread in frequency is narrow or small. This line width is an outcome of the homogeneous broadening factors and

inhomogeneous broadening factors. Despite these broadening mechanisms the line width in a laser is generally very small as compared to the normal lights. A laser cavity forms a resonant system. The photons are emitted by the stimulated emission where in all the photons are in same phase and in the same state of polarization. Oscillations can sustain only at the resonance frequency of the cavity. This leads to the narrowing of the laser line width.

Brightness: This is defined as the power emitted per unit area of the output mirror per unit solid angle and is extremely high compared with that

of a conventional source.

Coherence: Conventional sources of radiation are incoherent, which means that the electromagnetic waves associated with any two photons of the same wavelength are, in general, out of phase. The coherence of laser radiation is both temporal and spatial, the coherence lasting for a relatively long time and extending over a relatively large distance. Coherence of laser radiation is responsible for its use as a source of intense local heating, as in metal cutting and welding, and for holography [J. Michael Hollas (2004). {p 339}].

They are many methods in spectroscopy used laser like Laser-Induced Breakdown Spectroscopy (LIBS), Laser-Induced Fluorescence (LIF) Raman Spectroscopy and Fourier-transform Raman spectrometer**.**

2.3.7 Laser-Induced Breakdown Spectroscopy (LIBS)

Laser-induced breakdown spectroscopy (LIBS), also sometimes called laser-induced plasma spectroscopy (LIPS) or laser spark

spectroscopy (LSS) has developed rapidly as an analytical technique over the past two decades [David A. Cremers and Leon J. Radziemski (2006) {p 3}].

LIBS is a sensitive technique for analyzing the chemical or atomic compositions of solid or liquid materials. Here a laser pulse is focused onto the surface of a solid or liquid material. Due to the high peak intensity, fast evaporation of a small volume in the focus of the laser pulse occurs. The gaseous plume ejected from the surface contains molecules, atoms and ions contained in the focal volume.

The fluorescence emitted by the excited species is collected by a lens, focused into an optical fiber and sent to the entrance slit of a spectrograph (Figure.2.13). If the detector at the exit of the spectrograph is time-gated, the spectra can be recorded at specific times after the generation of the plume. Since the plume cools during its expansion, the ions recombine to excited states of neutral atoms or molecules and the emission from these states is a measure of the concentration of the atoms in the sample.

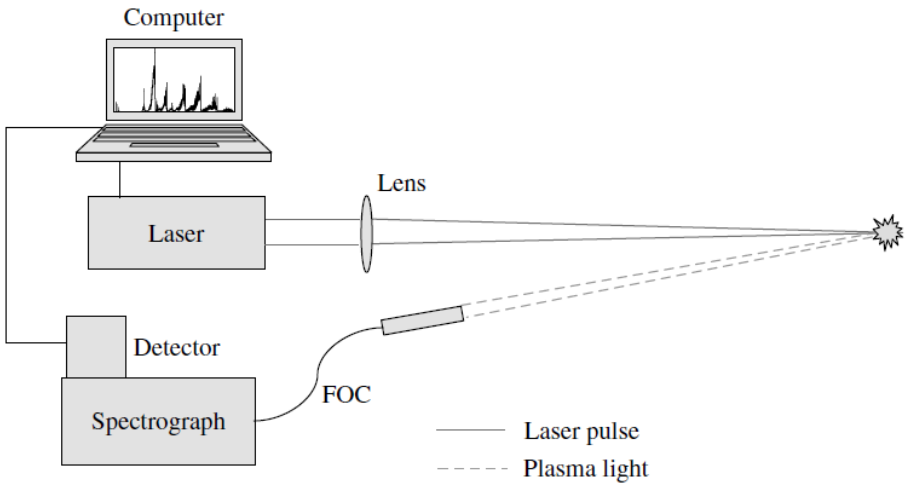

Figure (2.13) Laser-induced breakdown spectroscopy

With moderate laser power, molecules can evaporate without fragmentation. This is particularly useful for investigations of biological samples or for inspecting tissues in vitro. When a second weak probe laser is used, it can cross the plume at different locations, where it generates spatially resolved laser-induced fluorescence, which can be detected and analyzed. Using REMPI techniques, ionization of the neutral species can be achieved with subsequent mass-selective detection in a mass spectrometer [Wolfgan Demtröder (2008) {p 573}]

2.3.8 Laser-Induced Fluorescence

Laser-induced fluorescence (LIF) is the optical emission from molecules that have been excited to higher energy levels by absorption of laser radiation as shown in figure (2.14 a) [J.R. Lakowicz (1991)].

The fluorescence spectrum emitted from a selectively populated rovibronic level ($v'k,J'k$) ($vk\ ,Jk$: a rovibronic level in an excited electronic state of a diatomic molecule) consists of all allowed transitions to lower levels ($v''m\ ,J''m$) (Figure 2.15 b). The wavenumber differences of the fluorescence lines immediately yield the term differences of these terminating levels ($v''m\ ,J''m$).

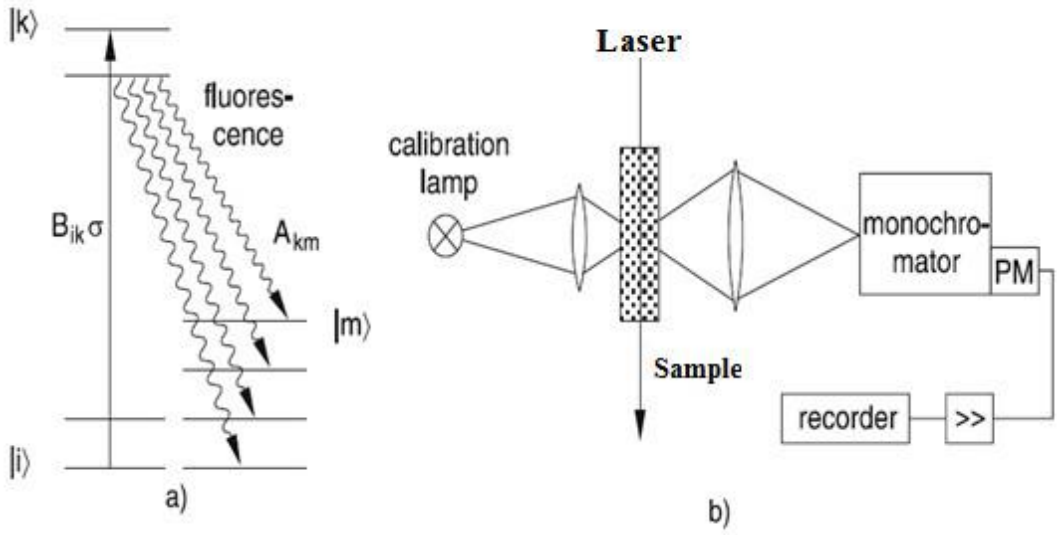

Figure (2.14): Laser-induced fluorescence: (a) level scheme and (b) experimental arrangement for measuring LIF spectra.

Laser-induced fluorescence (LIF) has a large range of advantages [J.L. Kinsey (1977)].

First, LIF serves as a sensitive monitor for the absorption of laser photons in fluorescence excitation spectroscopy.

Second, it is well suited to gain information on molecular states if the fluorescence spectrum excited by a laser on a selected absorption transition is dispersed by a monochromatic.

A third aspect of LIF is the spectroscopic study of collision processes. If the excited molecule is transferred by inelastic collisions from the level ($v'k$,$J'k$) into other rovibronic levels, the fluorescence spectrum shows new lines emitted from these collisionally populated levels which give quantitative information on the collision cross sections. Another aspect of LIF concerns it is application to the determination of the internal-state distribution in molecular reaction products of chemical reactions. Under certain conditions the intensity of LIF excited on the transition

$|i\rangle \rightarrow |k\rangle$ is a direct measure of the population density *Ni* in the absorbing level $|i\rangle$.

2.3.9 Raman Spectroscopy

Raman effect can be described as the inelastic scattering of light by matter. When a photon of visible light, too low in energy to excite an electronic transition, interacts with a molecule it can be scattered in one of three ways. It can be elastically scattered and thus retain it is incident energy or it can be inelastically scattered by either giving energy up to, or by removing energy from, the molecule [D. J. Gardiner P. R. Graves (1989) {p4}].

The scattered light consists of two types: one, called Rayleigh scattering, is strong and has the same frequency as the incident beam ν_0, and the other, called Raman scattering, is very weak (~ 10^{-5} of the incident beam) and has frequencies $(\nu_0 \pm \nu_m)$ where ν_m is a vibrational frequency of a molecule. The $(\nu_0 - \nu_m)$ and $(\nu_0 + \nu_m)$lines are called the Stokes and anti-Stokes lines, respectively. Thus, in Raman spectroscopy, we measure the vibrational frequency ν_m as a shift from the incident beam frequency ν_0 [John R. Ferraro, et al (2003) {p14}].

2.3.9.1 C1assical Theory

The classical approach to a description of the Raman effect regards the scattering molecule as a collection of atoms undergoing simple harmonic vibrations and takes no account of quantisation of the vibration al energy. When a molecule is placed in The electric field strength (E). of the electromagnetic wave (laser beam) fluctuates with time (t) as shown by Equation (2.10)

$$E = E_0 \cos 2\pi\nu_0 t \ldots\ldots\ldots \quad (2.10)$$

Where E_0 is the vibration amplitude and ν_0 is the frequency of the laser. If a diatomic molecule is irradiated by this fight, an electric dipole moment *P* is induced:

$$P = \alpha E = \alpha E_0 \cos 2\pi\nu_0 t \text{ ….. (2.11)}$$

Here, α is a proportionality constant and is called polarizability. If the molecule is vibrating with a frequency ν_m, the nuclear displacement *q* is written

$$q = q_0 \cos 2\pi\nu_m\, t \text{ ……. (2.12)}$$

where q_0 is the vibrational amplitude. For a small amplitude of vibration, α is a linear function of q . Thus, we can write

$$\alpha = \alpha_0 + \left(\frac{\partial\alpha}{\partial q}\right)_0 q_0 + \cdots \text{ ……. (2.13)}$$

Here, αis the polarizability at the equilibrium position, and $\left(\frac{\partial\alpha}{\partial \mathrm{q}}\right)_0$ is the rate of change of a with respect to the change in *q*, evaluated at the equilibrium position. Combining (2-11) with (2-12) and (2-13), we obtain

$$P = \alpha E_0 \cos 2\pi\nu_0 t$$

$$P = \alpha_0 E_0 \cos 2\pi\nu_0 t + \left(\frac{\partial\alpha}{\partial q}\right)_0 q E_0 \cos 2\pi\nu_0 t$$

$$P = \alpha_0 E_0 \cos 2\pi\nu_0 t + \left(\frac{\partial\alpha}{\partial q}\right)_0 q_0\, E_0 \cos 2\pi\nu_0 t \cos 2\pi\nu_m\, t$$

$$P = \alpha_0 E_0 \cos 2\pi\nu_0 t + \tfrac{1}{2}\left(\tfrac{\partial\alpha}{\partial q}\right)_0 q_0 E_0[\cos\{2\pi(\nu_0+\nu_m)t\} + \cos\{2\pi(\nu_0-\nu_m)t\}] \text{.. (2.14)}$$

According to classical theory, the first term represents an oscillating dipole

that radiates light of frequency ν_0 (Rayleigh scattering), while the second term corresponds to the Raman scattering of frequency $(\nu_0 + \nu_m)$ (anti-Stokes) and $(\nu_0 - \nu_m)$ (Stokes). If $\left(\frac{\partial \alpha}{\partial q}\right)_0$ is zero, the vibration is not Raman-active. Namely, to be Raman-active, the rate of change of polarizability (α) with the vibration must not be zero.

Figure (2.15) illustrates Raman scattering in terms of a simple diatomic energy level. In IR spectroscopy, we observe that $\nu = 0 \rightarrow 1$ transition at the electronic ground state. In normal Raman spectroscopy, the exciting line (ν_0) is chosen so that its energy is far below the first electronic excited state. The dotted line indicates a "virtual state" to distinguish it from the real excited state. the population of molecules at $\nu = 0$ is much larger than that at $\nu = 1$ (Maxwell-Boltzmann distribution law). Thus, the Stokes *(S)* lines are stronger than the anti-Stokes *(A)* lines under normal conditions. Since both give the same information, it is customary to measure only the Stokes side of the spectrum [John R. Ferraro, et al, (2003) {16}].

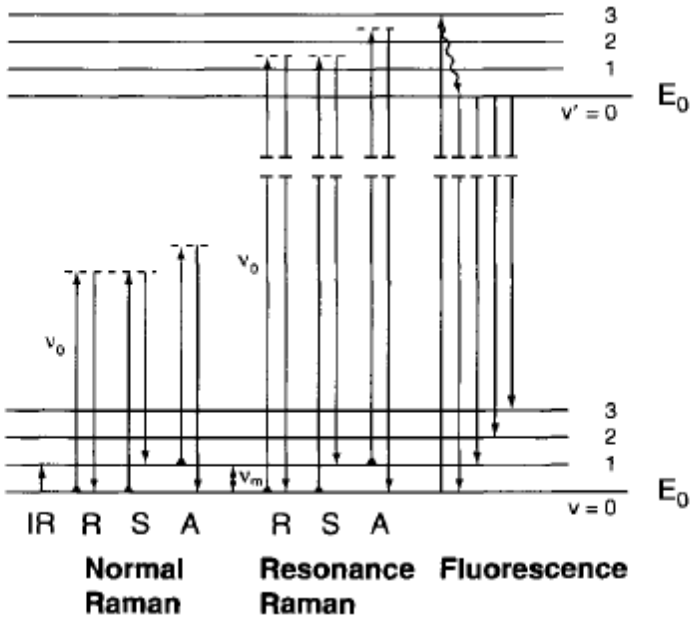

Figure 2.15 Comparison of energy levels for the normal Raman, resonance Raman, and fluorescence spectra.

2.3.9.2 Selection Rules for Raman Spectra

To determine if the vibration is active in the Raman spectra, the selection rules must be applied to each normal vibration. Since the origins of Raman spectra are markedly different than IR spectroscopy, their selection rules are also distinctively different. According to quantum mechanics a vibration is Raman active, if the polarizability is changed during the vibration. To discuss Raman activity, let us consider the nature of the polarizability.

When a molecule is placed in an electric field (laser beam), it suffers distortion since the positively charged nuclei are attracted toward the negative pole, and electrons toward the positive pole (Figure. (2.16)). This charge separation produces an induced dipole moment (P) given by:

$$P = \alpha E \ldots\ldots (2.15)$$

$\alpha \equiv$ Polarizability

$E \equiv$electric field

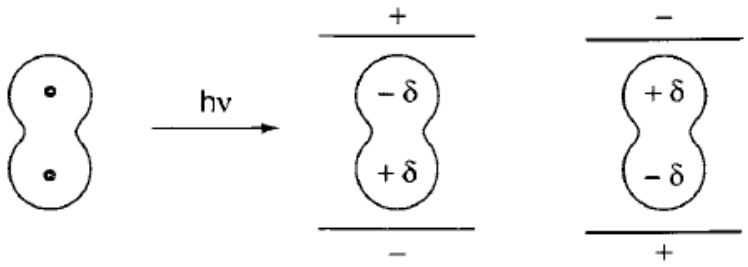

Figure (2.16): Polarization of a diatomic molecule in an electric field.

In actual molecules, such a simple relationship does not hold since both P and E are vectors consisting of three components in the x, y and z direction. Thus, (Equation. (2.15) must be written as to obtain resonance. Raman scattering, a laser beam is chosen which has an excitation frequency close to that of an electronic transition. Ideally, a tunable laser would be used for excitation and the frequency would be chosen to correspond exactly to the energy difference between the ground vibrational state and the first or second vibronic state of the excited state.

This condition is shown in (Figure (2.17)), the maximum resonance Raman scattering is not required for observing the effect or to obtain some enhancement. It is often more practicable to use an existing laser line available in the laboratory which has a frequency as near as possible to the true resonance frequency. (Figure (2.17)), could also be used to explain the nature of the absorption process in electronic absorption spectroscopy. It shows a transition from the ground state to an excited state. The key

difference, which cannot be seen in the diagram, is the length of time the molecule remains in an excited state.

In contrast, in absorption, the upward transition is also fast but the electron is absorbed into the molecule and the nuclei relax to the equilibrium geometry of the excited state. Thus, the processes of resonance Raman scattering and absorption are separated clearly by time, a variable not shown in the diagram.

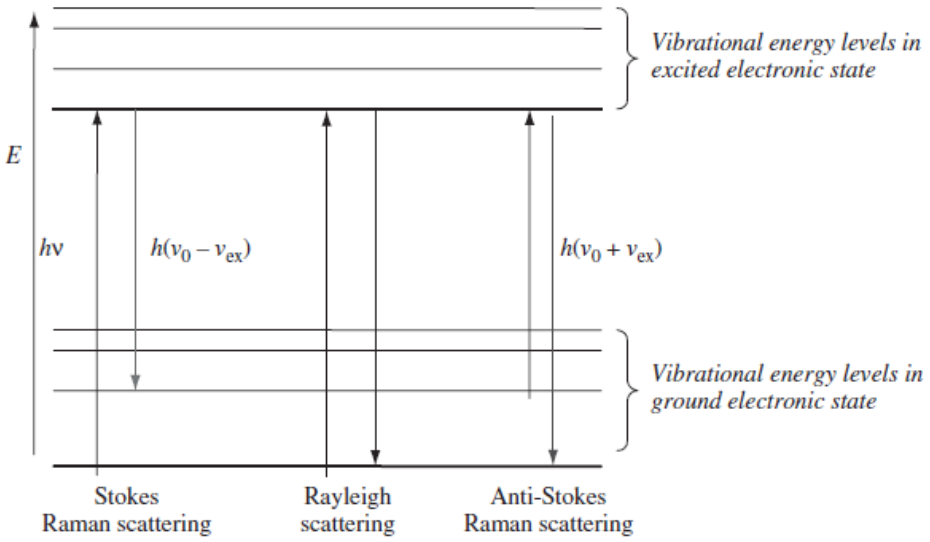

Figure (2.17) Diagram of the basic process of resonance Raman scattering.

Further, in the practice of absorption spectroscopy, the light irradiating the sample is usually polychromatic covering a wide range of frequencies, and under these circumstances a number of transitions are involved. Often, the most intense transition is to one of the higher vibronic levels [Ewen Smith, Geoffrey Den (2005). {p 93} D. L. Rousseau, et al, (1979) {p203}].

Raman spectroscopy has a number of advantages, but also some disadvantages compared to other methods. Advantages include the following:

The wavelength of the light source can, in principle, be chosen arbitrarily. Due to the non-resonant nature of the Raman scattering process, the incident light does not have to match a molecular transition in the species of interest. Consequently, all Raman-active species can be detected with a single laser source at the same time. Most molecules, in particular those in typical fuels, are Raman-active and hence can be detected simultaneously. This includes the homo-nuclear diatomic, which cannot be measured using IR spectroscopy. Good sensitivity can be obtained. Depending on the scattering cross-section it can be in the order of ~0.1%. Multi-pass arrangements, the use of cavities, resonant or near-resonant excitation, and the utilization of plasmonic enhancement (surface enhanced Raman scattering, SERS) allow a further significant improvement of the sensitivity for selected species. An LOD in the order of ppm and sub-ppm can be achieved. Fiber-coupled probes allow *in situ* measurements without the requirement of large optical accesses to the sample. The technique allows fast measurements at high repetition rate. The measurement time can be sub-second. However, it must be kept in mind that the shorter the measurement/acquisition time the lower the sensitivity and accuracy as the noise level increases. Pulsed laser sources are suitable to bring acquisition times down to nanoseconds should extremely high temporal resolution be required. Water has a weak Raman scattering cross section. Therefore, even in aqueous systems, Raman scattering does not suffer from water interference like in IR ((Johannes Kiefer 2015, Meyer, M.W.; Lupoi, J.S.; Smith, E.A. 2011)).

2.3.9.3 Fourier-transform Raman spectrometer

Many FT-Raman instruments are adaptations of existing FT-IR spectrometer and the components of an FT-Raman spectrometer are shown in (figure 2.18). All currently available commercial FT-Raman spectrometers use neodymium: yttrium aluminum garnet (Nd-YAG) lasers operating at 1064 nm. The use of long wavelength is necessary to avoid exciting fluorescence, but long wavelength results in a loss in scattering cross-section since the Raman scattering cross-section is proportional to v^4. The laser is directed to the sample either in 180° or 90° geometry. Since an interferometer has a larger aperture than the slit of a dispersive/CCD system, it is not necessary to focus the laser to a small spot. An unfocused or weakly focused laser is advantageous in FT-Raman because it lowers the power density at the sample and relaxes the tolerances on alignment of laser, collection optics, and sample. The scattered radiation from the sample then pass through a filter module which remove the Rayleigh line. Then, the scattered filtered radiation passes through an aperture called a *Jacquinot stop* which permits control of the degree of collimation in the interferometer and excludes severely off-axis radiation. The filtered radiation then passes to an interferometer where it is split by a beam splitter into two beams of equal intensity. Using moving and fixed mirrors, one beam is subjected to an optical delay, and the two beam are then recombining. When recombined, the two beams interfere producing either a constructive or destructive interference pattern. The modulated radiation leaving the interferometer is directed toward the detector which measures variations in the intensity of the emergent beam as a function of

the difference in path length. The interferogram is the sum of the cosine waves for all of the wavelength elements in the polychromatic source.

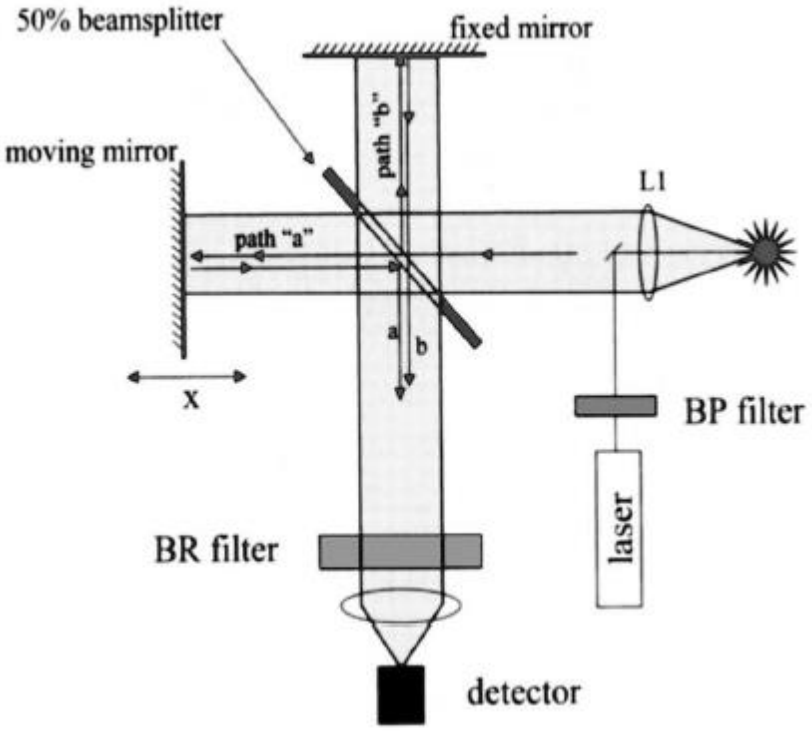

Figure (2.18) Schematic of FT-Raman spectrometer

The interferogram is then converted into a Raman spectrum of signal intensity against wavenumber by the Fourier-transform operation. Indium gallium arsenide (In Ga As) or liquid nitrogen-cooled germanium (Ge) detectors are usually used for FT-Raman spectroscopy. These detectors are very sensitive, but are noisy and still less sensitive for near-infrared radiation than the silicon CCD is for visible radiation [Hendra, P., Jones, C., Warnes, G. (1991), McCreery, R.L., (1999), Chase, B., (1987)].

2.3.9.4 Dispersive versus non-dispersive Raman spectrometers

1- The use of UV-Visible lasers as excitation sources in dispersive systems increase the Raman scattering intensity (dependent on the v^4 of the excitation frequency) so short acquisition times are

required to obtain the Raman data. It also offers a high sensitivity when coupled with low noise CCD detectors in contrast to the relatively high level noise and low sensitivity of the germanium detector. The scattered radiation is dispersed by the diffraction grating across an array of pixels on the CCD detector and the intensities of the incident light at all frequencies are analysed simultaneously (multi-channel advantage). However, the integrity of the sample may be compromised and fluorescence emission may occur due to the high energy power of these lasers. Moving to the near infrared excitation at 1064 nm inhibits the onset of fluorescence but reduces the Raman scattering intensity due to the relatively low energy power of near- infrared lasers.

2- A grating-based dispersive spectrograph with a CCD at its focal plane (multichannel spectrometer) monitors many wavelengths simultaneously and acquires a spectrum faster than a scanning, single-channel system that must monitor each wavelength in turn. This is called the multichannel advantage. A multiplex spectrometer (FT-Raman) does not separate the different wavelengths scattered by the sample but rather modulates them at frequencies dependent on their wavelengths.

The result is a single beam, detected by a single detector, which contains all wavelengths of interest. Since each wavelength is modulated at a different frequency, a Fourier transform of the multiplex detector output yields a Raman spectrum (multiplex or Felgett advantage). This difference between multichannel and multiplex approaches has major effects on the characteristics of the Raman spectrum, in terms of resolution, spectral coverage, signal magnitude, and signal/ratio (SNR). For multichannel and multiplex approaches, the simultaneous measurement over the

whole spectral range results in an improved S/N ratio. FT-Raman system also offers a constant spectral resolution over the whole spectral range.

3- In dispersive spectrometers, the dispersed light entering a monochromator must enter through a narrow slit so a fraction of the Raman scattering is lost. In addition, reflective losses from gratings and mirrors exacerbate the situation. On the other hand, the entrance of an interferometer is a large circular hole which allows high throughput of scattered radiation to the detector (Jacquinot advantage).

4- In theory, all spectrometers can show an improved S/N ratio if the spectra are averaged. In dispersive Raman systems, frequency precision and accuracy depend on calibration with external standard e.g. silicon and the ability of electomechanical mechanisms to uniformily move gratings and slits during and between the scans. Displacement errors due to mechanical wear may result in band shape distortion and low S/N ratio. Internal caliberation of the interferometer against a helium-neon laser provides exceptional wavenumber reproducibility, which facilitate the superposition of spectral data (accumulation) and data subtraction e.g solvent, background. This is called the Connes advantage.

5- Both dispersive and non-dispersive instruments provide the same spectral information and both offer all the advantages of Raman spectroscopy. However, one solutions, polymers or environmental sampling. Raman spectroscopy offers the ability to measure vibrational spectra of aqueous samples. aqueous samples, cannot be analyzed using FT-Raman spectroscopy as water has strong interactions in the near-infrared region and therefore, laser

radiation and Raman scatter are both susceptible to absorbance by water. Dispersive Raman spectroscopy, with visible laser excitation, is often more sensitive for aqueous samples because water absorbance of the radiation is not present. The confocal approach has been used in dispersive systems and as long as fluorescence is not a problem, the highest spatial resolution can be achieved. FT-Raman spectroscopy is the best choice in situations where samples fluoresce or are likely to contain minor impurities that may fluoresce. This is because of the use of longer excitation wavelengths at the near infrared region (commonly 1064 nm). FT-Raman has experienced great success in forensic analyses through sample containers or evidence bags, negating the need to break the container seal. It has been used to analyze illicit drug substances, clandestine lab samples, explosives and fibres. In particular, street drugs and clandestine lab samples often fluoresce with visible laser excitation but can be analyzed by FT-Raman spectroscopy. {Edwards, H.G.M., Chalmers (2005)}

2.3.10 Raman versus Infrared spectroscopy

There are several advantages of Raman spectroscopy over IR spectroscopy:

1- Unlike transmission IR spectroscopy, sample preparation is not required and samples can be analysed directly without destroying the sample.

2- Since water is a weak Raman scatterer, Raman spectra of samples in aqueous solution can be obtained without major interference from water vibrations. Thus, Raman spectroscopy is ideal for the studies of biological compounds in aqueous solution.

In contrast, IR spectroscopy suffers from the strong absorption of water.

3- Raman spectra of hygroscopic and/or air-sensitive compounds can be obtained by placing the sample in sealed glass tubing. In IR spectroscopy, this is not possible since glass absorbs IR radiation.

4- In-situ or in vivo analysis as well as analysis with optical fibres are more easily carried out by Raman spectroscopy which demonstrates the flexibility and versatility of Raman spectroscopy in comparison with IR.

5- Since the diameter of the laser beam is normally 1-2 mm, only a small sample volume is needed to obtain Raman spectra. This is a great advantage over conventional IR spectroscopy when only a small quantity of the sample is available. Also, the spatial resolution of Raman micro-spectroscopy is very high (1μ) compared with the spatial resolution of IR microscopy which is about 10 mm.

6- Lattice modes which appear below 200 cm^{-1} can be examined using Raman spectroscopy as Raman instruments allow spectral data to be obtained to within 50 cm^{-1} of the incident laser whereas IR data can normally be obtained to approximately 400 cm^{-1} unless special instrumentation is adopted. This gives Raman spectroscopy a very big advantage over IR spectroscopy where low wavenumber bands can be quite definitive for sample identification and characterization.

7- There is a special type of Raman scattering known as the resonance Raman (RR) effect that has no counterpart in the IR. The resonance Raman effect is an effect in which intensities of Raman bands are significantly increased in cases where the wavelength of the excitation radiation overlaps with an absorption

band of the sample molecule. In addition to huge signal enhancement, which significantly increases sensitivity, resonance Raman spectroscopy allows for selective examination of a particular chromophore in the molecule. To the contrary, IR spectroscopy only allows for the acquisition of average spectra of the sample [Šašić,S, (2008)].

2.4 Optical properties

Optical properties fall easily into two mutually exclusive categories: intrinsic and virtual. Intrinsic optical properties (IOP's) are those properties that depend solely on the medium, and are therefore independent of the ambient light field within the medium. The two primary factors in IOP are the absorption coefficient and the volume dispersion function. Other IOPs include the refractive index, band attenuation index, and single scattering albedo. Apparent optical properties (AOP's) are those properties that depend both on the median (IOP's) and on the geometric (directional) structure of the ambient light field, and that display enough regularities and stability to be useful recipes for samples.

The inherent optical properties (IOP's) specify the optical properties of samples in a form suited to the needs of radiative transfer theory.

Consider a small volume V of cell of thickness t illuminated by a narrow collimated beam of monochromatic light as schematically illustrated in Figure (2.19).

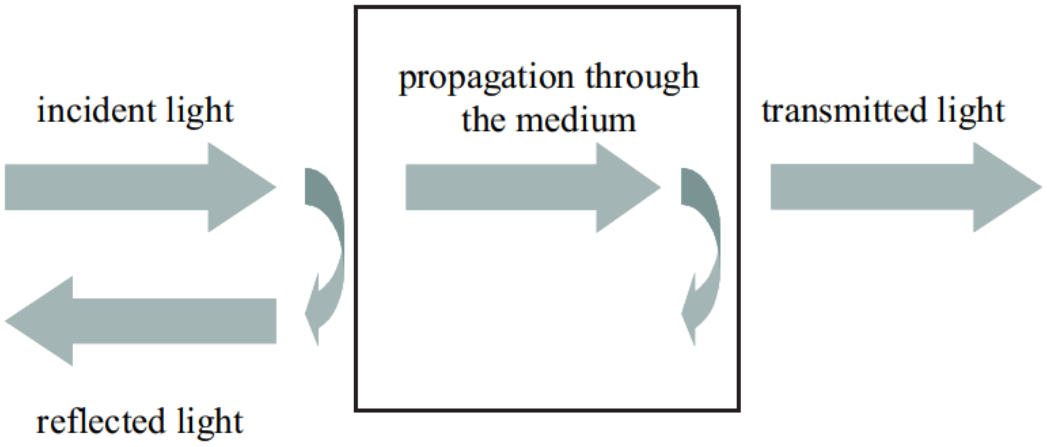

Figure 2.19 Reflection, propagation, and transmission of a light beam incident on an optical medium

Some part of the incident power I is absorbed within the volume of cell (A). Some part is scattered (R) out of the beam at an angle, and the remaining power is transmitted (T) through the volume with no change in direction. be the total power that is scattered into all directions. Furthermore, assume that no inelastic scattering occurs, i.e. assume that no photons undergo a change in wavelength during the scattering process. Then by conservation of energy

$$I = A + T + R \ldots (2.16)$$

2.4.1 Absorption

Absorption occurs during the propagation if the frequency of the light is resonant with the transition frequencies of the atoms in the medium. In this case, the beam will be attenuated as it progresses. The transmission of the medium is clearly related to the absorption, because only unabsorbed light will be transmitted. Selective absorption is responsible for the colouration of many optical materials. The spectral absorptance A is the fraction of

incident power that is absorbed within the volume: The spectral transmittance $T$is

$$T = I_T/I_0 \ldots\ldots (2.17)$$

$I_T \equiv$ transmission power

$I_0 \equiv$ incident power

The inherent optical properties usually employed in hydrologic optics are the spectral absorption, is the spectral absorbance per unit distance in the medium.

2.4.2 Absorption Coefficient

The absorption coefficient describes the attenuation of the intensity of light passing through a material. It can be understood as the sum of the absorption cross-sections per unit volume of the material for an optical process. The higher the length, the shorter the length of the light can penetrate the material before it is absorbed. Even if the amount of light absorbed by a cell is precisely measured, it is difficult to determine how much incident light is absorbed by the samples, the rate of light absorption can be well described by the Beer-Lambert Law. the spectral absorption coefficient α a is defined as

$$\alpha = 2.303A/t \ldots\ldots (2.18)$$

A≡ Absorbance

t ≡ path length (centimeters).

2.4.3 Extinction Coefficient

The extinction coefficient refers to "a measure of the rate of light transmitted through the scattering and absorption of a medium. The extinction coefficient (K_0) is a characteristic of a given substance under a precisely defined set of conditions, such as wavelength, solvent, and temperature. In practice, the measured extinction coefficient is also only partially on the characteristics of the instrument used. It is given by

$$K_0 = \frac{\alpha\lambda}{4\pi} \text{ …… (2.19)}$$

α≡Absorption Coefficient

λ≡ wavelength

2.4.4 The refractive index

Refractive index (RI) is an important characteristic of oils because of the ease and speed with which it can be determined precisely, the small quantity of sample needed, and its relationship to structure. It generally gives a good idea about the degree of unsaturation of fats and oil, as well as its correlation with the iodine value.

index of refraction of a medium, and symbolized by the symbol n, is the ratio of the speed of light in a vacuum to it is speed in that medium. It is a parameter that shows the extent to which the material is affected by electromagnetic waves. The refractive index consists of two parts, real and imaginary. (The propagation of light in an absorbing material can describe it is refractive index as a complex number. The imaginary part of this complex number expresses the attenuation of the light ray, while it is real part

expresses the refraction of light in the material.) The refractive index is calculated from the twitch spectrum by the relationship

$$n = 1/T + \sqrt{(1/(T-1))} \ldots. (2.20)$$

The refractive index of oils is one of the natural properties that distinguish it, as it is characterized by stability, and therefore it is widely used in many fields, including the identification of the substance itself, in addition to the detection of it is purity and quality.

2.5 Literature Reviews

Guzman et al, in 2011 used chemometric methods jointly with Raman spectra to assess oxidative stability in olive oil Primary and secondary oxidation parameters such as peroxide value, K_{232} and K_{270} were studied. Low-resolution Raman spectra ranging from 200 to 2700 cm^{-1} in a set of 126 oxidized and virgin olive oil samples were collected directly using a probe. Partial Least Squares was used to calibrate the Raman instrument for the different targeted parameters. The performance of the models was determined by using validation sets, and the best results obtained were: R^2 = 0.91, RMSEP = 2.57 for the peroxide value content; R^2 = 0.88, RMSEP = 0.37 for K_{232}; and R^2 = 0.90, RMSEP = 0.08 for K_{270}. These results demonstrated that low-resolution Raman spectroscopy could be a relevant technique for evaluating the oxidation status of olive oils because the key oxidation parameters can be determined quickly and in a non-destructive and direct way. The most salient changes occurred below 1800 cm^{-1}, particularly at 1267 cm^{-1} (symmetric rocking of cis C = C bonds), 1302 cm^{-1} (in-phase twisting of methylene groups), 1442 cm^{-1}

(scissoring of methylene groups, δCH_2), 1655 cm^{-1} (stretching of cis C = C bonds), and 1747 cm^{-1} (stretching of C = O bonds in esters) [Guzm_an, E., et al. (2011)].

Carmona, et al. in 2014 assessed the oxidative stability of four extra virgin olive oils, an olive pomace oil, and a mixture of virgin and refined olive oil, for the 2995–3040 cm^{-1} region, the Raman spectra for the four oils before heating were very similar. The 2800–3050 cm^{-1} region exhibited five bands at ca. 2855, 2874, 2894, 2932, and 2969 cm^{-1} typical of C–H stretching vibrations in methyl and methylene groups in addition to a sixth band above 3000 cm^{-1} corresponding to H–C–H stretching vibrations. Obviously, these bands should be largely due to the major fatty acid in the oils: oleic acid. Heating the oils at $190C^0$ for 2 or 5 h altered the band at. 3010 cm^{-1} for H–C–H bonds and that at 2874 cm^{-1} for C–H bonds in a with respect to the double bonds. However, it was the band at 3010 cm^{-1} which best allowed the effect of the thermal treatment to be monitored—those around 2874 cm^{-1} were more difficult to normalize. As can be seen from heating for 2 or 5 h decreased that band in all oils, albeit to a smaller extent in extra virgin olive oil. These results were ascribed to it is containing increased amounts of antioxidants such as carotenoids and tocopherols [Carmona, M.A., et al. (2014)].

In another study, Carmona, M.A., Lafont et al in 2015. used Raman spectroscopy to determine the degree of unsaturation of 12 vegetable oils including extra virgin olive oils and correlated their results with the corresponding iodine values as determined with a standard method. A plot of DU against the signal intensity for stretching vibrations in H–C–H bonds, which appeared in the zone from 3009–3013 cm^{-1} for all oils, exhibited excellent correlation

and so did iodine values. These results confirm that Raman spectroscopy is an accurate tool for assessing unsaturation in vegetable oils and an effective alternative to the “traditional” methods. The signal at 1658 cm^{-1} in the spectra for all oils, which was assigned to cis C = C bonds, provided DU values that were also highly correlated with the iodine values [Carmona, M.A., Lafont, F., et al. (2015)].

Muik, B., Lendl, B., Molina-Dıaz, A., and Ayora-Ca~nada, M.J. in 2003 used Raman spectroscopy in combination with partial least squares (PLS) regression for the direct determination of the fatty acid content of olive oils and olives. For this purpose, they compared the spectra for pure oleic acid, olive oil and milled olives. All spectra were similar and contained the typical strong bands at 1267 cm^{-1} ($\delta_{\ =\ C-H}$ deformation), 1302 cm^{-1} (in-phase methylene twisting), 1442 cm^{-1} (δ_{CH2}), 1655 cm^{-1} ($v_{C\ =\ C}$), 1747 cm^{-1} ($v_{C\ =\ O}$, only in oil and olives), 2852 cm^{-1} (v_{CH2} sym), and 2970 cm^{-1} (v_{CH3} sym). Milled olives additionally exhibited a band at 1604 cm^{-1} that was assigned to stretching of aromatic rings in lignin —a major constituent of olive kernels. The 1200–1800 cm^{-1} and 1000 1800 cm^{-1} regions were used to quantify free fatty acids in olive oil, using PLS regression. Although the results were less accurate than those obtained with the official method, they showed that the Raman technique is useful for fast, on-line quality control of oil production. Also, the Raman methodology is much more expeditious than the official method for olives as the only pretreatment needed is milling the fruits [Muik, B., Lendl, et al. (2003)].

In March 2020 M. Saleem, Naveed Ahmad et al used Raman spectroscopy has been utilized for the first time to characterize

pure canola oil samples extracted directly from its seeds through cold press and chemical method and six commercial oil brands. Raman spectra were acquired directly from oil samples by using laser at 785 nm to investigate their valuable ingredients. It has been observed that Raman bands evolving at 1156 and 1525 cm^{-1} represent beta-carotene, which are present in pure canola oil samples and absolutely absent in commercial brands. Furthermore, the effect of temperature on the molecular composition of pure and commercial oil brands has been investigated by heating individual samples at the temperatures of 100, 110, 120, 130, 150, 160, 170, 180, and 200 °C, each for 30 min. It has been found that pure canola oil retains beta-carotene and other valuable fatty acids until heated up to 150 °C; however, it showed a trend of thermal oxidation at all temperatures, whereas, in commercial brands, heating does not induce much spectral variations, which might be due to already treated with high temperatures during refining processes. Statistical analysis has been performed through principal component analysis (PCA) to produce classification among oil samples based on their minute spectral variations [M. Saleem, et al 2020)].

In a pioneering study in this field, in 2005 Muik, B., et al. examined chemical changes in edible oils including virgin olive oil upon heating at $160C^0$ for 9 h. Prior to heating, the Raman spectrum for virgin olive oil exhibited a band at 1525 cm^{-1} that was assigned to C = C stretching vibrations in highly conjugated compounds such as carotenoids. Because these compounds disappear during the refining process, they should only be present in virgin olive oil. The large number of conjugated double bonds in carotenoids impart them antioxidant properties. Because

heating for 90 min caused the band at 1525 cm^{-1} to disappear, this length of time was taken to be the stability period for virgin olive oil. Other oils exhibited different stability times (e.g., 60 min in sunflower oil and 120 min in corn oil) which the authors ascribed to the presence of tocopherols added as antioxidants. The greatest differences between the Raman spectra for the six oils studied were those in the bands for C-H C stretching vibrations, which appeared at 1620, 1680, and 1655 cm^{-1}. The ratio of the difference between the areas under the former two to the intensity of the latter, $A_{1620–1680}/I_{1655}$, was used to successfully monitor the oxidation of vegetable oils because it represented the formation of conjugated compounds (dienes and trienes) and cis–trans isomerization during the oxidation process. Virgin olive oil was that exhibiting the lowest ratio at any heating time, the other five oils (peanut, rapeseed, corn, sunflower, and safflower) exhibiting similar results in this respect after 7 h of heating [Muik, B., Lendl, B., et al. in (2005)].

Yang and Irudayaraj, in 2001 used near-infrared, mid-infrared, and Raman spectroscopic techniques were used to quantify the amount of olive pomace oil adulteration in extra virgin olive oil. The concentration of olive pomace oil in extra virgin olive oil was in the range between 0 and 100% in 5% increments by weight. Of the methods studied, Fourier Transform-Raman spectroscopy gave the highest correlation with a correlation coefficient of 0.997 and a standard error of prediction of 1.72%. The spectroscopic techniques have the potential to become a tool for rapid determination of adulteration in extra virgin olive oil, because they are easy to use and cost-effective, and compared the efficiency of Raman spectroscopy with that of near- and mid-

infrared spectroscopy in detecting adulteration of extra virgin olive oil with pomace oil. Although they succeeded in quantifying the amount of pomace oil contained in the extra virgin olive oil with the three techniques, Raman spectroscopy provided the highest correlation coefficient and the lowest standard error of prediction. These results further testify to the potential of the Raman technique for oil authentication [Yang, J. and Iridayaraj, J. (2001)].

Gauglitz and Vo-Dinh (2003) stated that infrared (IR) spectroscopy is a rapid, nondestructive and sensitive method easy to handle and provide all sampling techniques for gases, liquids and solids. Important aspects are the convenient qualitative and quantitative evaluation of the spectra. The mid- (fundamental) infrared region (IR or MIR) extends from 4000 cm^{-1} to 400 cm^{-1}. It is surrounded by the far-IR region (FIR) from 400 cm^{-1} to 10 cm^{-1} and the very important near-IR region from 12500 cm^{-1} to 4000 cm^{-1}. The features of an IR spectrum (number of infrared absorption bands, their intensities and their shapes) are directly related to the molecular structure of a compound. The IR spectrum is a unique physical property of an individual compound; it is its molecular fingerprint. The IR region comprises fundamental vibrations of bound atoms. Whenever such bound atoms vibrate, they absorb infrared energy, i.e. they exhibit IR absorption bands. The condition for a normal vibration to be IR active is a change in molecular dipole moment during vibration.

(Karoui et al., 2010). For vibrational spectroscopy, the success of the analysis for detecting adulterants in the edible oil will depend on the data analysis methods used. Information in an infrared spectrum is captured by the positions, shapes and intensities of the

bands. The band positions contain information about the chemical structure whereas information about the concentration of the compounds giving rise to specific bands are contained in the band intensities which are described by the Beer-Lambert law. The fact that edible oils contain hundreds of compounds explains the complex nature of their spectra which have overlapping bands. Hence, there is a need for the use of multivariate analysis to extract qualitative and quantitative information from the spectra [Karoui, R., Downey, G., & Blecker, C. (2010).].

In a recent study, Giulia Vicario et al, in December 2020 used UV-VIS spectroscopy for distinct set of samples of extra virgin olive oil (cultivar Frantoio) from a specific region in Tuscany (Italy), were examined by UV-absorbance spectroscopy. To identify and quantify various chemical components, such as the contents of dyes, sugars, and squalene. The acquisition of near UV absorbance spectra of EVOO samples was extremely fast (1 to 2 min), and quantitative analysis of the experimental spectra was performed using a mathematical approach. The UV absorption spectral profiles were inherent in virgin olive oils and were similar for all samples. From the absorbance values, it turned out that EVOO 2 has a greater number of pigments relative to EVOO 1 and EVOO 3. Among the different mathematical models tested, the best model for quantitative characterization of EVOO dyes was the five-pigment (six-function) model of oil. This model allowed for the quantification of carotene, fovitin-A, vitin-B, lutein and cis-neoxanthin [Giulia Vicario, et al (2020)].

Oguz Uncu, Banu Ozen, in 2019 used fluorescence, Fourier transform infrared (FT-IR), and ultraviolet–visible (UV–vis) spectroscopic methods. to detect and quantify adulteration of

fresh olive oils with old olive oils from the previous harvest year. Adulterated samples prepared in varying concentrations (10-50%(v/v)) Orthogonal partial least square-discriminant analysis (OPLS-DA) and partial least squares (PLS) regression techniques were used for the differentiation of adulterated oils from the pure oils and prediction of adulteration levels, respectively. After the application of various pre-treatment methods, all of the OPLS-DA classification models generated for every spectroscopic technique successfully differentiated adulterated and non-adulterated oils with over 90% correct classification rate. FT-IR + UV–VIS and fluorescence spectral data were also successfully used to predict adulteration levels with high coefficient of determinations for both calibration (0.94 and 0.98) and prediction (0.91 and 0.97) models and low error values for calibration (4.22% and 2.68%), and prediction (5.20% and 2.82%), compared to individual FT-IR and UV–VIS spectroscopy was obtained. Therefore, FT-IR + UV–VIS and fluorescence spectroscopy as being fast and environmentally friendly tools have great potential for both classification and quantification of adulteration practices involving old olive oil [Oguz Uncu, Banu Ozen, (2019)].

Jiulin Shi, et al in 2019 proposed a Brillouin absorption spectroscopy method to validate vegetable oils and detect adulteration of olive oil in visible areas. In this work, the natural spectra of vegetable oils and adulterated oils are presented. By employing two related wavelengths, the actual and fitted values were highly consistent, and the linear fitting of their absorption values produced high R^2 values and low MSE values. SBS spectra were also measured for vegetable oils and cheat oils, and the SBS frequency shifts were obtained by fitting the spectra with

Lorentzian functions, and the results presented here showed that different vegetable oils and cheat oils show Statistically significant differences in the normalized absorption values of two related wavelengths (455 and 670 nm) and frequency shifts of SBS. The results demonstrate that vegetable oil validation and detection of olive oil adulteration can be successfully achieved by SBS combined with visible absorption spectroscopy [Jiulin Shi, Dapeng Yuan. (2019)].

In another study, Fernando da Silveira Minuceli et al. in 2021 investigated the adulteration of oils, and methods such as UV-visible spectroscopy were used to quantify the amount of vegetable oil present in extra-virgin olive oil. This study aimed to understand the UV-Vis technology in a previous reading in the evaluation and examination of adulteration in extra virgin olive oils available in the market through quantitative research. Praying laboratory samples tampered with four types of vegetable oils to assess reading spectrum responses. The calibration curves had implications and there was no difference between the results obtained from 0 to 70% replacing olive oil with vegetable oil. Also, the synthesized oils were analyzed to verify respect for the prescribed percentage, yielding results of up to 96% soybean oil in a product that should contain a maximum of 88%. Therefore, it was possible to verify that the 456 nm region could be used to check cheating with efficiency and agility and that UV-visible spectroscopy could be considered as a fast and low-cost method for previous analyses.

In another study, Mohammad E. Khosroshahi. in 2018 UV-Vis absorption and fluorescence spectroscopy were used to test the quality and changes in the composition of extra virgin olive oil

(EVOO) and canola oil (CO) with temperature. The increase of temperature caused a change in the molecular structures of both types of oils seen as a gradual decrease of intensity amplitudes of absorption and fluorescence signals. A significant alteration occurred at ≈200˚C where almost the main spectra of pheophytin-a, b, carotenoids, lutein and vitamin E in EVOO and linoleic acid and oleic acid in CO disappeared. An independent experiment showed the output of laser changes linearly with the input in oil at constant temperature (i.e., room temperature) where the transmission values of ≈33% and ≈75% are determined for EVOO and CO respectively. However, the transmission through a heated oil exhibited a non-linear behavior which indicates the molecular optical response to thermal changes. The effect of storage time and adulteration of oils were also evaluated.

H. E. Hassan1 H.A. Badawy 2010. They heated corn oil at 180 ^{o}C. for six durations (3, 6, 9, 12, 15, and 18 hrs) to measure some optical, physical and chemical properties of oil with exposure by visible and invisible lights. Three light regions, ultraviolet (200-400nm), visible light (400-700nm), and near infrared (700-900nm) were used in the present work. The obtained results are summarized as follows: (1) The highest transmission light percentages were 94.89, 88.57 and 33.17 % for using wavelengths of 900 nm (IR), 700 nm (VIS) and 400 nm (UV), respectively.; (2) The highest absorption light percentages from heated corn oil were 0.09, 0.12, and 1.26 % at using 900 nm (IR, 700 nm (VIS), and 400 nm (UV) wavelengths.; (3) The wavelength (400 nm) of UV is the highest measure of absorption light of corn oil. Meanwhile, 900 nm of IR and 700 nm of VIS are the highest measure of transmission light can be used to measure corn oil

quality.; (4) The heating times were increased from 3 to 18 hrs lead to increase oxidized fatty acid, Polemer, acid value, peroxide value, and reflective index, while, the iodine value and viscosity were decreased compare with control sample.; and (5) The corn oil will start deterioration after 15 hrs of heating time whereas oxidization fatty acid more than 1% at transmission light percentages 13.69 % and 12.20% of wavelength 900 nm (IR) and 700 (VIS) and at absorption percentage 1.06% of wavelength 400 nm (UV).

Yang and Irudayaraj (2001) carried out a comparison study between several spectroscopic techniques in the infrared (IR) region. Near infrared (NIR), mid infrared (MIR), Fourier transform-infrared (FTIR) and Fourier Transform-Raman (FT-Raman) spectroscopic techniques were used to quantify the amount of olive-pomace oil adulteration in extra virgin olive oil. The concentration of olive-pomace oil in extra virgin olive oil was in the range between 0 and 100% in 5% increments by weight. The peaks in the NIR region (9091-4000 cm^{-1}) were broad and weak due to combinations and overtones of functional groups of sample chemical constituents, and hence NIR was mostly used in quantitative analysis. Unlike NIR, most of the peaks in the MIR region (4000-400 cm^{-1}) were narrow and sharp due to fundamental vibrations of molecules. Compared to dispersive NIR, FTIR spectroscopy in the MIR region had higher signal/noise ratio and resolution. FT-Raman spectroscopy can be regarded as a complementary method to the IR technique for analysis. Like FTIR spectroscopy, FT-Raman can also provide information on the functional/chemical groups for qualitative and quantitative characterization.

The classifications of edible oils and fats under investigation were performed by applying discriminant analysis using FTIR spectra between 400 and 4000 cm^{-1}. The whole spectra between 400 and 4000 cm^{-1} are the combination of many constituents of oil/fat whereas the region selected between 1400 and 1800 cm^{-1} mostly represents the combination of C–H bending, C=O stretching, and C=C stretching and hence is directly related to unsaturated C=C bond. Generally, FTIR, FT-NIR and FT-Raman spectroscopy techniques can be used for rapid classifying edible oils and fats without the need for sample preparation. Both FTIR and FT-Raman spectroscopy techniques provided exquisite structural insights into functional groups of oils and fats for discriminant analysis. FTIR spectroscopy was found to be the most superior and efficient for discrimination and classification of oils and fats when used with CVA and yielded about 98% classification accuracy, followed by FT-Raman (94%) and FT-NIR (93%) methods (Yang et al., 2005).

Chapter Three

Materials and Methods

3.1 Introduction

This chapter contains the section to describe the edible oils and devices used in this research which included the Raman Spectrometer (DXR 532nm DXR) IR Spectrometer and Ultraviolet – visible spectrometer.

3.2 Materials

Edible oil **(**Olive, Corn, Sunflower, Factory Sesame, Presses Sesame and Peanut) used in this research were collected from local market, the properties of these oils were shown in table (3.1) below.

3.3 Apparatus and Software

3.3.1 Raman Spectrometers (DXR 532nm)

The Thermo Scientific™ DXR™ Raman microscope is designed to produce the results demanded by Raman experts with the ease required by busy analytical laboratories. Smart Lock optical components and a patented auto alignment system make set-up easy, fast and precise. Automated calibration, focus and exposure ensure quality results with every measurement. Raman spectra were recorded with a Thermo Fisher Scientific DXR1xi Raman microscope with the following experimental parameters: laser

wavelengths 532 nm; power laser of 5–10 mW; 0–3400 cm^{-1} full range grating; 10×, 50× and 100× objectives; 25 μm confocal pinhole; 5 (FWHM) cm^{-1} spectral resolution. Integration time for acquiring a Raman spectrum was 5 s and 30 scans for any spectrum. All the spectra were recorded at room temperature about 25 C^{o} [Thaís Karine de Lima, et al, (2020)]. The experimental setup used in this work was arranged as shown in figure (3.1).

In order to identify the best experimental parameters, preliminary measurements were performed to optimize the signal-to-noise ratio, and minimize the sample fluorescence. The background-subtracted Raman spectra were normalized for the area under the curve for standardization of the Raman intensities. The samples did not undergo any kind of pre-treatment before Raman examination. In turn, to assess intra-sample variability, multiple measurements were carried out at different regions within the sample. The optical spectra analyses were conducted by Origin 9 [Origin Lab, Northampton, USA].

The study of samples was carried out by means of a Raman spectrometer located at King Khalid University, College of Science in Abha.

Figure (3.1) the experimental setup of DXR Raman microscope

Figure 3.2 shows the optical components. To run the Raman device perfectly, the work was divided to stages, carried out in order to get the best results. Features such as autoexposure, smart backgrounds and autofocus rely on the instrument and software intelligence to optimize data collection parameters. This is analogous to the way that the expertise required to achieve professional-level photography has been embedded into digital cameras.

• Components such as lasers, gratings, Rayleigh filters and sampling accessories should be easy to exchange, either through automation and a mouse-click, or by employing Smart Lock technology to ensure reproducible results. Smart components are readily recognized by the system software, their identities recorded for full traceability and the user is alerted if components are incompatible with each other.

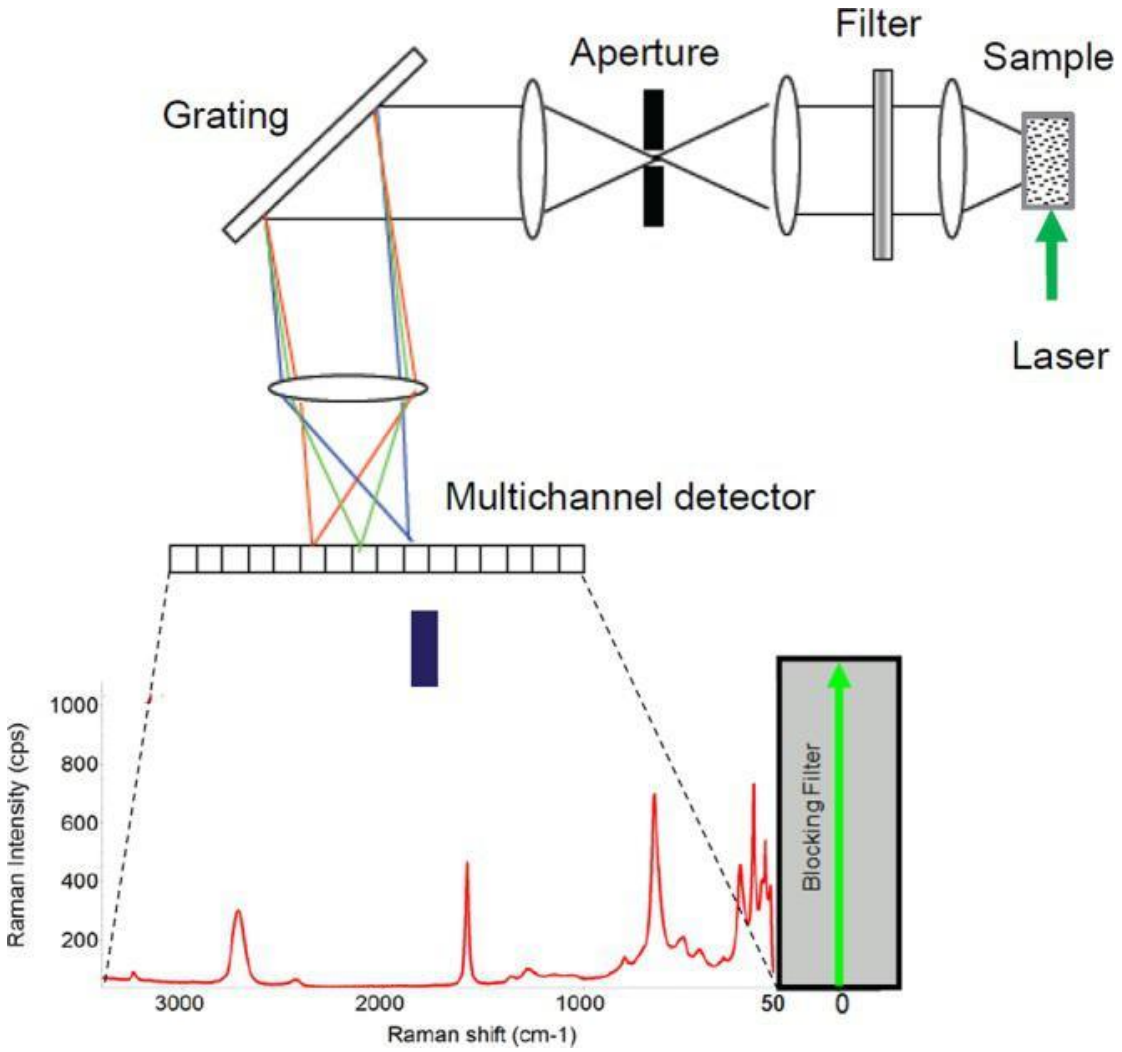

Figure (3.2) The schematic diagram of the Thermo Scientific™ DXR™ Raman microscope

3.3.2 Fourier Transform Infrared (FTIR) Spectroscopy

FTIR spectral analysis was carried out according to the method outlined by Guillén and Cabo (1999); (corn, olive, sunflower, factory sesame and peanut) oil, were exposed to FTIR analysis using an IRTracer-100 Spectrum FTIR Plus 460 (Shimadzu, Japan)) equipped with a deuterated tri-glycine sulphate (DTGS) detector was used to obtain FTIR spectra. The standard detector in routine FTIR instruments is the pyroelectric DTGS (deuterated tri-glycine sulfate) detector, whose response in the MIR range is

wavelength independent. The MIR spectral range extends from 4000 to 400 cm^{-1}. The detector operates at ambient temperature and shows good linearity across the whole transmittance scale. The DTGS detector responds to signal frequencies of up to several thousand Hz, hence the time needed to scan one spectrum at a resolution of 4 cm^{-1} is of the order of 1 s. A small quantity (one drop of the sample) was pressed between two well-polished KBr disks (liquid cell) creating a thin film. Each sample undergoes 64 scans which are accumulated in one measurement to acquire a sufficient signal-to-noise ratio. Samples were scanned between 4000 and 400 cm^{-1} with a nominal resolution of 4 cm^{-1} and the data interval was $1cm^{-1}$. Time required for acquiring a complete sample spectrum was 30 second. after each measurement, the plate was carefully cleaned of any previous residue by wiping with acetone and hexane and dried with soft tissues before filling the next sample.

Fourier transformed infrared spectra of these blends were recorded taking into account the close relationships found previously between the frequency data of some specific bands and the composition of the oil samples, frequency data of all samples were collected and used in

equations that relate frequency and composition. Special Lab Solutions software (Shimadzu, Japan) was used to collect and process FTIR data. The device is located in the Sudanese Forensic Evidence Laboratory.

Figure (3.3) FTIR (Mattson, model 960m0016) spectroscopy

3.3.3 Ultraviolet – visible spectrometer

visible spectra obtained in shimadzo mini 1240 spectrophotometer scanning between (190 to 1100) nm. The spectrophotometer measures how much of the light is absorbed by the sample. The device is located in the laser department, Faculty of Science, Al-Neelain University. The large liquid-crystal display (LCD) has been incorporated with easy-to-follow prompts, large fonts, and graphics to help reduce the time needed to get your results. The

description on the instruments' soft keypad quickly guides you through specific programs. Mighty Performance with Quantitative Methods Everything from simple concentration measurements up to sophisticated quantitative calibration curves. Some of the standard functions include:

- Factor method for input of simple constants
- One-point calibration curve with one standard sample and a point through the origin.
- Multi-point calibration curve of the application requiring various standards. 1st, 2nd, and 3rd order polynomial filling for calibration come standard.
- Two or three wavelength quantitative analysis for measuring turbid samples or for measuring the effects of another distinguishable component

Maximum Wavelength Scanning The UV mini comes standard with a Spectrum mode that allows for full spectral data acquisition over the wavelength range of 190nm to 1100nm. Upon completion of the spectral scan, the peaks and valleys can be marked within a few seconds. The standard peak pick function allows for clear and accurate detection of the most sensitive wavelengths. Methods, results and raw data can be saved on either the standalone instrument, optional dedicated IC Data cards, or within a directory of an IBM-Compatible PC with the help of the optional new UV data manager software. This provides unlimited storage and expanded capabilities in archiving methods and management of essential results. information directly from the screen. The PC printers can be utilized for the same functions and for finger print resolution of spectral data. Spectroscopic

techniques employ instruments that share several common basic components, including a source of energy, a means for isolating a narrow range of wavelengths, a sample holder, a detector for measuring the signal, and a digital processor that displays the signal filter, diffraction grating or prism, interferometer. Figure (3.5) shows the internal structure of shimadzo mini 1240 spectrophotometer. [Band, Y. B. (2006)]

Figure (3.4) UV-VIS mini 1240 spectrophotometer

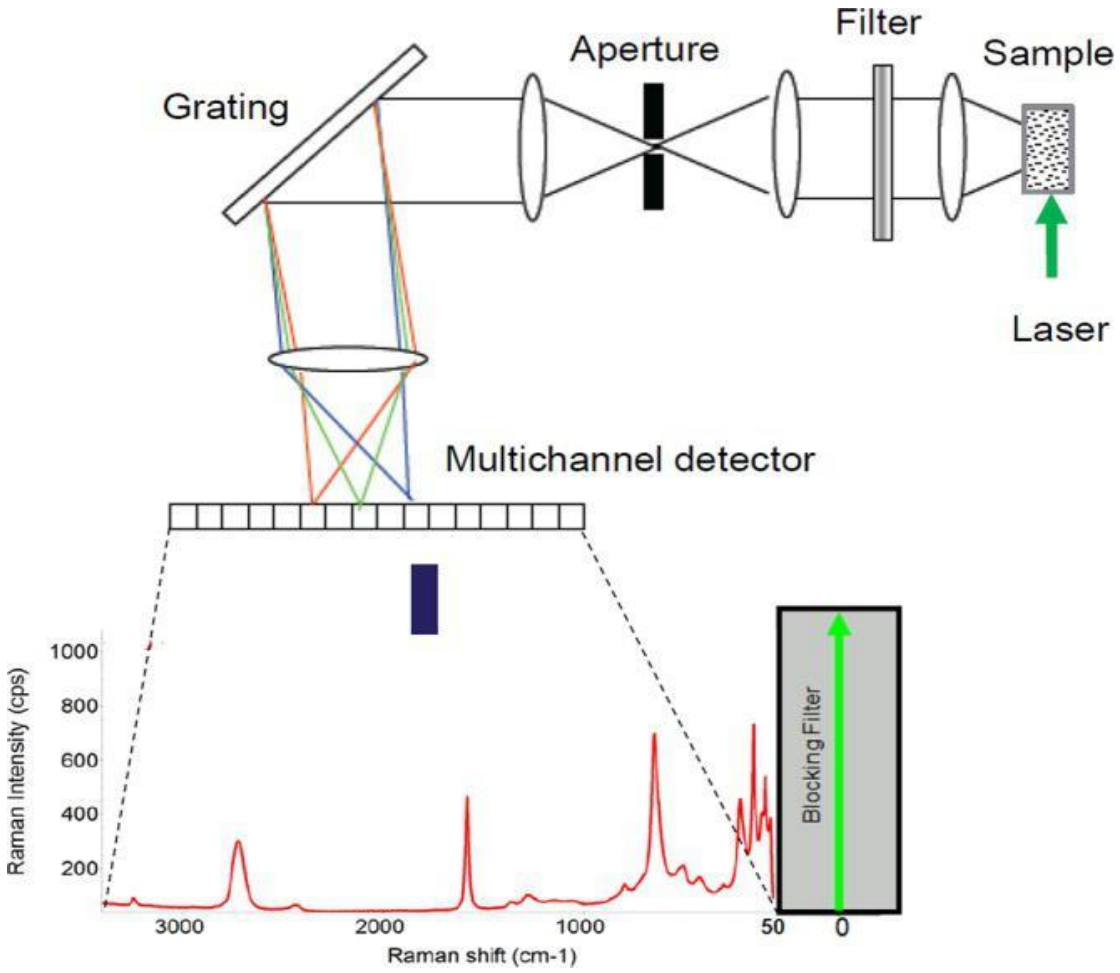

Figure (3.5) internal structure of Shimadzu mini 1240 spectrophotometer

3.3.4 Origin Pro 9 Software

Origin Lab, is a user-friendly and easy-to-learn software application that provides powerful data analysis and publication-quality graphing capabilities tailored to the needs of scientists and engineers. Origin Pro offers all of the features of Origin plus extended analysis tools for Peak Fitting, Surface Fitting, Statistics, Signal Processing, and Image Handling. Origin allows you to customize operations such as importing, graphing and analysis, all from the GUI. Origin also automatically updates all graphs, analysis results and reports when data or parameters change. This

allows for batch analysis of multiple files or datasets without the need for programming. All results of Raman spectroscopy and absorption spectroscopy were processed for all samples by Origin Pro 9 Software (Origin Lab, Northampton, USA).

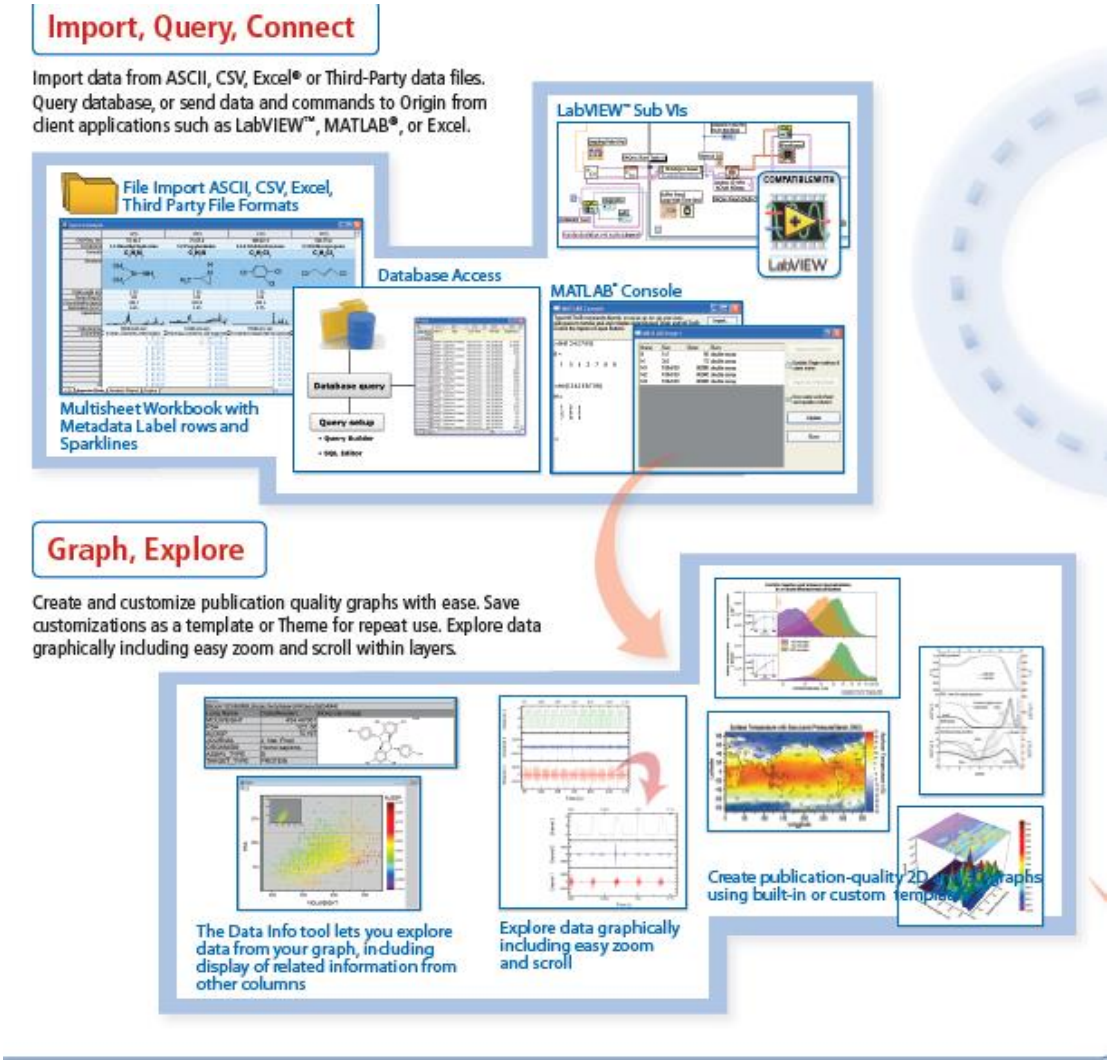

Figure (3.6) OriginPro desktop

3.4 Method

Six types of edible oils (corn, extra virgin olive, sunflower, sesame pressed, sesame plant and peanuts) were collected from local market. Raman spectroscopy and Fourier infrared spectroscopy were applied to identify functional groups presence on oils, then obtained results from FTIR and Raman were compared. ultraviolet visible was used to det absorbance spectrum from edible oils and optical properties were calculated such as transmission, reflection absorption coefficient, extinction coefficient and refractive index.

Chapter Four

Results and Discussion

4.1 Introduction

This chapter consist of all results obtained from Raman, Fourier Transform Infrared Spectroscopy and UV-VIS Spectrometer in addition to discussion.

4.2 Results and Discussion of Raman Spectroscopy

This study used of Thermo Scientific™ DXR™ Raman spectroscopy for analysis, quality, and characterization of edible oils, including six types of oils (corn, extra virgin olive, sunflower, factory sesame, pressed sesame, and peanut) purchased from local Sudanese stores.

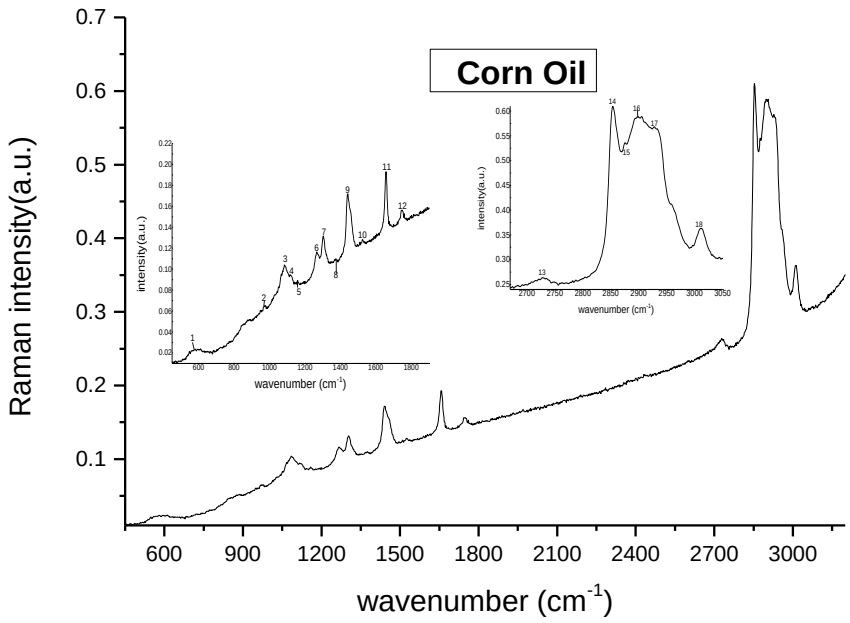

Figure (4.1) Typical Raman spectrum for Corn oil.

Figure (4.1) shows the Raman spectrum in the range from (3010.0 to 500.0) cm^{-1} of corn oil. It shows clear peaks represent the vibration of some components. Table (4.1) lists the Raman shifts and vibrational assignments of the Raman bands of the fiber substrates studied in this work. This will help to identify these bands if they appear in the Raman spectra of the corn oil and give an idea about the bands which may interfere with their identification. The intensity of all bands was also found.

Table (4.1) The wave number, intensities, and Functional Group/ Vibration of peaks in the Raman spectrum of the Corn Oil

Peak No	Wavenumber (cm^{-1})	Molecule/ group	Vibrational mode	Compound	Intensity (a.u.)	Reference
2	969.1	C=C	bending form trans	β-carotene	0.065	(Hong Yan, et al, 2018), (R.M. El-Abassy, et al 2009), (Shiyamala Duraipandian, et al, 2019)
3	1084.9	C-C	Aliphatic stretch		0.104	(Hong Yan, et al, 2018), (Shiyamala Duraipandian, et al, 2019)
4	1122.5	C-C	Aliphatic in phase stretch	Chlorophyll	0.093	(Hong Yan, et al, 2018)
5	1158.1	CH_2	Bending	β-carotene	0.089	(Qing Zhang, et al. December 2011)
6	1266.1	RHC=CHR	=CH symmetric rock cis isomer	Chlorophyll a	0.116	HANA VASKOVA, et al. 2014), (Hong Yan, et al, 2018), (R.M. El-Abassy, et al 2009))
7	1303.7	CH_2	Bending (twisting)	Alkene (unsaturated fatty acids)	0.131	(César Jiménez-Sanchidrián et al. 2016), (Hana Vaskova, et al. 2018), (Shiyamala Duraipandian, et al, 2019)
8	1374.1	CH_3	Symmetric bending	Alkene	0.110	(Qing Zhang, et al. December 2011), (Xiande Zhao, et al 2015)
9	1441.6	$-CH_2$	C-H bending (scissoring)	Methylene	0.171	(César Jiménez-Sanchidrián et al. 2016), (Michał Szmatoła, et

						al.2018), (V. Baeten, et al. 1996)
10	1524.5	RHC=CHR	C=C stretching	β-carotene	0.128	(HANA VASKOVA, et al. 2014), (R.M. El-Abassy, et al 2009), (Shiyamala Duraipandian, et al, 2019)
11	1657.6	Cis RHC=CHR	C=C stretching	Methyl linolenate	0.193	(César Jiménez-Sanchidrián et al. 2016). (Hong Yan, et al, 2018). (Lauren E. Jamieson, et al. 2018)
12	1749.2	RC=OOR	C=O stretching	Trielaidin (ester)	0.156	(César Jiménez-Sanchidrián et al. 2016). (HANA VASKOVA, et al. 2014). (Shiyamala Duraipandian, et al, 2019)
13	2727.9	Carbonyl group	Fermi resonance	Carbony	0.263	(Qing Zhang, et al.) 2011)
14	2853.3	$-CH_2$	Symmetric aliphatic stretch	β-carotene	0.610	(Hana Vaskova, et al. 2018). (Lauren E. Jamieson, et al. 2018). (Xiande Zhao, et al 2015)
15	2875.4	CH_2	Symmetric stretching	β-carotene	0.535	(Lauren E. Jamieson, et al. 2018). (Qing Zhang, et al. 2011). (Xiande Zhao, et al 2015)
16	2898.6	CH_2	Asymmetric stretching	β-carotene	0.588	(Qing Zhang, et al. 2011). (R.M. El-Abassy, et al 2009)
17	2927.5	$-C-H_2$	C-H asymmetric stretching	β-carotene	0.568	(César Jiménez-Sanchidrián et al. 2016). (R.M. El-Abassy, et al 2009)
18	3010.4	Cis RHC=CHR	=C-H symmetric stretching	methyl linoleate	0.362	(CésarJiménez Sanchidrián et al. 2016). (Lauren E. Jamieson, et al. 2018). (Michał Szmatoła, et al.2018)

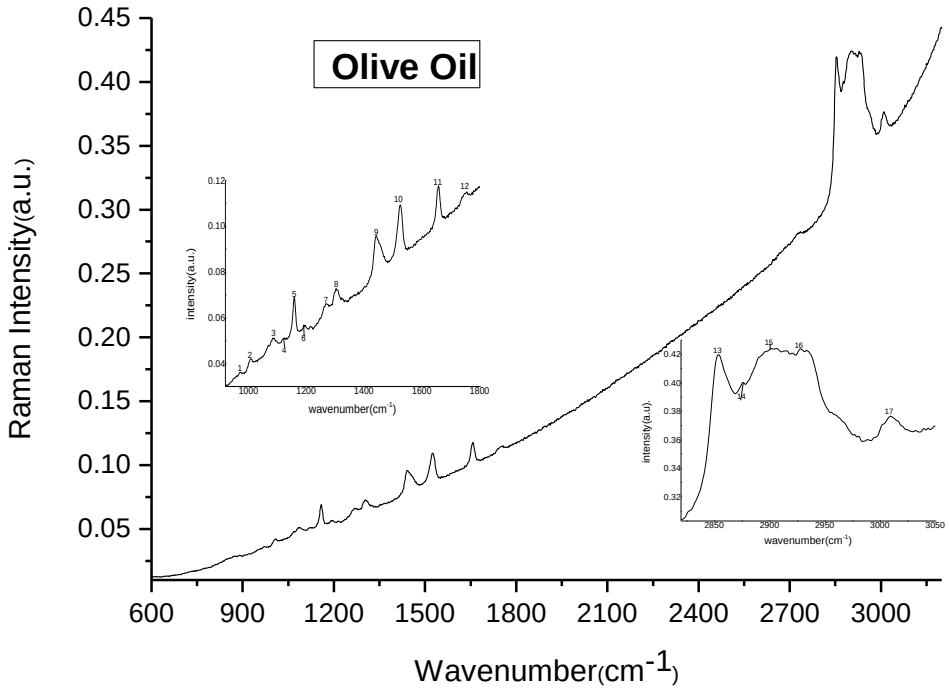

Figure (4.2) Typical Raman spectrum for Olive oil

Figure (4.2), shows Raman spectra acquired from Olive oil sample. The wavenumber region of (3089 to 600) cm^{-1} displayed provides a sufficient number of spectral peaks to afford unambiguous identification of the olive oil. The key signature bands of the olive oil are clearly observed in the spectra and the results compare favorably with the reference spectra recorded using a previous study.

Table (4.2) The wave number, intensities, and Functional Group/ Vibration of peaks in the Raman spectrum of the Olive Oil

Peak NO	Wavenumber (cm^{-1})	Molecule/ group	Vibration mode	Compound	Intensity (a.u.)	Reference
1	970.1	Trans RHC=CH R	C=C bending	β-carotene	0.036	(Hong Yan, et al, 2018), (R.M. El-Abassy, et al 2009), (Shiyamala Duraipandian, et al, 2019)
2	1007.7	HC-CH_3	bending	Carotenoids	0.042	(R.M. El-Abassy, et al 2009)

3	1088.7	C-C	Stretching		0.050	(Michał Szmatoła, et al.2018)
4	1125.3	C-C	Aliphatic in phase stretch	Chlorophyll b	00.51	(Hong Yan, et al, 2018
5	1158.1	CH_2	Bending	β-carotene	0.086	(Qing Zhang, et al. 2011)
6	1195.7	CH_2	Bending	β-carotene	0.056	(Qing Zhang, et al. 2011)
7	1268.1	RHC=CH R	symmetric rock cis isomer	Chlorophyll a	0.066	HANA VASKOVA, et al. 2014), (Hong Yan, et al, 2018), (R.M. El-Abassy, et al 2009)
8	1303.7	CH_2	Bending (twisting)	Alkene (unsaturated fatty acids	0.072	(César Jiménez-Sanchidrián et al. 2016), (Hana Vaskova, et al. 2018), (Shiyamala Duraipandian, et al, 2019)
9	1441.6	$-CH_2$	C-H bending (scissoring)	Methylene	0.095	(César Jiménez-Sanchidrián et al. 2016), (Michał Szmatoła, et al.2018), (V. Baeten, et al. 1996)
10	1525.5	RHC=CH R	C=C stretching	β-carotene	0.109	(HANA VASKOVA, et al. 2014), (R.M. El-Abassy, et al 2009), (Shiyamala Duraipandian, et al, 2019)
11	1657.6	Cis RHC=CH R	C=C stretching	Methyl linolenate	0.117	(César Jiménez-Sanchidrián et al. 2016). (Hong Yan, et al, 2018). (Lauren E. Jamieson, et al. 2018)
12	1756.0	RC=OOR	C=O stretching	oleic acid	0.115	(César Jiménez-Sanchidrián et al. 2016). (Shiyamala Duraipandian, et al, 2019). (V. Baeten and M. Meurens. 1996)
13	2854.2	$-CH_2$	C-H symmetric stretching	β-carotene	0.419	(Hana Vaskova, et al. 2018). (Lauren E. Jamieson, et al. 2018). (Xiande Zhao, et al 2015)
14	2876.4	$C-H_2$	Symmetric stretching	β-carotene	0.400	(Lauren E. Jamieson, et al. 2018). (Qing Zhang, et al. 2011). (Xiande

						Zhao, et al 2015)
15	2901.5	CH_2	Asymmetric stretching	β-carotene	0.424	(Qing Zhang, et al. 2011). (R.M. El-Abassy, et al 2009)
16	2928.5	-CH2	C-H asymmetric stretching	β-carotene	0.423	(César Jiménez-Sanchidrián et al. 2016). (R.M. El-Abassy, et al 2009)
17	3009.5	Cis RHC=CH R	=C-H symmetric stretching	methyl linoleate	0.376	(César Jiménez-Sanchidrián et al. 2016). (Lauren E. Jamieson, et al. 2018). (Michał Szmatoła, et al.2018)

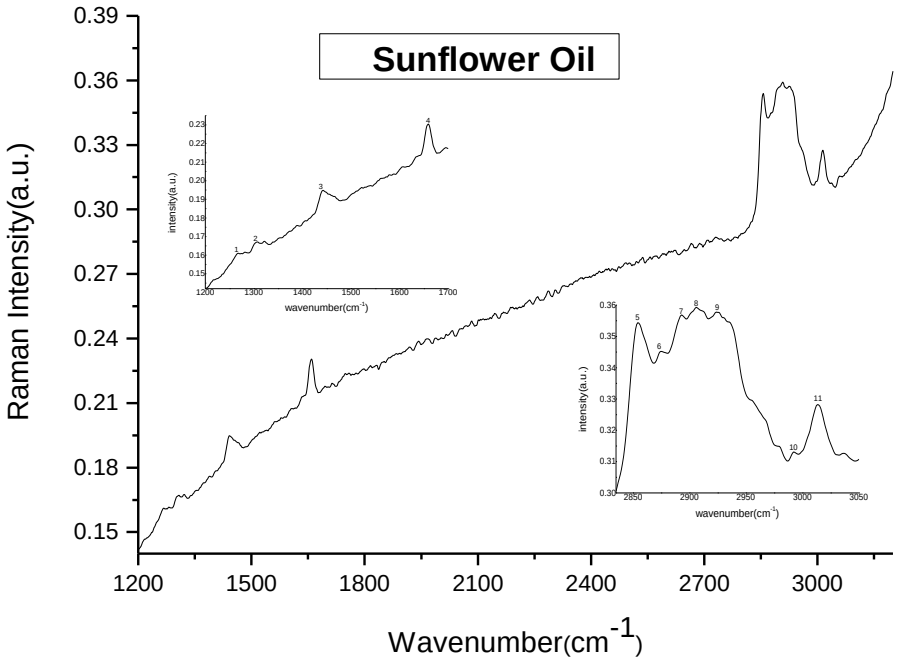

Figure (4.3) Typical Raman spectrum for Sunflower oil

Figure (4.3) shows the wavenumber region of 3200-900 cm^{-1} displayed provides a sufficient number of spectral peaks to afford unambiguous identification of the Sunflower Oil. It shows clear peaks and by comparison with the vibrations recorded in some

references, it was found that these vibrations are attributed to some bonds of Sunflower Oil as listed in Table (4.3).

Table (4.3) The wave number, intensities, and Functional Group/ Vibration of peaks in the Raman spectrum of the Sunflower oil.

Peak No	Wavenumber (cm^{-1})	Molecule/ group	Vibration mode	Compound	Intensity (a.u.)	Reference
1	1268.1	=C-H	Symmetric rock cis isomer	Chlorophyll a	0.161	(Hana Vaskova et al 2014), (Hewlett Packard, 1996), (P.NALLASAMY, et al.2000)
2	1303.7	$-CH_2$	C-H bending (twisting)	Alkene (unsaturated fatty acids	0.166	(César Jiménez-Sanchidrián et al. 2016), (Hana Vaskova, et al. 2018), (Shiyamala Duraipandian, et al, 2019)
3	1442.6	$-CH_2$	C-H bending (scissoring)	Methylene	0.194	(César Jiménez-Sanchidrián et al. 2016), (Michał Szmatoła, et al.2018), (V. Baeten, et al. 1996)
4	2854.2	$-CH_2$	C-H symmetric stretching	β-carotene	0.354	(Hana Vaskova, et al. 2018). (Lauren E. Jamieson, et al. 2018). (Xiande Zhao, et al 2015)
5	2874.5	C-H	Symmetric stretching	β-carotene	0.345	(Lauren E. Jamieson, et al. 2018). (Qing Zhang, et al. 2011). (Xiande Zhao, et al 2015)
6	2892.8	CH_3	symmetric stretching	β-carotene	0.356	(R.M. El-Abassy, et al 2009). (Xiande Zhao, et al 2015).
7	2906.3	CH_2	Asymmetric stretching	β-carotene	0.359	(Xiande Zhao, et al 2015).
8	2923.6	CH_2	Asymmetric aliphatic C-H stretching	β-carotene	0.357	(César Jiménez-Sanchidrián et.al. 2016)
9	2992.1	C=CH	Stretching	β-carotene	0.313	(César Jiménez-Sanchidrián et.al. 2016)
10	3013.3	=CH	Asymmetric olfinic C-H stretch	methyl linoleate	0.328	(Lauren E. Jamieson, et al. 2018). (R.M. El-Abassy, et al

						2009). (Thaís Karine de Lima, et al, 2020)

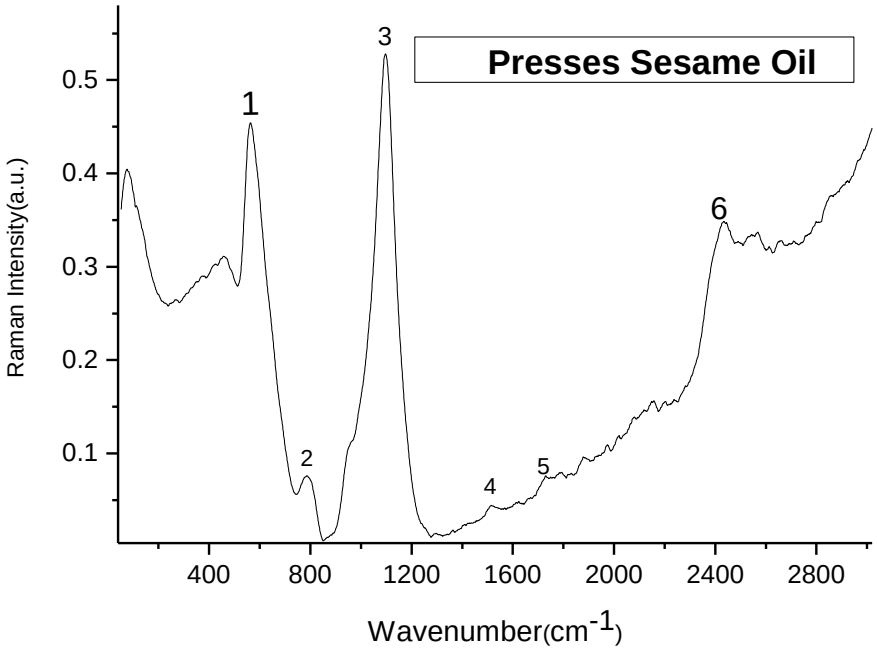

Figure (4.4) Typical Raman spectrum for Presses Sesame oil.

Figure (4.4) shows the Raman spectra of a Pressed Sesame Oil sample. In the region from (3000 to 50) cm^{-1} shown provides a number of spectral peaks to identify some bonds of the sample and compare the spectrum with previous studies of Sesame Pressed oil.

Table (4.4) the wavenumber, intensities, and Molecule Group/ Vibration of peaks in the Raman spectrum of the Pressed Sesame oil.

Peak N0	Wavenumber (cm^{-1})	Molecule/group	Vibration mode	Compound	Intensity (a.u.)	Reference
1	460	C=C-C	Bending In-plane		0.311	
2	785.9	CH_2	Rocking	Chlorophyll a	0.076	(Qing Zhang, et al. 2011).

3	1098.4	C=C	Stretching	Ester	0.528	(Qing Zhang, et al. 2011)
4	1523.6	RHC=CHR	C=C stretching	β-carotene	0.044	(HANA VASKOVA, et al. 2014), (R.M. El-Abassy, et al 2009), (Shiyamala Duraipandian, et al, 2019)
5	1730.6	RC=OOR	C=O stretching for ester	Carotenoid	0.075	(HANA VASKOVA, et al. 2014). (Hong Yan, et al, 2018)

Figure (4.5) Raman spectrum in the range from (3100 to 780) cm^{-1} of Factory Sesame Oil. It shows few peaks by comparison with the vibrations recorded in some references.

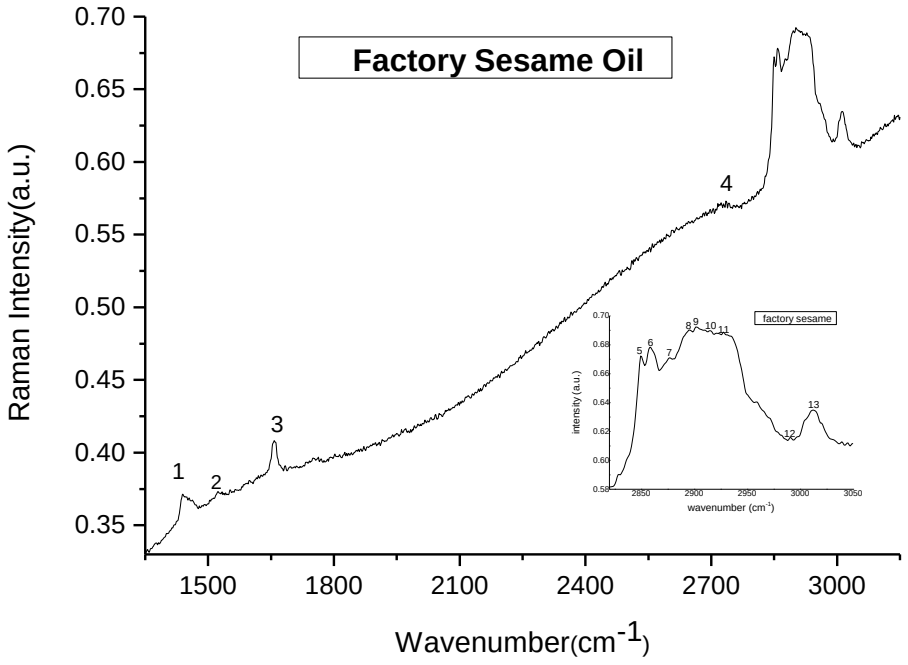

Figure (4.5) Typical Raman spectrum for Factory Sesame oil.

Table (4.5) the wavenumber, intensities, and Molecule Group/ Vibration of peaks in the Raman spectra of the Factory Sesame Oil

Peak N0	Wavenumber (cm^{-1})	Molecule/ group	Vibration mode	Compound	Intensity (a.u.)	Reference
1	1302.8	-CH2	C-H bending (twisting)	Alkene (unsaturated fatty acids	0.327	(César Jiménez-Sanchidrián et al. 2016), (Hana Vaskova, et al. 2018), (Shiyamala Duraipandian, et al, 2019)
2	1439.7	-CH2	C-H bending (scissoring)	Methylene	0.371	(César Jiménez-Sanchidrián et al. 2016), (Michał Szmatoła, et al.2018), (V. Baeten, et al. 1996)
3	1523.6	RHC=CH R	C=C stretching	β-carotene	0.373	(HANA VASKOVA, et al. 2014), (R.M. El-Abassy, et al 2009), (Shiyamala Duraipandian, et al, 2019)
4	1657.6	Cis RHC=CH R	C=C double bond stretching	Methyl linolenate	0.408	(César Jiménez-Sanchidrián et al. 2016). (Hong Yan, et al, 2018). (Lauren E. Jamieson, et al. 2018)
5	2728.9	Carbonyl group	Fermi resonance	Carbony	0.571	(Qing Zhang, et al. 2011)
6	2849.4	-CH2	C-H symmetric stretching	β-carotene	0.672	(César Jiménez-Sanchidrián et al. 2016). (Michał Szmatoła, et al.2018). (R.M. El-Abassy, et al 2009)
7	2858.1	CH2	Symmetric aliphatic CH stretching	β-carotene	0.678	(R.M. El-Abassy, et al 2009)
8	2877.4	CH2	Symmetric stretching	β-carotene	0.670	(César Jiménez-Sanchidrián et al. 2016). (Qing Zhang, et al. 2011). (Xiande Zhao, et al 2015).
9	2895.7	-CH3	C-H symmetric stretching	β-carotene	0.690	(R.M. El-Abassy, et al 2009). (Xiande Zhao, et al 2015).
10	2901.5	CH2	Asymmetric stretching	β-carotene	0.692	(Qing Zhang, et al. 2011). (R.M. El-

						Abassy, et al 2009)
11	2927.5	CH2	Asymmetric aliphatic CH stretching	β-carotene	0.688	(César Jiménez-Sanchidrián et al. 2016). (R.M. El-Abassy, et al 2009)
12	2991.1	C=CH	Stretching	Alkane	0.615	(César Jiménez-Sanchidrián et.al. 2016)
13	3012.4	=CH	C-H Asymmetric olefinic stretching	methyl linoleate	0.634	(Lauren E. Jamieson, et al. 2018). (R.M. El-Abassy, et al 2009). (Thaís Karine de Lima, et al, 2020

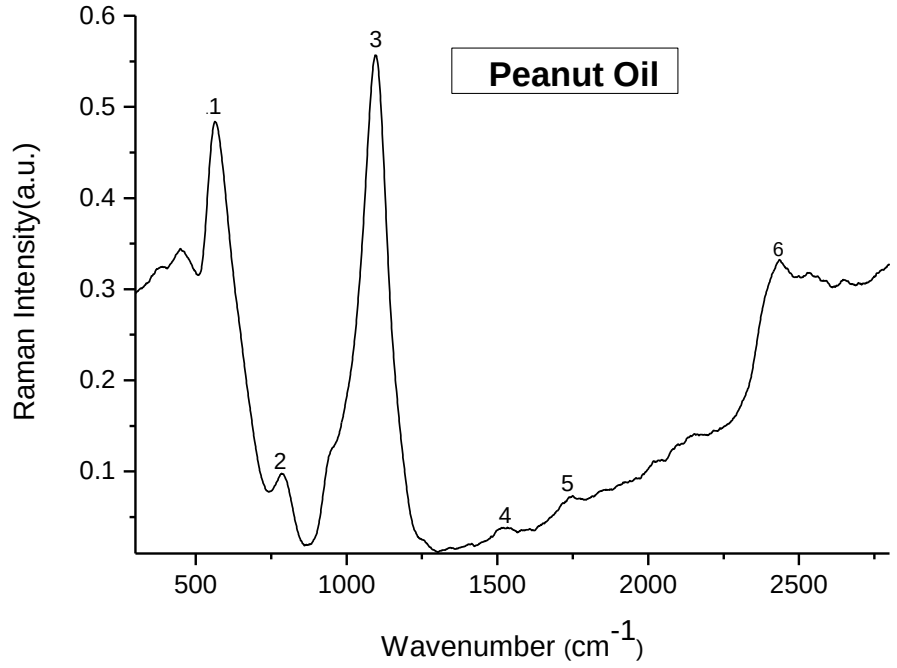

Figure (4.6) Typical Raman spectrum for Peanut oil.

Figure (4.6) show the spectrum of Peanut Oil the range from (2800 to 300) cm^{-1}, depicting the characteristics bands of saturated and unsaturated fats. In each figure, the significant Raman spectral features. The Raman features associated with the saturation are contributed. It shows clear peaks and by comparison with the vibrations recorded in some references, it was found that these

vibrations are attributed to some components of other materials as listed in Table (4.6)

Table (4.6) the wavenumber, intensities, and Molecule Group/ Vibration of peaks in the Raman spectra of the Peanut oil.

Peak N0	Wavenumber (cm^{-1})	Molecule/ group	Vibration mode	Compound	Intensity (a.u.)	Reference
1	585.7	-	-		0.483	-
2	785.0	CH2	Rocking	Chlorophyll a	0.097	(Qing Zhang, et al. 2011).
3	1097.4	C=C	Stretching	Ester	0.556	(Qing Zhang, et al. 2011)
4	1517.8	RHC=CH R	C=C stretching	Lutein	0.038	(R.M. El-Abassy, et al 2009)
5	1748.2	RC=OOR	C=O stretching	Trielaidin (ester)	0.073	(César Jiménez-Sanchidrián et al. 2016). (HANA VASKOVA, et al. 2014). (Shiyamala Duraipandian, et al, 2019)

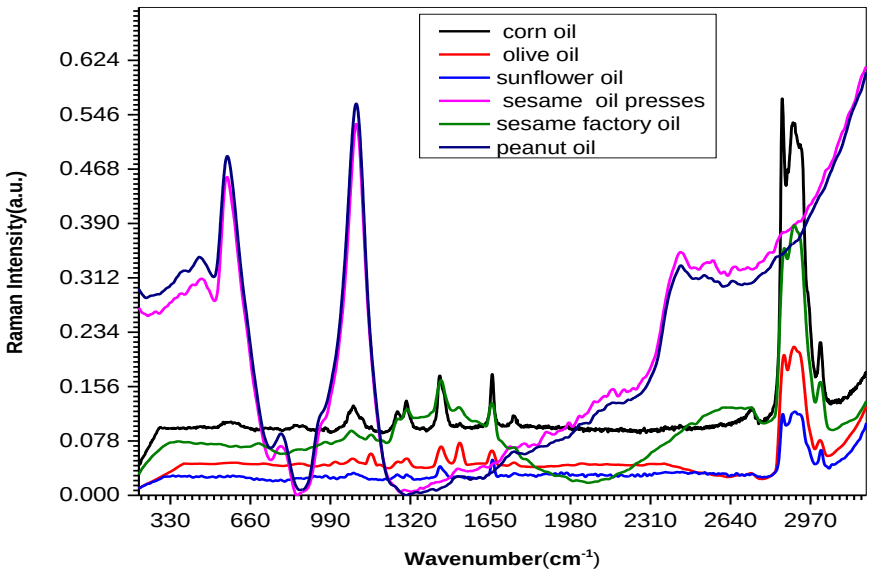

Figure (4.7) Typical Raman spectra for (corn, olive, factory sesame, peanut, presses sesame and sunflower) oil

Through the analysis of the six samples oils collected from Khartoum area it was found that the vibration modes of some sample are appeared in all the samples while other modes are appeared in some samples and disappeared in other samples.

In the region from the beginning of the spectrum to 600 cm^{-1}, bands appeared in this region of several oils, corn oil 580 cm^{-1}, pressed sesame oil 80cm^{-1} and 567cm^{-1}, and peanut oil at 448cm^{-1} and 585cm^{-1}, see figures (4.1, 4.4, 4.6).

In the fingerprint region, the range between (600 and 1800) cm^{-1}. This region gets its name from the variety of localized micro-spectral properties that give particles their unique "fingerprints". Molecular fingerprints can allow classification of samples and the chemical analysis. Bands appeared in this region in all samples. see figures (4.1 to 4.6).

The "silent region ", this spectral region of (1800 to 2500) cm^{-1} is mostly devoid of contributions from biological molecules, although there are some exceptions. Bands in this range only appeared in presses sesame oil, peanut oil. It was not possible to interpret the results in this region. See tables (4.4, 4.6).

In figures (4.1, 4.2, 4,3, and 4.5) the range from (2500 to 3400) cm^{1}, which is known as the "high wavenumber region" From the Raman spectrum. Changes in Raman ranges in the region of cm^{-1} are related to modifications of expansion vibrations C–H. Raman indicates the homologous expansion of CH_2, antagonist expansion of CH_2 symmetry, and symmetric stretching movement of CH_3, respectively. This region appears in corn, olives, sunflower, and factory sesame.

The 2800–3020 cm^{-1} region exhibited four bands at. 2858, 2877, 2901, and 2927 cm^{-1} typical of C–H stretching vibrations in

methyl and methylene groups in addition to a fifth band above 3012 cm^{-1} corresponding to =C–H– stretching vibrations. Obviously, these bands should be largely due to the major fatty acid in the oils: oleic acid (see Tables 4.1, 4.2, 4.3, 4.5).

Cis-trans appeared in the bands of corn at (969.1, 1266.1, 1657.6) cm^{-1}, olives at (970.1, 1268.1, 1657.6) cm^{-1} sunflower at (1268.1) cm^{-1} and factory sesame at (1657.6) cm^{-1}. **Cis**-trans isomerism is a direct result of the high energy barrier of rotation at the double bond it is most often encountered in unsaturated compounds. Groups can be arranged around C = C, =CH spatially to give two types of isomers it is called **Cis** (Latin for the same side) and Trans (Latin for the cross). The two shapes it has the same molecular formula but differs in structure. **Cis** and Tran's isomers have different solubility Points and boiling points [P. NALLASAMY P. M. ANBARASAN, S. MOHAN. (06.10.2000)]. See tables (4.1, 4.2, 4.3, 4.5).

The main difference between low-quality and high-quality edible oils is the appearance of the two vibration modes at 1155 cm^{-1} and 1525 cm^{-1}. In an oil samples, these two modes can be observed in high quality (corn, olive, factory sesame) oil, while in a low-quality oil samples, these two modes cannot be detected. Also, the intensity of these two modes varies with the free fatty acids (FFA) content in edible oils samples. The mode at 1155 cm^{-1} can be assigned to C–C stretching of carotenoids, and the mode at 1525 cm^{-1} can be assigned to C=C stretching of carotenoids. The carotenoids play an important role as natural antioxidants in edible oils. From this, the best oils for use are corn, olive and factory sesame oils

Raman band at 970 cm^{-1} has also been labeled for fatty acid methyl esters, and its relative concentration in cold press oil (olive) samples is higher than the others.

The carbonyl group or C = O is the ideal functional group to detect utilizing infrared spectroscopy (IR) because the peak of the expansion vibration is intense and located in a unique wavelength range. It did not appear in the pomegranate studies, but in the research, it was found at the band at 2728 cm^{-1} in corn oil and factory Sesame oil. See tables (4.1 and 4.4).

Obviously, the band intensities at 1265 and 1654 cm^{-1}, corresponding to the cis (=C–H) vibration and cis (C=C) vibration, respectively, which have a high correlation with unsaturated fatty acids in the oils

The spectra for (corn, olive, sunflower, factory sesame) oils were similar and contained the typical strong bands at (267, 1302, 1442, 1655, 1747, 2852 and 2970) cm^{-1}. See figure (4.7) and tables (4.1, 4.2, 4.3, 4.5).

From the figure (4.7) shows the similarity between the Raman spectrum for each of the corn, olive, factory sesame and sunflower oils, and the spectra are similar to the previous studies of oils.

The most substantial differences from figure (4.7) were those in the (1200–1800) cm^{-1} region. From the figure (4.7) there is a big difference between the Raman spectrum of factory sesame oil and presses sesame oil, but the Raman spectrum of peanut oil and presses sesame oil are identical. Detection of adulteration of pressed sesame oil mixed with peanut oil. To confirm this result, more samples must be studied.

4.3 Results and Discussion of FTIR Spectroscopy

To have a good understanding of the relationship between the FTIR spectrum of vegetable oils and it is chemical component structures and to achieve a proper analysis of the FTIR spectrum, all the specific information, including absorption band, corresponding functional group, vibration mode, and intensity**.**

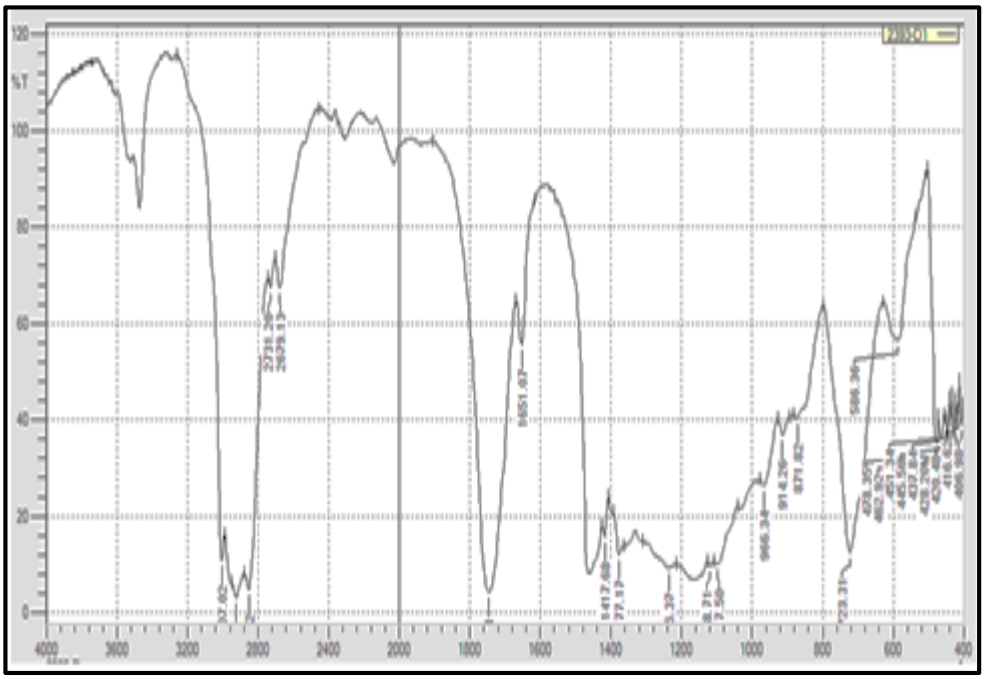

Figure (4. 8) Typical FTIR spectra for corn oil

Table (4.7) FTIR assignment for corn oil

Wavenumber (cm^{-1})	Assignment	Remark	Compound	Intensity (a.u.)
723.31	-(CH2)n-	Rocking(out of plane)	carbon skeleton	12.42
914.26	-HC=CH- (cis)	Bending (out-of plane)	vinyl group	38.76
966.34	-HC=CH- (trans)	Bending (out-of plane)	conjugated linoleic acids	28.38
1097.50	-C-O	Stretching	Ester	10.05
1118.71	-C-O	Stretching	Ester	9.82
1236.37	-C-H (CH2)	Bending	Methylene	9.35
1377.17	-C-H (CH3)	Bending (sym)	Methylene	12.07
1417.68	=C-H (cis)	Stretching (asym)	alkyl groups	15.79
1651.07	C=O (cis)	Stretching	protein	55.77
1747.51	C=O	Anhydride	Aldehyde	56
2679.13	Carbonyl group	Fermi resonance		67.46
2731.20	O=C-H	Rocking overtone		67.29
2852.72	-C-H (CH2)	Stretching (sym)	Dodecane	4.75

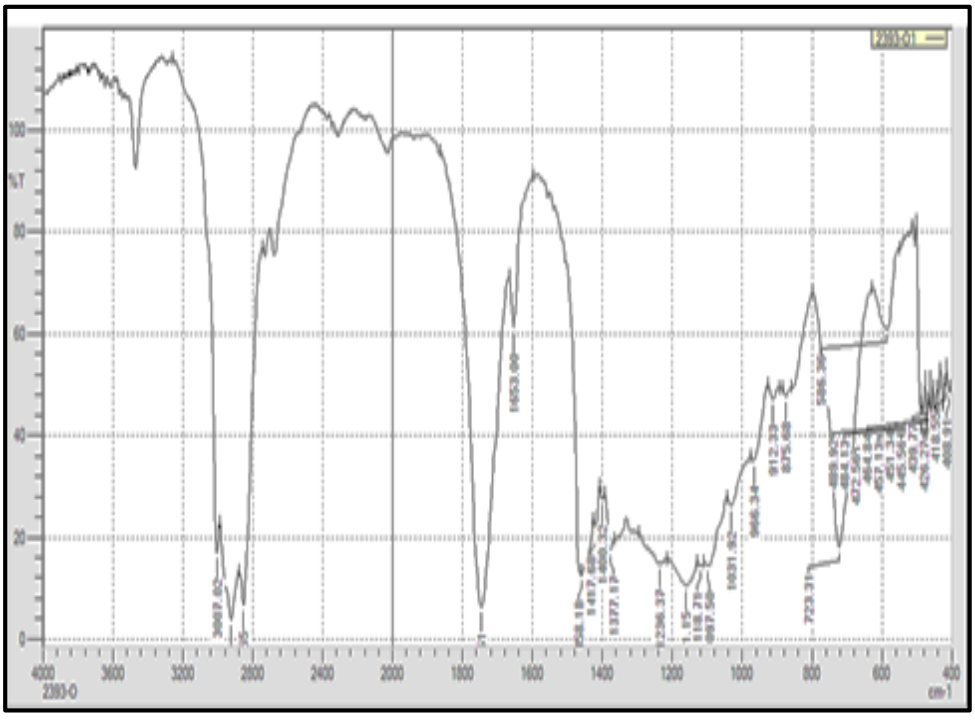

Figure (4.9) Typical FTIR spectra for Olive oil

Table (4.8) FTIR assignment for Olive oil

Wavenumber (cm^{-1})	Assignment	Remark	Compound	Intensity (a.u.)
723.31	-(CH2)n	Rocking (out of plane)	carbon skeleton	18.02
912.33	-HC=CH- (cis)	Bending (out-of plane)	vinyl group	47.23
966.34	-HC=CH- (trans)	Bending (out- plane)	conjugated linoleic acids	35.22
1031.92	C-O	Stretch	Ester	26.26
1097.50	C–N	Stretch	Ester	14.40
1118.71	-C-O	Stretching	Ester	14.37
1161.15	C–N	Stretch	Triglyceride	10.57
1236.37	-C-H (CH2)	Bending	Methylene	14.83
1377.17	-C-H (CH3)	Bending (sym)	Methylene	17.48
1400.32	=C-H (cis)	Bending		27.59
1417.68	=C-H (cis)	Bending (rocking)	alkyl groups	21.33
1458.18	-C-H (CH3)	Stretching (asym)	Methylene	12.70
1653.00	C=O (cis)	Stretching	Protein	61.27
1747.51	C=O	Stretch	Aldehyde	6.30
2854.65	C–H	Stretch	dodecane	6.79
2924.09	C–H	Stretch	Methylene	3.93
3007.02	=C-H (cis)	Stretching	Olefinic	17.04

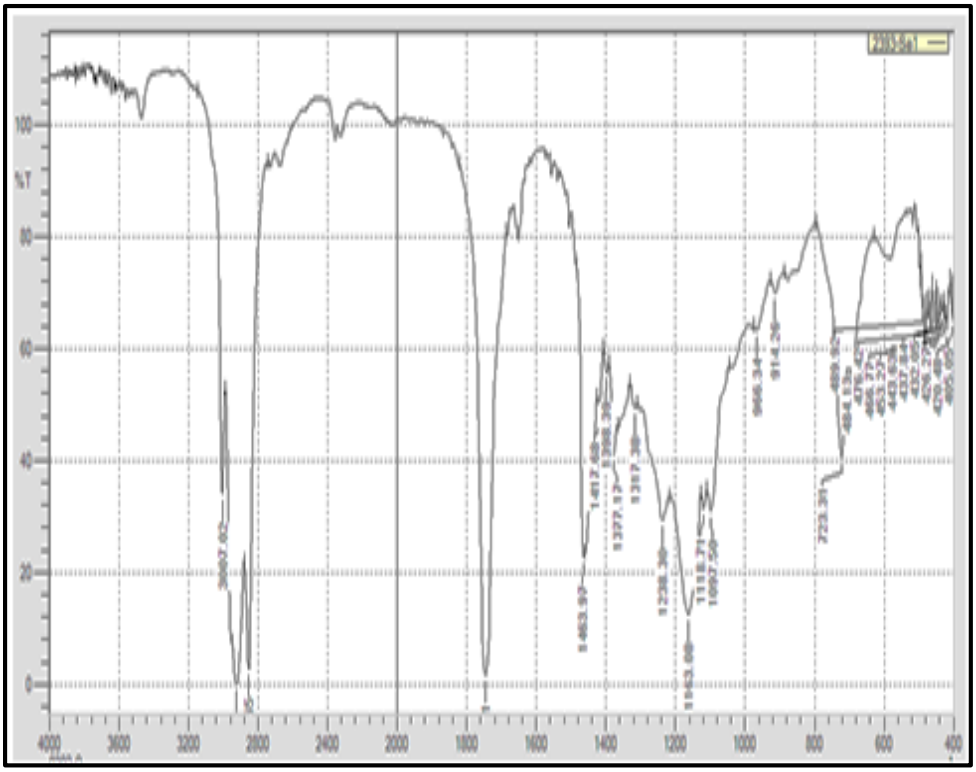

Figure (4.10) Typical FTIR spectra for sesame oil

Table (4.9) FTIR assignment for sesame oil

Wavenumber (cm^{-1})	Remark	Assignment	Compound	Intensity (a.u.)
723.31	$-(CH_2)_n-$	Rocking (out of plane)	carbon skele	18.02
912.33	-HC=CH- (cis)	Bending (out of plane)	vinyl group	47.23
966.34	-HC=CH (trans)	Bending (out of plane)	conjugated linoleic acids	35.22
1031.92	C-O	Stretching	Ester	26.26
1097.50	-C-O	Stretching	Ester	14.40
1118.71	-C-O	Stretching	Ester	14.37
1163.08	-C-H (CH_2)	Bending	Triglyceride	10.57
1238.30	-C-H (CH_2)	Bending	Methylene	14.83
1377.17	-C-H (CH_3)	Bending (sym)	Methylene	17.48
1398.39	=C-H (cis)	Bending	-	27.59
1417.68	=C-H (cis)	Bending (rocking)	alkyl groups	21.33
1463.97	-C-H (CH_2)	Scissoring	Methylene	12.70
1747.51	-C=O	Stretching	Aldehyde	6.30
28.54.65	-C-H (CH_2)	Stretching (sym)	Dodecane	6.79
2924.09	-C-H (CH_2)	Stretching (asym)	Methylene	3.93
3007.02	=C-H (cis)	Stretching	Olefinic	17.04

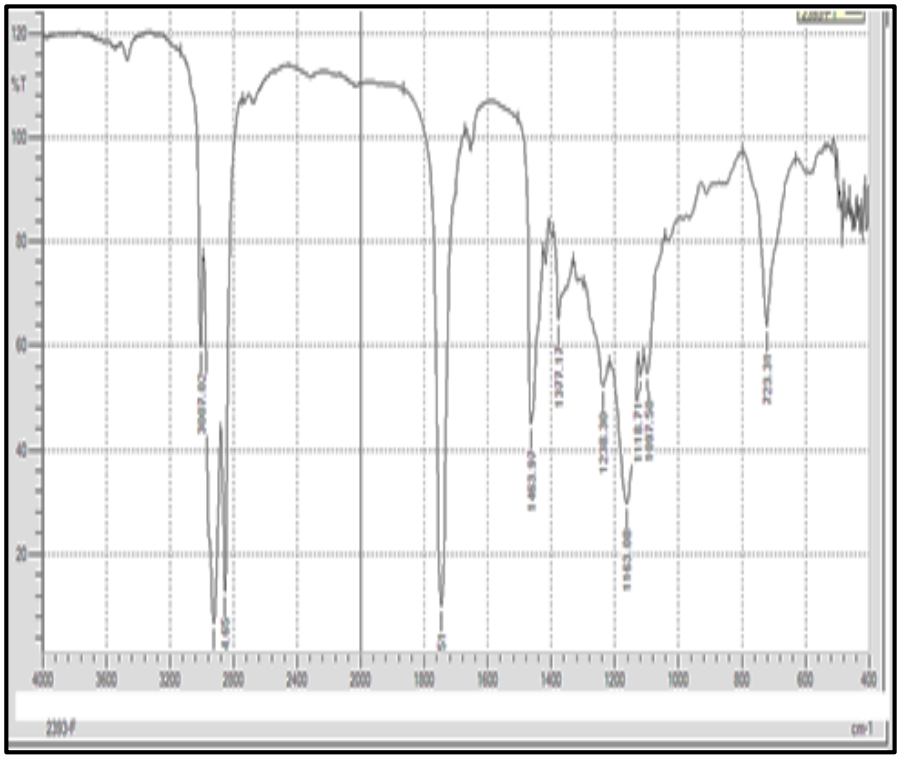

Figure (4.11) Typical FTIR spectra for Peanut oil

Table (4. 10) FTIR assignment for Peanut oil

Wavenumber (cm^{-1})	Remark	Assignment	Compound	Intensity (a.u.)
723.31	-(CH2) n-	Rocking (out of plane)	carbon skeleton	63.72
1097.50	-C-O	Stretching	Ester	54.52
1118.71	-C-O	Stretching	Ester	54.29
1163.08	-C-H (CH2)	Bending	Triglyceride	29.66
1238.30	-C-H (CH2)	Bending	Methylene	52.35
1377.17	-C-H (CH3)	Bending (sym)	Methylene	65.07
1463.97	-C-H (CH2)	Scissoring	Methylene	45.17
1747.51	C=O	Stretch	Aldehyde	10.20
2854.65	-C-H (CH2)	Stretching (sym)	dodecane	12.93
2924.09	-C-H (CH2)	Stretching (asym)	methylene	6.72
3007.02	=C-H (cis)	Stretching	olefinic	58.86

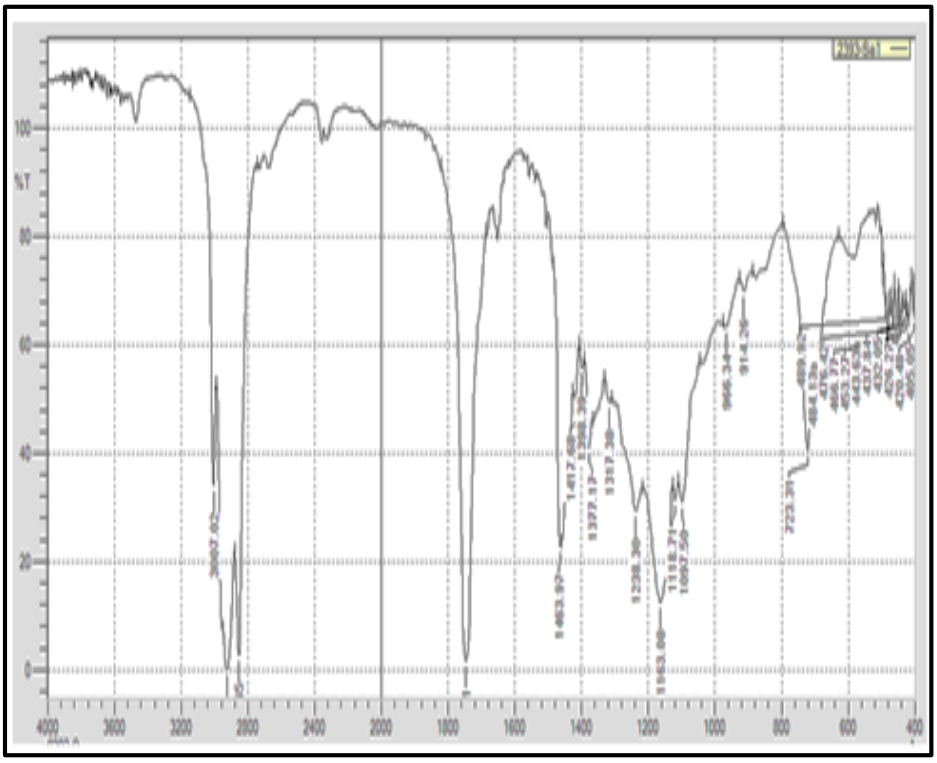

Figure (4.12) Typical FTIR spectra for Sunflower oil

Table (4.11) FTIR assignment for Sunflower oil

Wavenumber (cm^{-1})	Remark	Assignment	Compound	Intensity (a.u.)
723.31	-(CH2)n-	Rocking (out of plane)	carbon	37.78
914.26	-HC=CH- (cis)	Bending (out-ofplane)	vinyl group	69.66
966.34	-HC=CH- (trans)	Bending (out-ofplane)	linoleic acids	63.40
1097.50	-C-O)	Stretching	Esters	31.05
1118.71	-C-O	Stretching	Esters	31.44
1163.08	-C-H (CH2)	Bending	Triglyceride	12.60
1238.30	-C-H (CH2)	Bending	Methylene	29.41
1377.17	-C-H (CH3)	Bending (sym)	Methylene	40.96
1398.39	=C-H (cis)	Bending	-	55.72
1417.68	=C-H (cis)	Bending (rocking)	alkyl groups	48.34
1463.97	-C-H (CH2)	Scissoring	Methylene	22.79
1747.51	C=O	Stretching	Aldehyde	1.73
2854.65	-C-H (CH2)	Stretching (sym)	Dodecane	2.74
2926.01	-C-H (CH2)	Stretching (asym)	Methylene	0.22
3007.02	=C-H (cis)	Stretching	Olefinic	34.23

IR spectra of the (corn, olive, peanut, factory sesame, and sunflower) oils are presented in Fig. (4.8 to 4.12).

Infrared spectroscopy (IR) is conventionally divided into three wavelength regions: the near-infrared (NIR: 750–2500 nm or 13 333–4000 cm^{-1}), mid-infrared (MIR:2500–25 000 nm or 4000–400 cm^{-1}), and far-infrared (25–1000 μ m or 400–10 cm^{-1}).

It is well known that every oil or fat differs in composition, length and unsaturated degree of the fatty acids as well as their positions in the chain. The triglyceride, which is a major component in edible oils and fats, was dominant in the spectra.

Even though the spectra of all the tested vegetable oils demonstrated very similar, their absorbance units were found as different from each other depending on the functional groups of the oils.

The whole spectra between 400 and 4000 cm^{-1} are the combination of many constituents of oils whereas the region selected between 1400 and 1800 cm^{-1} mostly represents the combination of C–H bending, C=O stretching, and C=C stretching and hence is directly related to unsaturated C=C bond.

In the IR spectra, the major bands in oil samples can be attributed to the following vibrations: 723 cm^{-1} (overlapping of the CH_2 rocking vibration and the out-of-plane vibration if cis-disubstituted olefins), (1163 and 1238) cm^{-1} (stretching vibration of the C-O ester groups), 1377 cm^{-1} (bending vibrations of CH_2 groups), 1417 cm^{-1} (rocking vibrations of CH bonds of cis-disubstituted olefins), 1654 cm^{-1} (C=C stretching vibration of cis-olefins).

At ~1,750 cm^{-1}, a strong band arises from the ester linkage attaching fatty acids to the glycerol backbone of triglycerides.

These IR spectra was known as general absorption bands of triglycerides (1747 cm^{-1} C=O of triglycerides or esters).

Small peak seemed at 3007 cm^{-1} associated with the stretching of cis double-bond (=CH). One of the greatest peaks were observed at around 2923 and 2854 cm^{-1} which results from the asymmetric or symmetric stretching vibration of the aliphatic CH_2.

The most important spectral, however, appear in the fingerprint region. Two bands near 1121 and 1098 cm^{-1} show interesting spectral features. The absorbance intensity in the vicinity of 1121 cm^{-1} shows a positive correlation with the amount of oleic acid, whereas the intensity near 1098 cm^{-1} is correlated with the amount linoleic acid. In addition, the peak centered at 913 cm^{-1} is very weak in high oleic, but it is more intense in the samples rich in polysaturated fatty acids.

The peaks detected at 3007, 2924 and 2852 cm^{-1} are attributed with the stretching of hydrogen bonds. At higher wavenumbers, stretching is occurred with the double bonds associated in the structure of vegetable oils.

Edible oils contain mainly triacylglycerols, including three long chain fatty acids attached via ester links. The IR regions of 2924–2853, 1747 cm^{-1} are attributed to the fatty acid chain length and the absorption of free fatty acids (FFAs), also at 723 cm^{-1}, the increased absorption intensity indicates the oxidation to alcohols or secondary oxidized products.

The fingerprint region from 1500–900 cm^{-1} is generally used to identify their authenticity: the out-of-plane bending vibrations of isolated trans double bonds ranges between 967–969 cm^{-1}, while those of cis double bonds occur at approximately 914 cm^{-1}.

The degree of unsaturation of oils can be detected through characteristics of cis and trans peaks at 3006 and 968 cm^{-1}, respectively, while a second band at 975 cm^{-1}, is associated also to secondary oxidation products (aldehydes and ketones with trans-double bonds).

Also, if we examine again the FTIR spectra of olive oil and corn oil, we will find an important peak ascribed to the very weak stretching of the C=O of the acid group located at 1653 cm^{-1} with considerable absorption intensity and this peak appears as a shoulder of the very strong band of the C=O stretching band of the ester group located at 1747 cm^{-1}. This peak is considered as an important tool because it represents the acidity of the oil.

Concomitantly, an increase in absorption at 1747 cm^{-1} is associated with the carboxyl group of FFAs, associated with the carbonyl group of aldehydes.

For an edible oil, the higher-frequency end of the spectrum (3700–3400 cm^{-1}) corresponds to hydroxyl groups (e.g., water and hydroperoxides). If an edible oil sample is clean, dry, and mostly unoxidized, there is no appreciable MIR absorption in this region.

The 1950-1450 cm^{-1} region exhibits IR absorption from a wide variety of double-bonded chemical groups, in particular C=O. This region is of particular importance for investigations of biological molecules. Conjugation, ring size, hydrogen bonding, steric and electronic effects often result in significant shifts in absorption frequencies.

4.4 Results and Discussion of UV-VIS Spectroscopy

This work was devoted to the detection of the total quantitative components of carotenoids and chlorophyll derivatives, as they are responsible for the color, which is an important qualitative characteristic of the oil because it contains antioxidants. Some optical properties of edible oils used in Sudan (corn, olive, peanut, factory sesame, pressed sesame, and sunflower) oil. The absorbance spectrum reflects the organization of the conjugated double bond system and constitutes the fingerprint of pigments. Absorbance spectroscopy considered to be the simplest way to identify major pigments present in an oils. The absorption properties of vegetable oils depend on the content of pigment components such as chlorophylls, pheophytins, carotenoids, and lutein

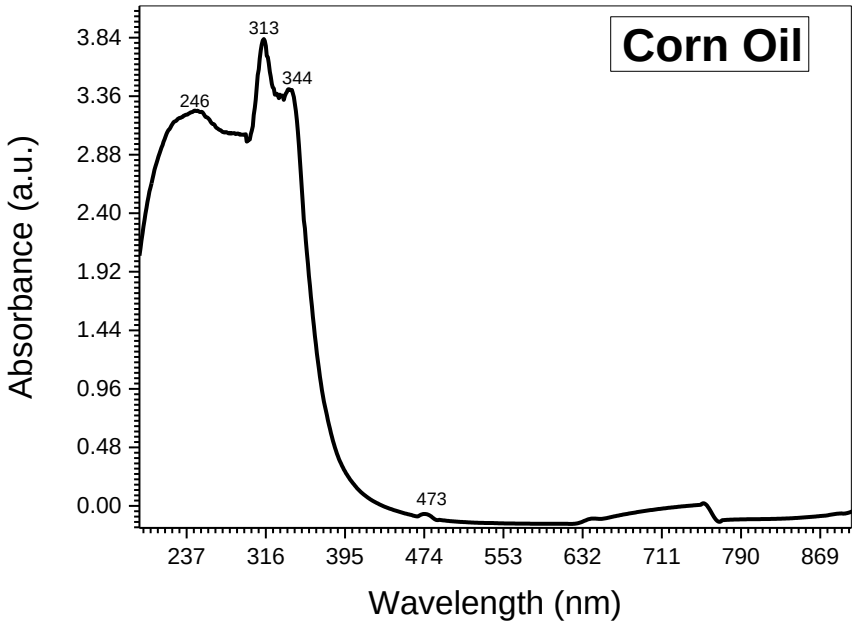

Figure (4.13) absorption spectra of corn oil

Table (4.12) analyzed data of UV-VIS spectrum of Corn

Peak Center (nm)	Amplitude (a.u.)	Pigment	Reference
246	3.235	conjugated dienes	(Oguz Uncu, Banu Ozen, 2019)
313	3.999	Polyphenols	(Francieli C.G.B.S. Alves, et al, 2018)
344	3.413	Polyphenols	(Francieli C.G.B.S. Alves,et al, 2018)
473	-0.066	Lutein	(Cristina Lazzerini, et al, 2016)

Absorption intensities acquired for the corn oil plotted as the function of wavelength is shown in Figure (4.12) and table (4.11). It can be seen that the corn oil sample exhibits differences in absorbance, making it possible to distinguish between the corn oil and other five types of oil samples on the basis of their absorption spectra. Absorbs at the wavelengths are 246 nm, 313 nm, 344 nm and 473 nm. It is universally acknowledged that these four peaks, contributed by dienes 246 nm, Polyphenols (313 and 344) nm, and Lutein pigments at 473 nm. The absorption spectrum of lutein shows weak absorption band. Corn oil does not show the pigment absorption peaks of chlorophyll, so it has a light yellow or colorless color

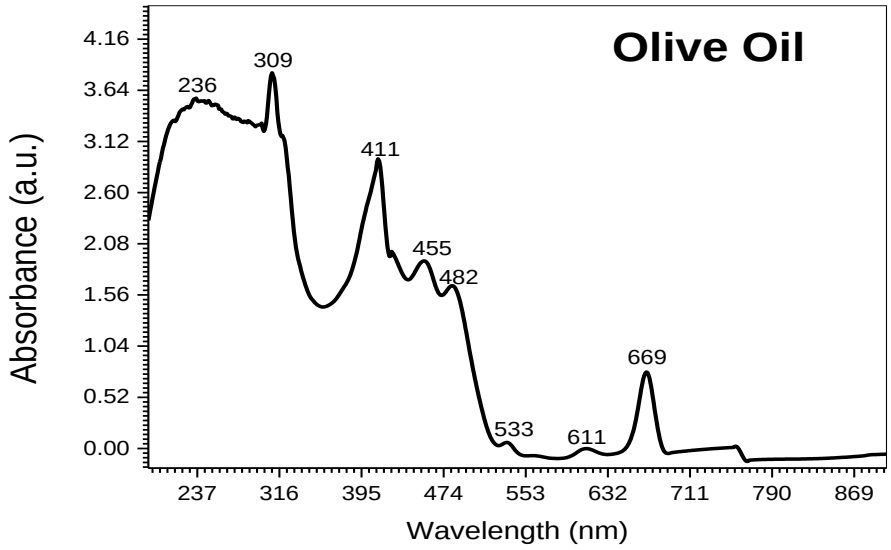

Figure (4.14) absorption spectra of Olive Oil

Table (4.13) The analyzed data of UV-VIS spectrum of olive oil

Peak Center (nm)	Amplitude (a.u.)	Pigments	Reference
236	3.560	Conjugated dienes	(Oguz Uncu, Banu Ozen, 2019), (Chmielarz, et al, 1995)
309	3.818	polyphenolic	(Francieli C.G.B.S. Alves,et al, 2018)
411	2.945	Carotenoids	(Karla Danielle Tavares Melo Milanez, et al, 2017)
455	1.905	Lutein	(Valentina Domenici, et al, 2014)
482	1.654	Lutein	(Mínguez - Mosquera, et al, 1990)
533	0.0565	Carotenoids	(M Rinawati, 2020)
612	-0.002	Chlorophyll	(Mínguez - Mosquera, et al, 1990)
669	0.777	Pheophytin-a	(Oguz Uncu, 2019), (Jose. Cayuela et al, 2014), (Valentina Domenici, et al, 2014)

Absorption intensities acquired for the olive oil plotted as the function of wavelength is shown in Figure (4.14) and table (4.13) It can be seen that the olive oil sample exhibits differences in absorbance, making it possible to distinguish between the olive oil and other five types of oil samples on the basis of their absorption spectra. The absorption spectrum of olive oil presents some characteristic bands that correspond to lutein, carotenoid and chlorophyll pigments, respectively, in which the lutein contributes a strong band with several peaks between 455 and 482 nm, carotenoid contribute a weak band with several peaks between 411 and 533 nm and the chlorophylls contribute another strong band at approximately 612 and 670 nm. The Conjugated dienes appearance from the beginning of the spectrum at 236 nm. polyphenolic compounds which show absorption at 309 nm. These compounds have an impact on the sensorial and quality aspects, and also have relationships with the health benefits. polyphenolic compounds are one of the secondary polar components for edible oils.

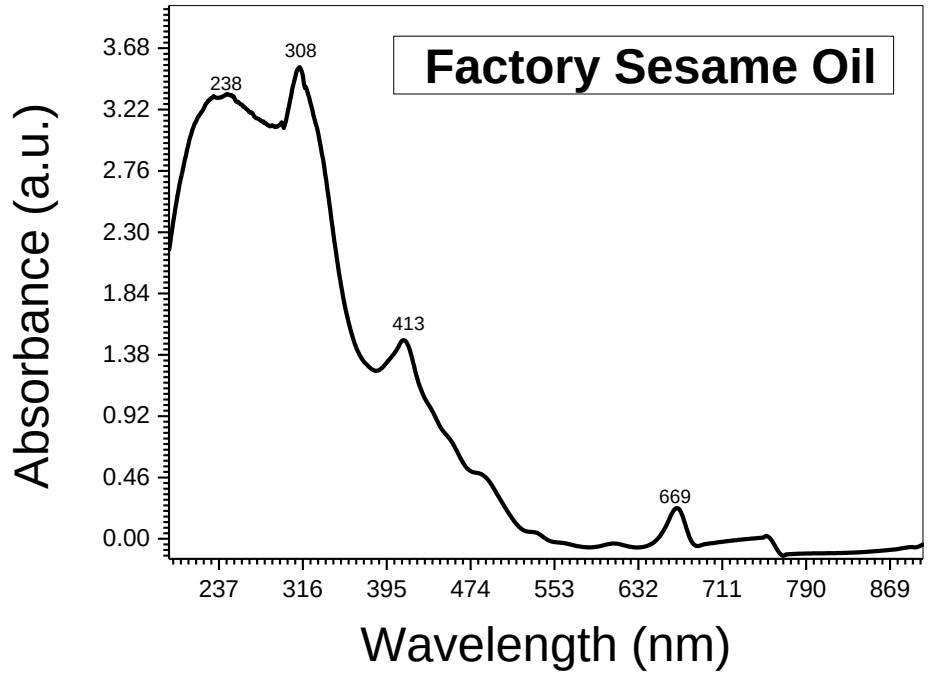

Figure (4.15) absorption spectra of Factory Sesame Oil

Table (4.14) The analyzed data of UV-VIS spectrum of Factory Sesame Oil

Peak Center (nm)	Amplitude (a.u.)	Pigments	Reference
238	3.310	Conjugated dienes	(Oguz Uncu, Banu Ozen, 2019), (Chmielarz, et al, 1995)
308	3.999	polyphenolic	(Francieli C.G.B.S. Alves,et al, 2018)
413	1.504	Carotenoid	(Valentina Domenici, et al, 2014)
669	0.241	pheophytin-a	(Oguz Uncu, 2019), (Jose. Cayuela et al, 2014), (Valentina Domenici, et al, 2014)

The absorption spectrum of factory sesame oil shown in Figure (4.15) and table (4.14) presents characteristic bands that correspond to Conjugated dienes appearance from the beginning

of the spectrum at 238 nm, polyphenolic compounds which show absorption at 308 nm, carotenoid contribute a weak band at 413 and pheophytin-a pigments, in which a strong band with peak at 669 nm.

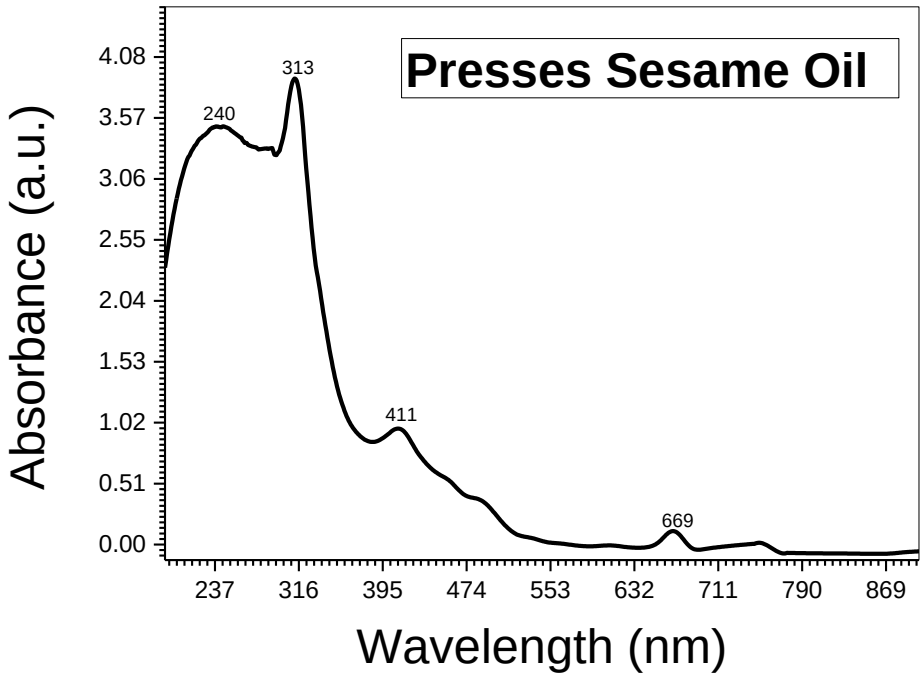

Figure (4.16) absorption spectra of Presses Sesame Oil.

Table (4.15) The analyzed data of UV-VIS spectrum of Presses sesame oil

Peak Center (nm)	Amplitude (a.u.)	Pigments	Reference
240	3.511	Conjugated dienes	(Oguz Uncu, Banu Ozen, 2019), (Chmielarz, et al, 1995)
313	4.102	polyphenolic	(Francieli C.G.B.S. Alves,et al, 2018)
411	0.980	Carotenoid	(Karla Danielle Tavares Melo Milanez, et al, 2017)
669	0.126	Pheophytin-a	(Oguz Uncu, 2019),

			(Jose. Cayuela et al, 2014), (Valentina Domenici, et al, 2014)

The absorption spectrum of presses sesame oil shown in Figure (4.16) and table (4.15) presents characteristic bands that correspond to Conjugated dienes appearance from the beginning of the spectrum at 240 nm, polyphenolic compounds which show absorption at 313nm, carotenoid contribute a weak band at 411 and pheophytin-a pigments, in which a strong band with peak at 669 nm.

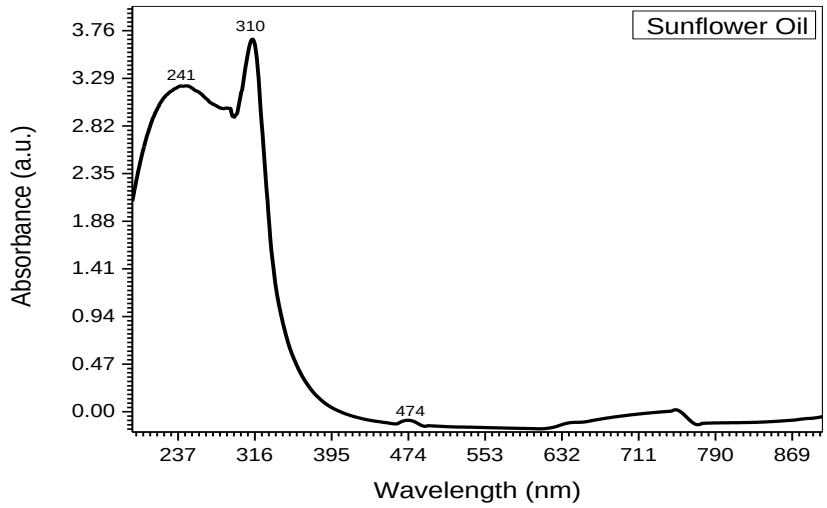

Figure (4.17) absorption spectra of Sunflower Oil

Table (4.16) The analyzed data of UV-VIS spectrum of Sunflower oil

Peak Center (nm)	Amplitude (a.u.)	Pigment	Reference
241	3.228	Conjugated dienes	(Oguz Uncu, Banu Ozen, 2019), (Chmielarz, et al, 1995)
310	3.901	polyphenolic	(Francieli C.G.B.S. Alves,et al, 2018)
474	-0.0522	Lutein	(Cristina Lazzerini, et al, 2016)

The acquired absorption intensity of sunflower oil plotted as a function of wavelength is shown in Figure (4.17) and table (4.16). It can be seen that the sunflower oil sample shows differences in absorbance, the first band was contributed by Dines at 241 nm, second band by Polyphenols 310 nm, and the last band by

pigments Lutein at 474 nm. Lutein absorption spectrum shows a weak absorption range. Sunflower oil does not show the pigment absorption peaks of chlorophyll, so it is light yellow.

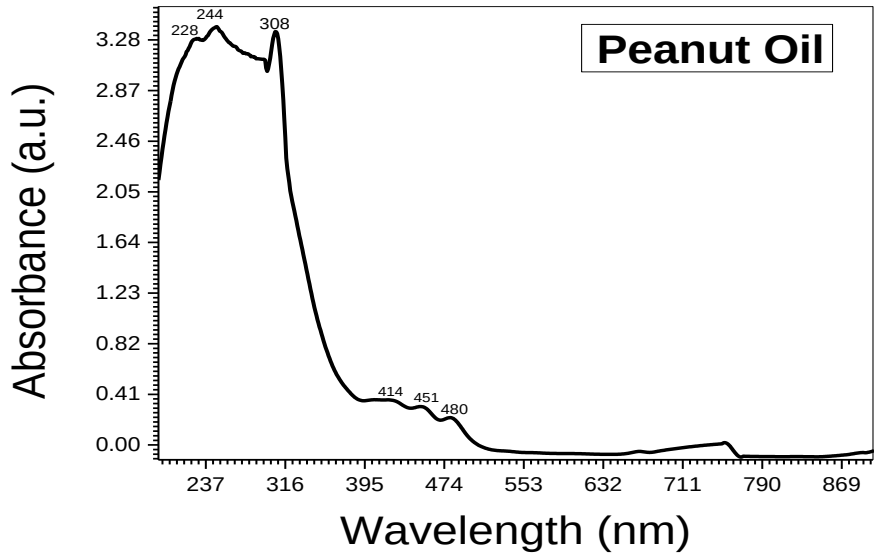

Figure (4.18) absorption spectra of Peanut Oil

Table (4.17) analyzed data of UV-VIS spectrum of Peanut oil

Peak Center (nm)	Amplitude (a.u.)	Pigment	Reference
228	3.310	Dienes	(Francieli C.G.B.S. Alves,et al, 2018)
244	3.389	Dienes	(Chmielarz, et al, 1995), (Oguz Uncu, Banu Ozen, 2019)

308	3.575	polyphenolic	(Francieli C.G.B.S. Alves,et al, 2018)
414	0.364	pheophytin-a	(Valentina Domenici, et al, 2014)
451	03122	β-carotene	(Francieli C.G.B.S. Alves,et al, 2018)
480	0.223	Carotenoid	(Marta Ferreiro-González, 2017)

Absorption intensities acquired for the peanut oil plotted as the function of wavelength is shown in Figure (4.18) and table (4.17). It can be seen that the peanut oil sample exhibits differences in absorbance, making it possible to distinguish between the peanut oil and other five types of oil samples on the basis of their absorption spectra. The absorption spectrum of peanut oil presents some characteristic bands that correspond to pheophytin-a, β-carotene and carotenoid pigments, respectively, in which the pheophytin-a contribute a weak band peak at 414 nm, β-carotene contribute a weak band peak 451 nm and the carotenoid contribute weak band at 480 nm. The Conjugated dienes appearance from the beginning of the spectrum with several peaks between (228 and 244) nm. polyphenolic compounds which show absorption at 308 nm.

4.5 Optical Properties of Edible Oils

Optical properties of edible oils were calculated from absorbance spectrum which using UV-VIS spectrometer (shimadzo mini 1240 spectrophotometer) scanning between (190 -1200) nm.

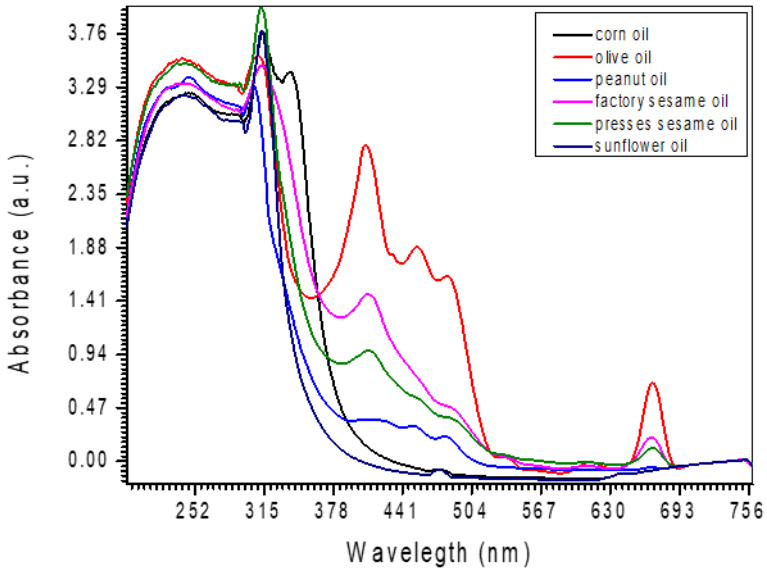

Figure (4.19) the Absorbance of corn, olive, factory sesame, peanut, presses sesame and sunflower oil

The spectrum in figure (4.19) can be divided into three main regions the first region is from the beginning of the spectrum to 340 nm. The second region is (400 - 500) nm. The last region is from 600 nm at the end of the spectrum. The excitation wavelengths are in the region 450 to 280 nm, where the absorption spectra of the oil are high, and in the visible region, 500-650 nm, where the absorption spectra are much lower absorption intensities acquired for all the selected six important Sudanese oils plotted that an additional chemical group caused a shift in the absorption peaks of these oils. Olive oil is distinguished in this field from the rest of the oils by its clear and multiple peaks, as it possesses three (420, 454 and 480) nm.

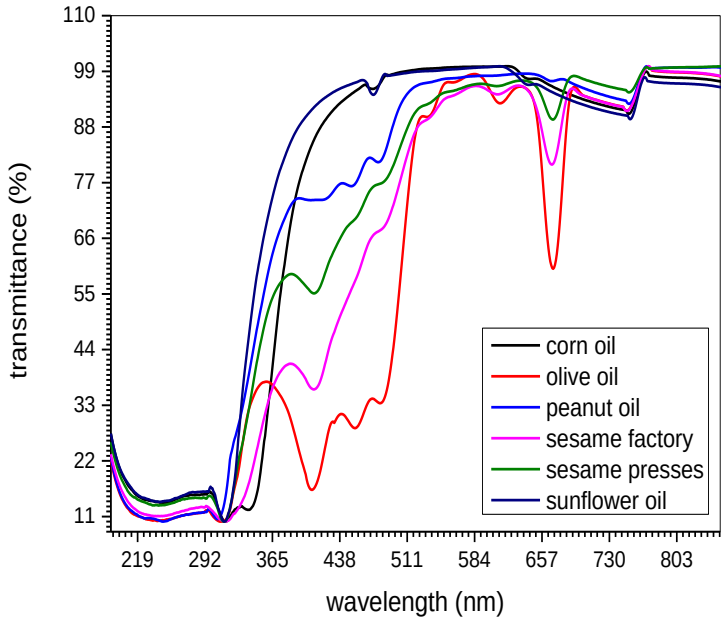

Figure (4.20) transmission of corn, olive, factory sesame, peanut, presses sesame and sunflower oil

The transmittance spectrum is characterized by its opposite behavior to the absorption spectrum, as Figure (4.20) shows the transmittance spectrum as a function of the wavelength of the oil samples. It is clear from the figure that the transmittance generally begins to appear at the wavelength that represents the boundary between the absorption and permeability of oils, or the so-called cut-off wavelength ($\lambda_{cut\text{-}off}$), and then the transmittance generally increases with the increase in the wavelength of the electromagnetic radiation falling on the samples. The sample oils reach their peak and hold in the visible region of the electromagnetic spectrum. It can be seen from Figure (4.20) that corn and sunflower oils have the greatest transmittance value about 99.2%. We find that olive oil has the lowest transmittance

points about (16 and 60.1) % at wavelengths (407 and 670) nm respectively.

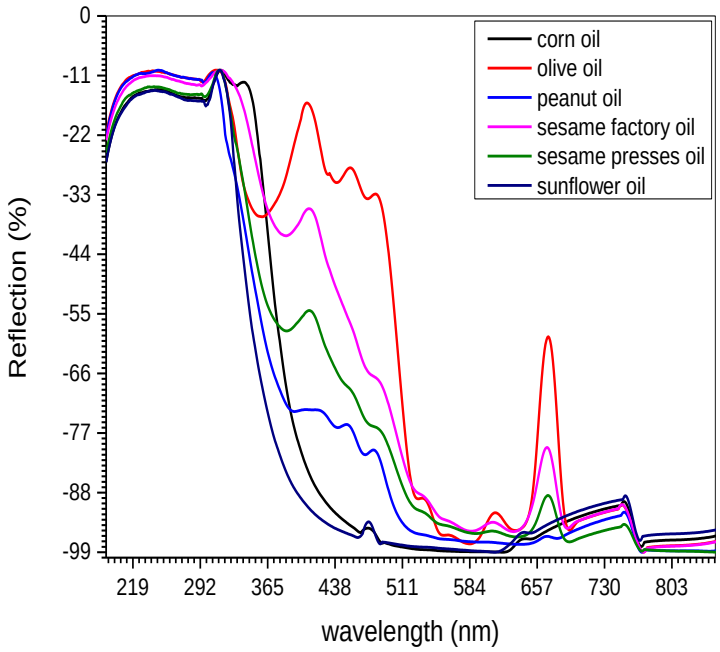

Figure (4.21) reflection of corn, olive, factory sesame, peanut, presses sesame and sunflower oil

The reflectivity spectrum was calculated from the absorption and transmittance spectrum according to the equation (2.19) of energy conservation. Figure (4.21) shows the reflectivity spectrum of six Sudanese edible oils as a function of wavelength, it is clear that the reflectivity decreases with increasing wavelength.

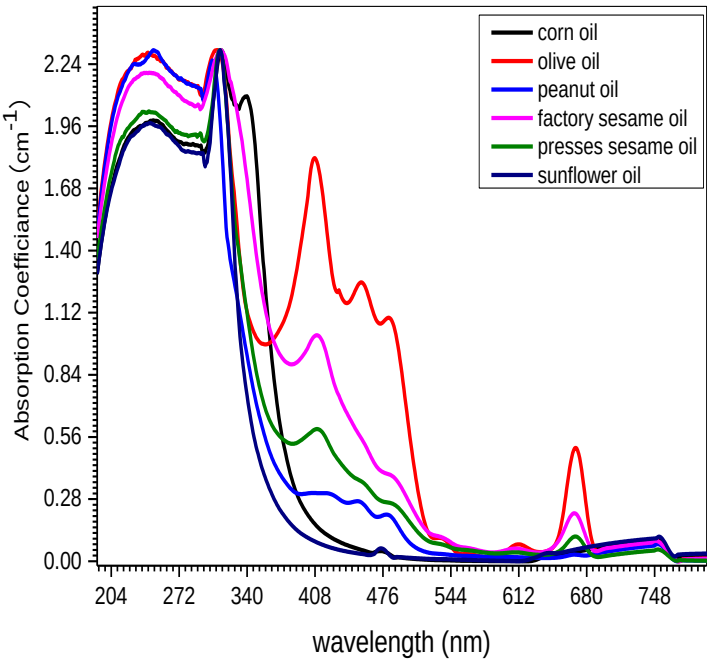

Figure (4.22) Absorption Coefficient (α) of corn, olive, factory sesame, peanut, presses sesame and sunflower oil

Figure (4.22) shows the absorption coefficient as a function of the wavelength of the incident photon on six samples of edible oils used in Sudan. It is clear from the figure that the absorption coefficient behaves in a behavior similar to the behavior of the absorption spectrum, and this is due to the fact that the absorption coefficient is a function of absorption as in the equation (2.18). From the figure (4.22), it becomes clear that the absorption coefficient begins in general with a gradual increase with the increase in wavelength at the beginning of the spectrum and then begins to decrease. It is noted that the absorption coefficient of all samples was different. It is noted that olive oil has the highest absorption coefficient, while corn oil and sunflower oil have the lowest absorption coefficient.

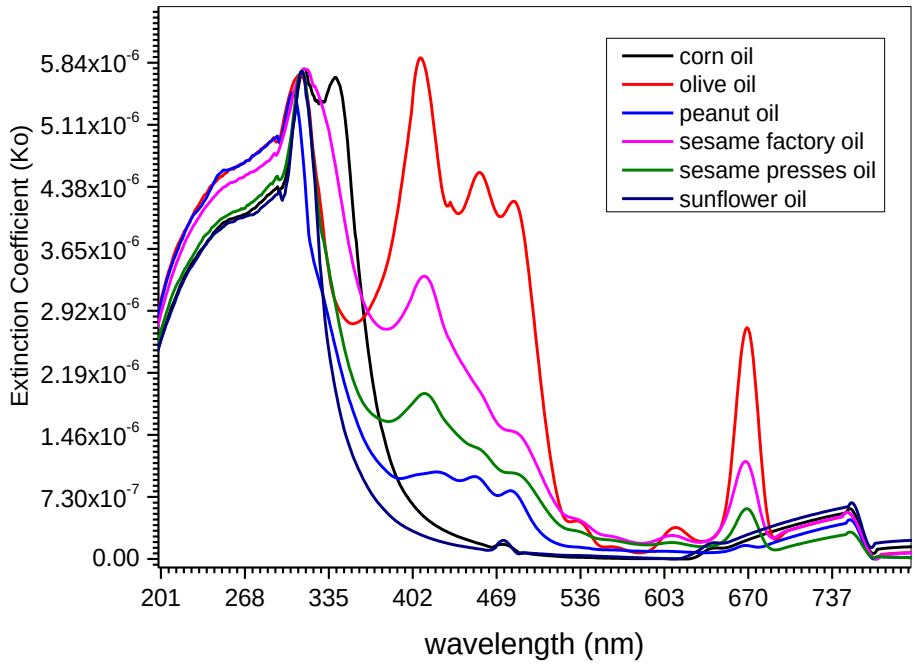

Figure (4.23) Extinction Coefficient (K_o) of corn, olive, factory sesame, peanut, presses sesame and sunflower oil

The extinction coefficient indicates the amount of attenuation obtained by the electromagnetic wave as it passes through the material medium, the extinction coefficient can be calculated by equation (2.19), figure (4.23) shows the change of the extinction coefficient as a function of the wavelength of the incident photon on edible oil samples.

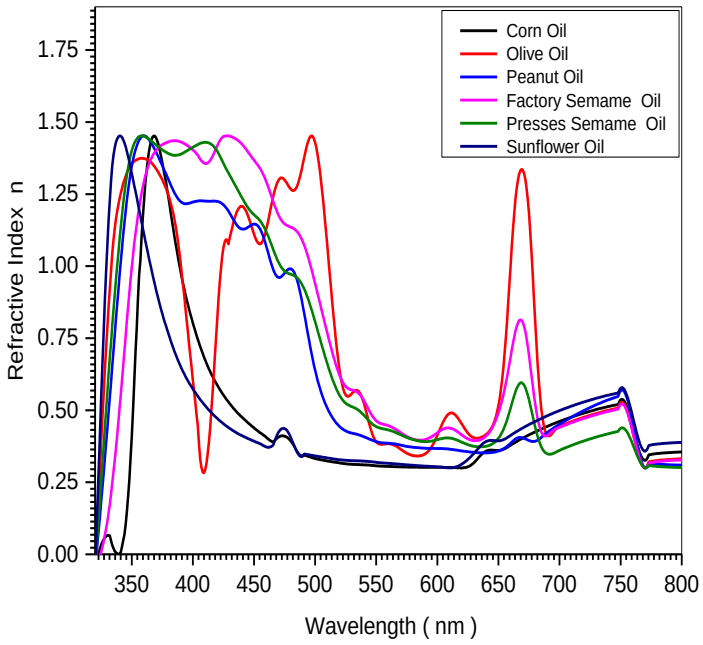

Figure (4.24) Refractive Index (n) spectra of corn, olive, factory sesame, peanut, presses sesame and sunflower oil

Refractive index (RI) is an important characteristic of oils because of the ease and speed with which it can be determined precisely, the small quantity of sample needed, and its relationship to structure. It generally gives a good idea about the degree of unsaturation of oil, as well as its correlation with the iodine value. The refractive indices of extra virgin olive, sunflower, corn, and refined olive oils were determined and the results in figure (4.24) and table (4). From this table, it could be seen that the refractive index value Calculated from the transmission spectrum using equation (2.20) at room tempura the olive oil was the smallest Refractive index in uv spectrum region (1.374) and factory sesame (1.435) comparing to the value of 1.452, for other samples oils. These variations in refractive indices of the corresponding oils under

investigation were attributed to the differences in fatty acid composition of these oils containing different.

As for the visible spectrum region, we find that olive oil has the highest refractive index of 1.452, followed by factory sesame oil, 1.45

4.6 Discussion

Six types of edible oils (corn, extra virgin olive, sunflower, factory sesame, pressed sesame and peanut) were collected from local market. Raman spectroscopy and Fourier infrared spectroscopy were applied to identify functional groups presence on oils, Optical properties of edible oils were calculated from absorbance spectrum which using UV-VIS spectrometer. FTIR and Raman spectroscopy were used to collect spectral information from the oils without requiring any sample preparation. The Raman spectra showed an apparent difference between the oils and it was easy to distinguish between them. As for the IR spectra, there was no clear difference between the spectra of oils. Raman spectrum of corn oil in range (3010.0 to 500.0) cm^{-1}, olive oil sample in region of (3089 to 600) cm^{-1}, Sunflower Oil in region of (3200-900) cm-^{1}, Pressed Sesame Oil sample in region (3000 to 50) cm^{-1}, Factory Sesame Oil in range from (3100 to 780) cm^{-1} finally spectrum of Peanut Oil in range (2800 to 300) cm^{-1}, while FTIR spectrum of all samples ranged from (400-4000) cm^{-1}. From the comparison of IR and Raman spectra of edible oil samples, the frequencies of some characteristic peaks were identical, while the relative intensities differed markedly. On the contrary, Raman scattering signal at (560, 969) cm^{-1} was quite weak, but corresponding infrared absorption peak was obvious. Both techniques probe vibrational transitions, but the selection rules

applying for IR and Raman spectroscopy are different, in the FTIR spectra, the major bands in oil samples can be attributed to the following vibrations: (523, 723, 1458, 1653, 1747,) cm^{-1} but in Raman spectra of edible oils samples, the major bands can be found at (1084, 1266, 1303, 1441, 1657, 1749,) cm^{-1}. It is of particularly significance for edible oils that stretching of C=C bonds gave rise to strong Raman signals and C=O stretching bands were very weak; the contrary can be found in infrared spectra. The general appearance of the IR spectra of these vegetable oils was found to be very similar to a previously reported study. In the Raman spectrum, the spectrum of peanut and presses sesame differed from the previous studies. Thus, the combination of these two different techniques can be very usefully in the study of oil provide comprehensive information about the chemical compositions of edible oils.

The visible region (350–800 nm) is zone where electronic transitions occur. Molecules exhibiting a large number of conjugated double bonds such as carotenoids, chlorophylls, and porphyrins absorb energy in this region. And their absorption properties may be used to evaluate the color of oils products.

Shift in the absorption peaks of these oils refer to different chemical group that oils contain.

The absorption peaks of all oil samples at room temperature in the range (200-400) nm are similar. This range provides some information about polyphenol antioxidants.

Compared to the relative intensities of IR and Raman bands differ considerably, the information provided being complementary. The 1700-1600 cm-1 spectral region has a particular importance for the characterization of oils from the unsaturation point of view.

The dominant features in this region are the intense absorption bands corresponding to C=C bonds, in contrast with FT-IR spectra, where the equivalent absorptions are displayed as weak bands. Moreover, in Raman spectra the C = C stretching vibrations corresponding to the cis and trans configurations appear at (1656 cm^{-1}), therefore Raman spectroscopy is considered a valuable analytical method in the oils field for the determination of the unsaturation type and degree.

Absorption peaks characterizing olive oil located at positions about 455 and 488 nm are due to the presence of carotenoids. The 533 nm peak corresponds to vitamin E and the chlorophyll band has a maximum at 612 and 669 nm, respectively. Chlorophyll and carotenoids significantly affect the color of olive, factory sesame and pressed sesame oil. It was found that olive oil had the greatest absorption value and the least transmission in all samples, then factory sesame and pressed sesame.

It was found that corn oil had the greatest transmission value and the least absorption in all samples, then sunflower oil and then peanut oil.

The (411-414) nm peak of pheophytin-a, a chemical compound that acts as an electron carrier in electron transfer. In the path of the photosynthesis system in plants.

Corn, sunflower, and peanut oil does not show the pigment absorption peaks of chlorophyll, so it has a light yellow or colorless, olive oil presents some characteristic bands that correspond to lutein, carotenoid and chlorophyll pigments, respectively so it has green light, Factory and presses sesame oil presents polyphenolic compounds carotenoid and pheophytin-a pigments this means it were colorless, the color of sunflower oil is

slightly amber due to Dines, Polyphenols and pigments Lutein bands. Finally, peanut oil presents some characteristic bands that correspond to pheophytin-a, β-carotene and carotenoid pigments, so it has a light-yellow color.

carotenoid contribute in the Raman scattering spectrum at bands (961, 1158, 1525, 2853, 2875, 289 and 2927) cm^{-1} while it appeared in the spectrum of absorption of ultraviolet visible rays at wavelengths (411and 533) cm.

Lutein appeared in the Raman spectrum of peanut oil in the range of 1517 cm^{-1}, while it appeared in the UV- visible absorption spectrum of all samples around the values (455, 473, 482) cm.

chlorophyll pigments contribute to the Raman scattering spectrum around the bands (785, 1122 and 1266) cm^{-1}, while it appeared in the UV-visible absorption spectrum at wavelengths (414, 612 and 669) cm.

Absorption coefficient and refractive index of all oils under study were different because structure components of each oil were different and this confirm with Raman and FTIR results. High values of the absorption coefficient indicate the possibility of direct electronic transitions between the valence and conduction bands at these energies.

The Raman spectral characteristic bands have been proved to be the Raman-active molecular vibration of pigment components.

The effect of vacuum occlusion on the spectrum, where butadiene has a Cis and Trans position and in the trans form, the π orbitals are all in one plane because the molecule is flat and this helps to overlap between the π orbitals better than the Cis position, which is uneven and has a vacuum occlusion. The higher the inter-orbital overlap, the lower the π-π transition energy, so the trans position

gives a longer wavelength transition, lower energy, and higher absorption intensity than the cis mode cis.

These results is in a good agreement with the work of (César Jiménez-Sanchidrián & José Rafael Ruiz; 2016) (Xuemei Liu, et al , 2021)

4.7 Conclusions

Combined FTIR spectroscopy has been shown to be a rapid and reliable method for the stabilization and quality control of edible oils.

Spectroscopic methods are very successful in evaluating edible oil quality. These methods are used for the qualitative and quantitative analyses of some Sudanese edible oils.

Raman Spectroscopy was used, it is a promising tool for evaluating edible oils safety because it allows rapid detection of large numbers of samples in a short time and, as a nondestructive method, it requires no sample preparation. In combination with chemometric analysis, Raman Spectroscopy is a highly powerful tool for extracting physical and chemical information from complex matrices.

This work is demonstrating that Raman spectroscopy is a valuable and useful technique for determining the degree of unsaturation of a vegetable oils.

In addition to, the detection of adulterants and the determination of minor components of vegetable oils can be achieved.

it is evident that Raman Spectroscopy has produced promising results and thus could be a powerful technique for oil product quality surveillance as well as for reducing the occurrence of edible oils product safety issues.

Raman spectroscopy techniques have proven useful and accurate in evaluating changes in the chemical profile and viscosity of oils samples. FTIR spectroscopy has been successfully used to analyze the oxidation levels of various oil samples with acceptable levels of prediction accuracy.

The Raman spectrum showed the difference in the samples, but in the FTIR spectrum, the results were similar for all samples.

The second study, sample of edible oils were studied to determine their pigment content and to find some optical properties, used UV-VIS spectroscopy.

The absorption properties of edible oils have been studied in the region of visible wavelengths near ultraviolet rays. Each oil exhibits unique absorption properties over the wavelength range from (200 to 800) nm. Olive oil has unique absorbing properties that set it apart from other oils.

In the visible UV-visible wavelength region, the edible oils can be distinguished from each other.

The work points out the advantages of using UV Vis spectroscopy. The advantages are related to the non-destructive properties, speed, and low cost of each sample from spectroscopy plus no specific sample preparation or specially qualified laboratory personnel. In conclusion, it can be a reliable, fast, obtainable, and cheap classification tool.

4.8 Recommendations

- Expand the study to include all edible oils used in Sudan.
- Conducting more experiments by taking samples from different production companies for comparison.
- Use different spectrophotometers covers all frequencies of electromagnetic wave and compare the results

- Study the effect of low and high temperatures on oils.
- Verify the effect of storage method on optical properties.
- Study the effect of boiling oils more than once
- Find the electrical properties of oils.
- Using atomic spectra to identify the elements in oils.
- Comparison of molecular and atomic spectra

Reference

1- Bernhard Schrader. (1995). ***Infrared and Raman spectroscopy****: methods and applications*. VCH Verlagsgesellschaft mbH, Weinheini (Federal Republic of Germany) VCH Publishers. Inc., New York.

2- Blachut, D., Wojtasiewicz, K., Czarnocki, Z., 2002***, Identification and synthesis of some contaminants present in 4-methoxyamphetamine (PMA) prepared by the Leuckart method***, Forensic Science International, 127(12), 45-62.

3- Baudot, P., Vicherat, A., Viriot, M.L., Carre, M.C., 1999, ***Identification of N-methyl-1-(1,3-benzodioxol-5-yl)-2-butanamine (MBDB), a homologue derivative of "ecstasy***", Analusis, 27(6), 523-532.

4- Breck Hitz, J.J. Ewing, Jeff Hecht. (2001). ***Introduction to laser technology***, Third Edition http://www.ieee.org/store.

5- Carmona, M.A., Lafont, F., Jim_enez-Sanchidri_an, C., and Ruiz, J.R. (2015) ***Characterization of macadamia and pecan oils and detection of mixtures with other edible oils by Raman spectroscopy***. Grasas y Aceites, 66:94–102.

6- Carmona, M.A., Lafont, F., Jim_enez-Sanchidri_an, C., and Ruiz, J.R. (2014). ***Raman spectroscopystudy of edible oils and determination of the oxidative stability at frying temperatures.*** Eur. J.Lipid Sci. Technol. 116:1451–1456.

7- César Jiménez-Sanchidrián & José Rafael Ruiz. (2016). ***Use of Raman spectroscopy for analyzing edible vegetable oils***. http://dx.doi.org/10.1080/05704928.2016.1141292.

8- Chase, B., 1987, ***Fourier transform Raman spectroscopy***, Microchimica Acta 93(1), 81-91.

9- Chmielarz, Bajdor, Labudzinska, Klukowska-Majewska, (1995), ***Studies on the double bond positional isomerization process in linseed oil by UV, IR and Raman spectroscopy,*** Journal of Molecular Structure 348 3 13-3 16

10- Cristina Lazzerini, Mario Cifelli and Valentina Domenici, (2016), ***Pigments in Extra-Virgin Olive Oil: Authenticity and Quality***, http://dx.doi.org/10.5772/64736

11- David A. Cremers and Leon J. Radziemski. (2006). ***Handbook of Laser-Induced Breakdown Spectroscopy***. John Wiley & Sons Ltd, The Atrium, Southern Gate, Chichester, West Sussex PO19 8SQ, England.

12- Daniel Barrera-Arellano, .. Sergio O. Serna-Saldivar, (2019), ***Chapter 21 - Corn Oil: Composition, Processing, and Utilization***, https://doi.org/10.1016/B978-0-12-811971-6.00021-8

13- David W. Ball. (2001). ***The Basics of Spectroscopy***. The International Society for Optical Engineering P.O. Box 10. Email: spie@spie.org.

14- D. J. Gardiner, P. R. Graves. (1989). ***Practical Raman spectroscopy***. Springer-Verlag Berlin Heidelberg New York London Paris Tokyo.

15- D. L. Rousseau, J. M. Friedman, and P. F. Williams, (1979). ***Raman Spectroscopy of Gases and Liquids***. Springer-Verlag Berlin Heidelberg New York.

16- Doi, K., Miyazawa, M., Fujii, H., Kojima, T., 2006, ***The analysis of the chemical drugs among structural isomer***, Yakugaku Zasshi-Journal of the Pharmaceutical Society of Japan, 126(9), 815-823.

17- Edwards, H.G.M., Chalmers, J. M., 2005, ***Raman spectroscopy in archaeology and art history, The Royal Society of Chemistry***, Cambridge,UK, pp.48-51.

18- Éric Dufour. (2009). ***Infrared Spectroscopy for Food Quality Analysis and Control***, First edition. Oxford, UK: phone (_44) (0) 1865 843830; fax (_44) (0) 1865 853333; email: permissions@elsevier.com.

19- Esam M. A. Ali, 2016, ***Raman, spectroscopic investigation of cocaine hydrochloride on human nail in a forensic context***, University of Bradford

20- Ewen Smith, Geoff Dent. (2005). ***Modern Raman spectroscopy: a practical approach***. John Wiley & Sons Ltd, The Atrium, Southern Gate, Chichester, West Sussex PO19 8SQ, England.

21- Fernando da Silveira Minuceli, Jiuliane Martins da Silva, Roberta da Silveira, Oscar Oliveira Santos**, (**06/08/2021**), *UV-VIS methodology for the quantification ovegetable oil in adulterated olive oil,*** Research, Society and Development, v. 10, n. 6, e50210612822 | ISSN 2525-3409 | DOI: http://dx.doi.org/10.33448/rsd-v10i6.12822

22- Francieli C.G.B.S. Alves, Aline Coqueiro, Paulo H. Março, Patrícia Valderrama, (2018), ***Evaluation of olive oils from the Mediterranean region by UV–Vis spectroscopy and Independent Component Analysis***, https://doi.org/10.1016/j.foodchem.01.126

23- FRANK D. GUNSTONE, (2000), ***VEGETABLE OILS IN FOOD TECHNOLOGY Composition, Properties and Uses,*** Osney Mead, Oxford OX2 0EL, UK Tel: +44 (0)1865 206206.

24- Gauglitz, G. and T. Vo-Dinh (2003). Handbook of Spectroscopy. Published by: WILEY-VCH Verlag GmbH & Co. KGaA, Weinheim, Federal Republic of Germany.

25- G. Gauglitz and T. Vo-Dinh. (2003). ***Handbook of Spectroscopy***. WILEY-VCH Verlag GmbH & Co. KGaA, Weinheim ISBN 3-527-29782-0.

26- Hana Vaskova and Martina Buckova, (2014), ***Measuring and Identification of Oils.*** CEBIA-Tech No. CZ.1.05/2.1.00/03.0089.

27- HANA VASKOVA, MARTINA BUCKOVA***. (***2018***), Multivariate study of Raman spectral data of edible oils.*** vaskova@fai.utb. cz http://www.utb.cz

28- Hartwig Schulz, Malgorzat Baranska***.*** (2007)***. Identification and quantification of valuable plant substances by IR and Raman spectroscopy***. www.elsevier.com/locate/vibspec.

29- H. Chalmers, J.M., Griffiths, P.R. (2002). ***Handbook of IR Spectroscopy***. Hardcover. ISBN 3-527-28896-1.

30- H. Charlotte Grinter and Dr. T. L. Threlfall. (1992). ***UV-VIS Spectroscopy and Its Applications.*** Springer- Verlag Berlin Heidelberg.

31- H. E. Hassan1 H.A. Badawy, (2010) ***QUALITY DETECTION OF HEATING CORN OIL USING VISIBLE AND INVISIBLE LIGH,*** Misr J. Ag. Eng., 27 (2): 613 - 627

32- Hendra, P., Jones, C., Warnes, G. (1991). ***Fourier Transform Raman spectroscopy: Instrumentation and chemical applications***. Ellis Horwood Limited, Chichester, England, 1991, chapter 2, p.p.17-20

33- Herman A. Szymanski, (1967) ***RAMAN SPECTROSCOPY Theory and Practice.*** PLENUM PRESS· NEW YORK.

34- Hewlett-Packard, (1996), ***Fundamentals of UV-visible spectroscopy***. Printed in Germany 09/96, publication number12-5965-5123E

35- Hong Yan, Jixiong Zhang, Jingxian Gao, Yangming Huang, Yanmei Xiong & Shungeng Min. (2018). ***Towards improvement in prediction of iodine value in edible oil system based on chemometric analysis of portable vibrational spectroscopic data.*** http://creativecommons.org/licenses/by/4.0/

36- J.L. Kinsey (1977), ***Laser-induced fluorescence***. Ann. Rev. Phys. Chem. 28, 349.

37- Johannes Kiefer. (2015). ***Recent Advances in the Characterization of Gaseous and Liquid Fuels by Vibrational Spectroscopy***. www.mdpi.com/journal/energies.

38- J. Michael Hollas. (2004). ***MODERN SPECTROSCOPY***, Fourth Edition. The Atrium, Southern Gate, Chichester, West Sussex PO19 8SQ, England, www.wileyeurope.com.

39- John R. Ferraro, Kazuo Nakamoto and Chris W. Brown. (2003). ***Introductory Raman Spectroscopy*** *(Second edition*). ISBN: 978-0-12-254105-6.

40- Jose. Cayuela • Khaled Yousfi • M. Carmen Martınez • Jose M. Garcı, (2014***), Rapid Determination of Olive Oil Chlorophylls and Carotenoid by Using Visible Spectroscopy***, DOI 10.1007/s11746-014-2515-1

41- José L. Quiles, M. Carmen Ramيrez-Tortosa and Parveen Yaqoob, (July 2005) ***OLIVE OIL AND HEALTH***, A catalogue record for this book is available from the British Library,London, UK.

42- J.R. Lakowicz (1991), ***Topics in Fluorescence Spectroscopy***, (Plenum, New York). John R. et

43- Karla Danielle Tavares Melo Milanez, Thiago César Araújo Nóbrega, Danielle Silva Nascimento, Matías Insausti, Beatriz Susana Fernández Band, Márcio José Coelho Pontes, (2017), ***Multivariate modeling for detecting adulteration of extra virgin olive oil with soybean oil using fluorescence and UV–Vis spectroscopies: A preliminary approach,*** 10.1016/j.lwt.06.060

44- Karoui, R., Downey, G., & Blecker, C. (2010). ***Mid-infrared spectroscopy coupled with chemometrics: A tool for the analysis of intact food systems and the exploration of their molecular structure-***

quality relationships-A review. Chemical Reviews, 110(10), 6144-6168. doi:10.1021/cr100090k

45- Lauren E. Jamieson, Angela Li, Karen Faulds and Duncan Graham. (6 November 2018). ***Ratiometric analysis using Raman spectroscopy as a powerful predictor of structural properties of fatty acids.*** R. Soc. Open sci. 5: 181483. http://dx.doi. org/10.1098/rsos.181483**.**

46- Lewis, I.R., Edwards, H.G.M., 2001, ***Handbook of Raman Spectroscopy from the Research Laboratory to the Process Line***, Marcel Dekker, Inc., New York, USA,

47- Macomber, R.S., 1998, ***A complete introduction to modern NMR spectroscopy***, John Wiley & Sons, New York, USA,

48- Mc Creery, R.L., 1999, ***Raman spectroscopy for chemical analysis***, John Wiley & Sons, New York, USA, pp.1-247.

49- Marta Ferreiro-González , Gerardo F. Barbero , Jesús Ayuso **,** (2017)**,** ***Authentication of virgin olive oil by a novel curve resolution approach combined withvisiblespectroscopy,*** http://dx.doi.org/10.1016/j.foodchem.2016.10.015

50- Meyer, M.W.; Lupoi, J.S.; Smith, E.A. (2011). ***1064nm dispersive multichannel Raman spectroscopy for the analysis of plant lignin***. *Anal. Chim. Acta*, *706*, 164–170.

51- Michał Szmatoła, Justyna Chrobak, Rafał Grabowski, Jolanta Iłowska, JuliaWoch, Iwona Szwach, Izabela Semeniuk, Jolanta Drabik, MałgorzataWrona, Rafał Kozdrach, Beata Orli ´ nska and Mirosława Gryme. **(**December 2018***). Spectroscopic Methods in the Evaluation of Modified Vegetable Base Oils from Crambe abyssinica.*** http://creativecommons .org/licenses/by/4.0/**.**

52- Mínguez - Mosquera, M.I.; Gandul-Rojas, B.; Garrido - Fernández, J.; Gallardo-Guerrero, L (1990), ***Pigments Present in Virgin Olive Oil. J. Am. Oil*** Chem. Soc. 1990, 67, 192–196

53- Mohammad E. Khosroshahi, **(2018),** Effect of Temperature on Optical Properties of Vegetable Oils Using UV-Vis and Laser Fluorescence Spectroscopy. Optics and Photonics Journal, 8, 247-263.https://doi.org/10.4236/opj.2018.87021

54- M Rinawati, L A Sari and K T Pursetyo, (2020), ***Chlorophyll and carotenoids analysis spectrophotometer using method on microalgae***, IOP Conf. Series: Earth and Environmental Science 441 012056

55- M. Saleem, Naveed Ahmad, Rahat Ullah, Zulfiqar Ali & S. Mahmood & Hina Ali (March 2020). ***Raman Spectroscopy–Based Characterization of Canola Oil***. Food Analytical Methods https://doi.org/10.1007/s12161-020-01752-0.

56- Muhammad Akhyar Farrukh,2011, Atomic Absorption Spectroscopy, Janeza Trdine 9, 51000 Rijeka, Croatia

57- Muik, B., Lendl, B., Molina-D_ıaz, A., and Ayora-Ca~nada, M.J. (2005). ***Direct monitoring of lipid oxidation in edible oils by Fourier transform Raman spectroscopy***. Chem. Phys. Lipids, 134:173–182.

58- Muik, B., Lendl, B., Molina-D_ıaz, A., and Ayora-Ca~nada, M.J. (2003). ***Direct, reagent-free determination of free fatty acid content in olive oil and olives by Fourier transform Raman spectrometry***. Anal. Chim. Acta, 487:211–220.

59- Nafie A. Almuslet and Mohammed A. Yousif. (2016). ***Utilization of Raman Spectroscopy to Identify the Components of Groundwater in Some Western Areas of Saudi Arabia Kingdom*.**

60- Oguz Uncu, Banu Ozen, (2019), ***A comparative study of mid-infrared, UV–Visible and fluorescence spectroscopy in combination with chemometrics for the detection of adulteration of fresh olive oils with old olive oils,*** Food Control 105 209–218

61- Origin Lab, Northampton, USA

62- Peter F. Bernath. (2005), ***Molecular Spectroscopy and Structure***. Departments of Chemistry and Physics University of Waterloo, Ontario Canada N2L 3G1.

63- PETER LARKIN. (2011). ***Infrared and Raman Spectroscopy principles and spectral interpretation.*** ISBN: 978-0-12-386984-5

64- Peyronel Fernanda,(2018), ***Methods Used in the Study of the Physical Properties of Fats***, https://doi.org/10.1016/B978-0-12-814041-3.00011-3.

65- P. NALLASAMY, P. M. ANBARASAN, S. MOHAN. (06.10.2000). ***Vibrational Spectra and Assignments of cis- and Trans-1,4-Polybutadiene***. Raman School of Physics, Pondicherry University, 605014, Pondicherry-INDIA e-mail: s mohan@lycos.com

66- Qing Zhang, Cheng Liu, Zhijian Sun, Xiaosong Hu, Qun Shen, Jihong Wu**. (**December 2011**). *Authentication of edible vegetable oils adulterated with used frying oil by Fourier Transform Infrared Spectroscopy.*** Journal homepage: www.elsevier.com /locate/food chem**.**

67- R.M. El-Abassy, P. Donfack, and A. Materny, (27 April 2009), ***Visible Raman spectroscopy for the discrimination of olive oils from different vegetable oils and the detection of adulteration,*** (www.interscience.wiley.com) DOI 10.1002/jrs.2279.

68- Šašić,S, 2008, ***Pharmaceutical Applications of Raman Spectroscopy***, John Wiley &Sons, New York, USA, chapter 1, pp.1-5.

69- Shiyamala Duraipandian, Jan C. Petersen and Mikael Lassen. (June 2019). ***Authenticity and Concentration Analysis of Extra Virgin Olive Oil Using Spontaneous Raman Spectroscopy and Multivariate Data Analysis.*** License http://creativecommons.. org/licenses/by/4.0/

70- Sponsored by HORIBA Scientific, (2018***). Raman Spectroscopy and its Most Common Applications***. Knightsbridge Road Piscataway NJ, 08854 United States.

71- Sune Svanberg. (June 2001). ***Atomic and Molecular Spectroscopy***: basic aspects and practical applications. Springer-Verlag Berlin Heidelberg New York. http://www.springer.de.

72- Thaís Karine de Lima, supervised by D. Bertoldo Menezes, (2020), ***Using Raman spectroscopy and an exponential equation approach to detect adulteration of olive oil with rapeseed and corn oil***. https://doi.org/10.1016/j.foodchem.2020.127454

73- Tony Owen, (1996), ***Fundamentals of UV-visible spectroscopy***, Hewlett-Packard 12-5965-5123E

74- Turrell, G., Corset, J., 1996, ***Raman microscopy: Developments and applications***, Academic Press Limited, London, UK, chapter 3, pp.51-

75- Valentina Domenici, Donatella Ancora, Mario Cifelli, Andrea Serani, Carlo Alberto Veracini, and Maurizio Zandomeneghi (2014)**,** ***Extraction of Pigment Information from Near-UV Vis Absorption Spectra of Extra Virgin Olive Oils***, dx.doi.org/10.1021/jf503818k | J. Agric. Food Chem

76- V. Baeten and M. Meurens**.** (**1996,**)**.** ***Detection of Virgin Olive Oil Adulteration by Fourier Transform Raman Spectroscopy.*** J. Agric. Food Chem.**,** 44, 2225-2230

77- WALTER S. STRUVE, 1989, ***Fundamentals of molecular spectroscopy***, JOHN **WILEY** & SONS New York / Chichester / Brisbane / Toronto / Singapore.

78- Wikipedia, the free encyclopedia, (18 December 2021***), sunflower oil***, Wikipedia® is a registered trademark of the Wikimedia Foundation, https://en.wikipedia

79- Wolfgang Demtröder. (2008). ***Laser Spectroscopy*** Fourth edition. 67663 Kaiserslautern Germany demtroed@rhrk.uni-kl .de

80- Wolf Hamm, Richard J. Hamilton, Dr Gijs Calliauw, (2013), ***Edible Oil Processing, Second Edition,*** Print ISBN:9781444336849 |Online ISBN:9781118535202 |DOI:10.1002/9781118535202.

81- **OriginLab Corporation, (2019),** One Roundhouse Plaza, Northampton, MA 01060 USA, USA: 1.800.969.7720, Int'l: 1.413.586.2013, Fax: +1.413.585.0126 Email: sales@originlab.com.

82- Xiande Zhao & Daming Dong & Wengang Zheng & Leizi Jiao & Yun Lang**,** (2015). ***Discrimination of Adulterated Sesame Oil Using Mid-Infrared Spectroscopy and Chemometrics***. Food Anal. Methods DOI 10.1007/s12161-015-0125-7**.**

83- Xuemei Liu, Jianjun Zeng, Wen Ping, Alireza Sanaeifar, Xiao Xu, Wei Luo, Junjing Sha, Zhenxiong Huang, Yifeng Huang, Baishao Zhan, Hailiang Zhang, and Xiaoli Li, (2021), ***Quantitative visualization of photosynthetic pigments in tea leaves based on Raman spectroscopy and calibration model transfer,*** doi: 10.1186/s13007-020-00704-3

84- Yang, H. and J. Irudayaraj (2001). ***Comparison of near-infrared, Fourier transform-infrared, and Fourier Transform-Raman methods for determining olive-pomace oil adulteration in extra virgin olive oil.*** Journal of the American Oil Chemists Society, 78: 889-895**.**

85- Yang, H., J. Irudayaraj and M.M. Paradkar (2005). ***Discriminant analysis of edible oils and fats by FTIR, FT-NIR and FT-Raman spectroscopy***. Food Chemistry, 93: 25–32.

86- Zhao, J.; Carrabba, M.M.; Allen, F.S. (2002). ***Automated fluorescence rejection using shifted-excitation Raman difference spectroscopy***. *Appl. Spectrosc. 56*, 834–845.

Appendix

Raman and FTIR Spectra of edible oils

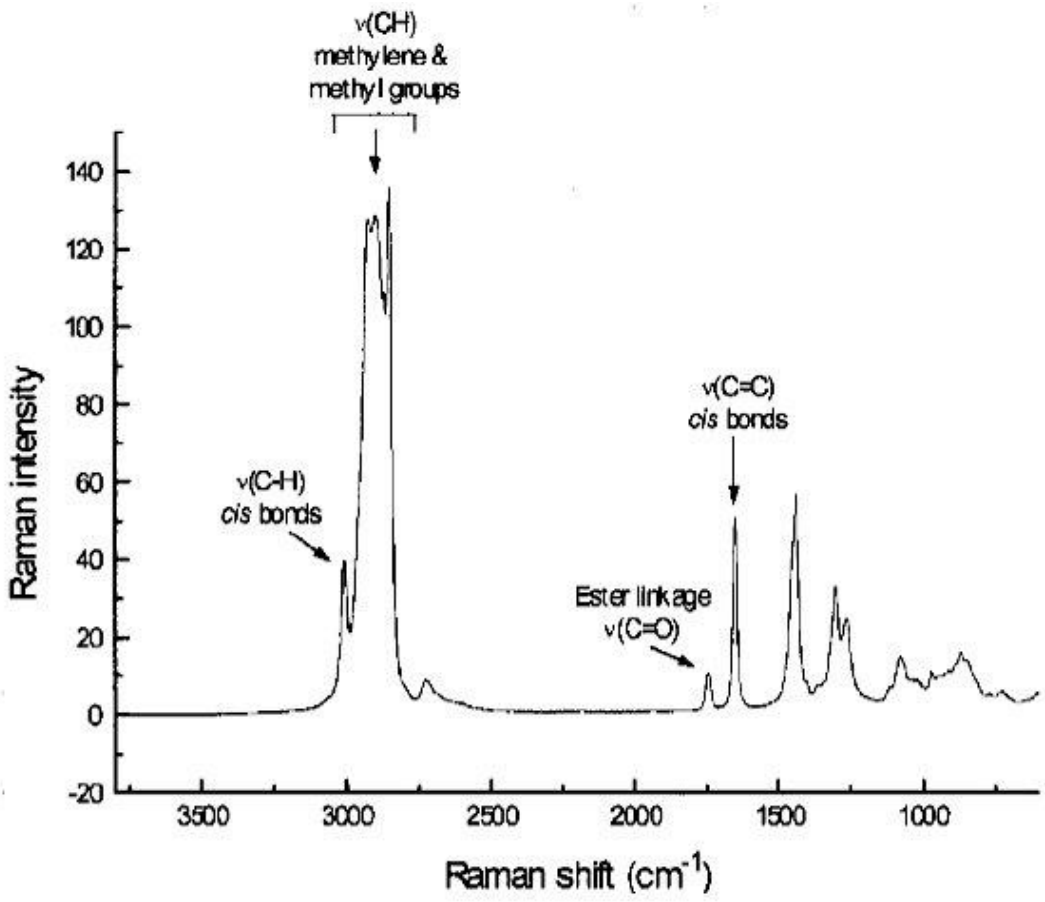

FT-Raman spectrum of an edible oil

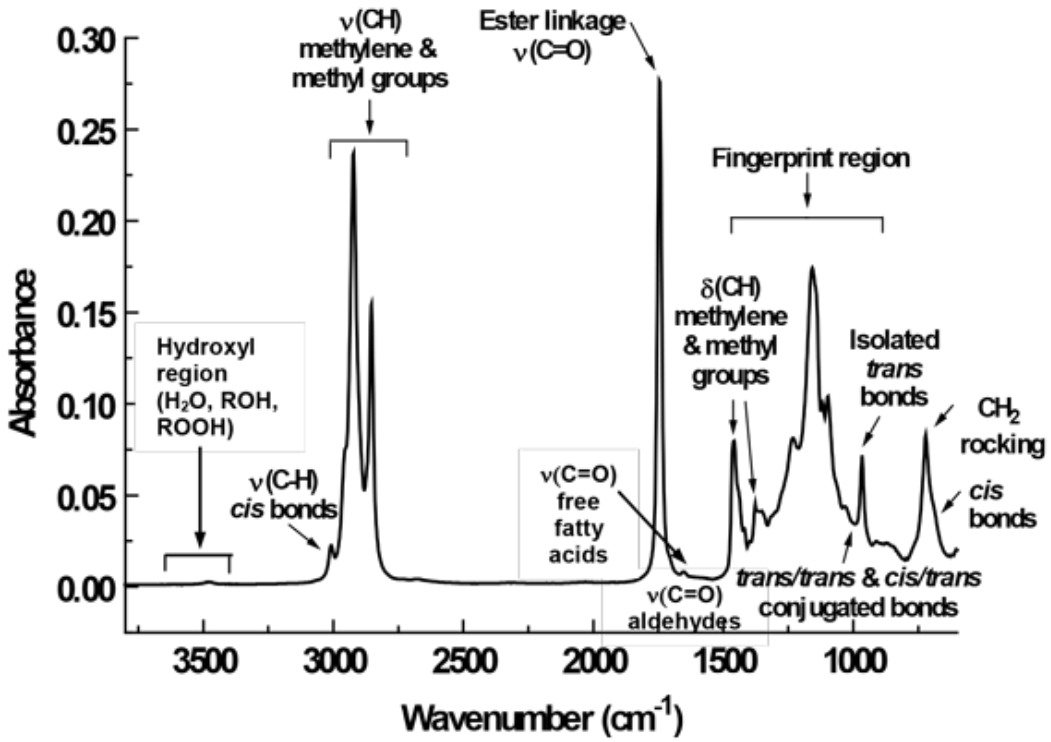

The FTIR spectrum of an edible oil

(Marta Ferreiro- González , et al, 2017)